

**A Study of Nitrogen-based Plasma Polymerisation from
Fundamentals to Design of Coatings for Fibrinogen
Adsorption Regulation**

Madhuwanthi Buddhadasa



Department of Chemical Engineering

McGill University, Montreal

November, 2017

A thesis submitted to McGill University in partial fulfillment of the
requirements for the degree of

Doctor of Philosophy

© Madhuwanthi Buddhadasa, 2017

Dedicated to my family and friends

Acknowledgements

Firstly, I would like to convey my heartfelt gratitude to my parents for planting the seed of learning within me without which I may not have come this far. Thank you for your unconditional love, patience and support that have given me the strength to overcome all obstacles and keep moving forward. Thank you to my sister who has always been there for me to listen to me and provide moral support. I am very lucky to have you all in my life.

I am sincerely grateful to Prof. Pierre-Luc Girard-Lauriault for his continuous support, patience and positive attitude which gave me the courage and confidence to persevere and progress in my research. My sincere gratitude to Prof. Sophie Lerouge for her thoroughness and resourcefulness which helped me think in different perspectives and widen my horizons. Accomplishing this thesis would not have been possible without the assistance and feedback from both my supervisors.

My sincere thanks to Cédric Vandenabeele and Prof. Rony Snyders for their valuable contribution and generous support on the plasma and film diagnostics project. I learnt a lot from our collaboration and enjoyed working with you.

I would like to acknowledge my group mates Sara, Larissa, Evelyne, Dominic, Francois and Mario for their contributions that made working in the lab a rewarding experience. Larissa, thank you for your help, especially at the time my laptop broke down, I greatly appreciated your thoughtfulness. To my summer student, Alex, thank you for your collaboration on the protein adsorption project, I enjoyed working with you. To the past and present undergraduate students in our group: Joey, Calvin, Cole, Mingxing, Azat and Cedric, thank you for your contributions, it was a pleasure working with you.

Special thanks to several staff members of the McGill chemical engineering department including Jo-Ann and Louise for administrative help, Lisa for patient assistance at the store,

Frank for help with my gas-cylinder problems and ensuring a safe working environment, Ranjan and Andrew for useful advice with the analytical equipment, Lou for help with my computer-related problems and Gerald for help with the electronics. Thank you all for your patient and kind support throughout my studies at McGill.

I would like to thank Prof. Anne Kietzig and Tanvir Ahmmed for valuable advice on contact angle measurements, and Prof. Jean-Luc Meunier and Prof. Sylvain Coulombe for kindly lending their lab items that helped with the protein adsorption experiments. Thank you to John Li, Alireza Mesgar and Sasa Ristic for assistance with gold/chromium coating. To Lihong Shang for help with XPS, and Kelly Sears and Weawkamol Leelapornpisit for help with platinum coating. To Prof. Richard Chromik and Yinyin Zhang for advice and kind support with tribometry measurements. To Mehdi Dargahi, Pablo Escuder and Jiri Nohava also for help with tribometry measurements.

Sandrine, thank you for your ideas, as well as the insightful and fun conversations. Norma, your advice, encouragements and the social events you organized, that brought a sense of community to our groups are much appreciated. Hanno, thank you for your advice and fruitful and enjoyable conversations. Natalie, your generous support and advice with the initially planned bio project and Lisa, your help with those bio experiments are sincerely appreciated.

Finally, I am thankful for all financial support received through McGill University.

Thank you!

Abstract

It has been over a century since plasma polymers were discovered and since then they are investigated for numerous potential applications in many fields including electrical, optical and biomedical. Plasma based deposition techniques are dry processes with which a wide variety of substrate materials and objects with 3-dimensional geometries can be treated. The coatings are highly cross-linked, conformal and pin-hole free providing good barrier properties. Surface chemistries can easily be controlled and precursor gases are relatively inexpensive. These are a few reasons that make plasma polymers attractive, especially for biomedical applications such as cell and tissue culture, controlled drug release, anti-fouling coatings, contact lenses, biosensors and so on.

In this thesis, application of nitrogen (N) based plasma polymer films is investigated, to regulate the adsorption of fibrinogen (Fg), a blood clotting protein, in light of achieving the long term goal of gaining control over blood coagulation, a useful criterion for studying aneurysm healing following an endovascular coiling procedure. In arriving at this main objective, several fundamental studies are first conducted to design a suitable set of coatings, which are produced using a low-pressure radio frequency (RF) glow discharge. In the first part of the thesis, a fundamental study on elucidating the characteristics of two distinct methods of producing N rich plasma polymer films is carried out, where the precursor types employed in each method are (i) single source precursors and (ii) precursor mixtures. A variety of characterisation tools are used to perform plasma diagnostics and thin film analyses, to understand the plasma-phase processes that result in coatings with specific functionalities.

The second part of this work aims at producing plasma polymer coatings with a high amine content as well as high resistance to film dissolution in aqueous media. Owing to the increased controllability of N to C ratio in the gas phase and thereby, in the solid phase, which is the film, the second method of producing N based coatings is employed. This method

involves using a functional group source gas, in this case ammonia, and a hydrocarbon (HC) precursor, in this case ethylene and/or 1,3-butadiene. Owing to the presence of two conjugated C-C double bonds, 1,3-butadiene is chosen to render better cross-linked coatings compared with those produced from ethylene, a common precursor used in many studies. Plasma deposition parameters varied in film optimisation are power, gas flow ratio and total gas flow rate. It is shown that butadiene based films, as required, yield a better compromise between amine content and water stability compared with that achieved by ethylene based films, under similar plasma deposition conditions.

The final part of this project focuses on developing a series of plasma polymer films that can effectively promote Fg adsorption to varying extents. It commences with a continuation of the optimisation of coatings from the previous section. This is carried out by varying the deposition pressure, a crucial process parameter that greatly influences plasma polymerisation, and studying its effect on film properties such as the amine content, aqueous stability as well as affinity for Fg adsorption. Next, the influence of the type of N based coatings, defined by the HC precursor used for deposition, on Fg adsorption is investigated. An oxygen (O) rich and a platinum (Pt) coating are also included in the study. Friction and wear tests are performed to ensure sufficient wear resistance against a polyethylene surface in aqueous media. Finally, a subset of these coatings is chosen to monitor Fg adsorption in the presence of a second protein, human serum albumin (HSA). It is shown that the designed plasma polymer coatings could successfully regulate the adsorption of Fg with and without the presence of a high concentration of competing HSA, opening up the possibility for controlling blood coagulation, a useful concept to improve aneurysm healing following an endovascular coiling treatment.

Abrégé

Cela fait plus d'un siècle que les polymères plasma ont été découverts et depuis, ils sont étudiés pour de nombreuses applications potentielles dans différents domaines, notamment électrique, optique et biomédical. Les techniques de dépôt par plasma sont des procédés à sec avec lesquels une grande variété de matériaux, de substrats et d'objets à géométries tridimensionnelles peuvent être traités. Les revêtements sont hautement réticulés, uniformes et exempts de trous d'épingle, ce qui leur confèrent de bonnes propriétés de barrière. La chimie de surface des polymères plasma peut être facilement contrôlée et les gaz précurseurs sont relativement peu coûteux. Ce sont quelques éléments qui les rendent attrayants, en particulier pour les applications biomédicales telles que la culture de cellules et de tissus, la libération contrôlée de médicaments, les revêtements antifouling, les lentilles de contact, les biocapteurs, etc.

Dans cette thèse, nous étudions l'utilisation de couches minces de polymères plasma à base d'azote (N) pour réguler l'adsorption du fibrinogène (Fg), une protéine de la coagulation sanguine, avec pour objectif à long terme de contrôler la coagulation sanguine, un critère déterminant pour la guérison des anévrismes après une procédure d'occlusion endovasculaire (coils). Pour atteindre cet objectif principal, plusieurs études fondamentales sont d'abord menées pour concevoir une série de revêtements qui sont produits en utilisant une décharge lumineuse radio-fréquentielle (RF). Dans la première partie de la thèse, une étude fondamentale sur l'élucidation des caractéristiques de deux méthodes distinctes de production de couches minces riches en N est réalisée, les précurseurs utilisés dans chaque méthode étant (i) des précurseurs purs et (ii) des mélanges de précurseurs. Plusieurs outils de caractérisation sont utilisés pour effectuer le diagnostic du plasma et l'analyse des couches minces afin de comprendre l'effet des processus ayant lieu dans la phase plasma sur les caractéristiques des revêtements fonctionnels.

La deuxième partie de ce travail vise à produire des revêtements de polymères plasma avec une haute concentration en amine ainsi qu'une bonne résistance à la dissolution en milieux aqueux. En raison du contrôle accru du rapport N sur C dans la phase gazeuse et par conséquent, dans la couche mince solide, le second procédé de production de revêtements à base de N est utilisé. Cette méthode implique l'utilisation d'un gaz générant des groupes fonctionnels, dans ce cas l'ammoniac, et d'un d'hydrocarbure (HC), dans ce cas l'éthylène et/ou le 1,3-butadiène. En raison de la présence de deux doubles liaisons C-C conjuguées, le 1,3-butadiène est choisi pour rendre les revêtements plus réticulés que ceux produits à partir d'éthylène, un précurseur utilisé dans de nombreuses autres études. Les paramètres de dépôt variés dans le cadre de l'optimisation des propriétés des couches minces sont la puissance, le rapport de débit des gaz et le débit total de gaz. Il est démontré que les couches à base de butadiène, présentent un meilleur équilibre entre la teneur en amine et la stabilité à l'eau lorsque comparés à celles obtenus avec des couches à base d'éthylène, dans des conditions de dépôt similaires.

La dernière partie de ce projet se concentre sur le développement d'une série de couches minces de polymères plasma qui ont la capacité de promouvoir l'adsorption de Fg à des degrés variables. Il commence par une poursuite de l'optimisation des revêtements présentés dans la section précédente. Ceci est effectué en faisant varier la pression de dépôt, un paramètre de procédé qui influence grandement le processus de polymérisation dans le plasma, et en étudiant son effet sur les propriétés des couches telles que la teneur en amine, la stabilité en milieu aqueux et l'affinité pour l'adsorption de Fg. Ensuite, on étudie l'influence du type de revêtements à base de N, défini par le précurseur HC utilisé pour le dépôt, sur l'adsorption de Fg. Un revêtement riche en oxygène (O) et une surface de platine (Pt) sont également inclus dans l'étude. Des essais de frottement et d'usure sont effectués pour assurer une résistance à l'usure suffisante contre une surface en polyéthylène dans des milieux aqueux. Enfin, un sous-ensemble de ces revêtements est choisi pour étudier l'adsorption de Fg en présence d'une seconde protéine, la sérum-albumine humaine (HSA). Il est démontré que les revêtements

de polymères plasma peuvent réguler l'adsorption de Fg, avec ou sans la présence d'une concentration élevée de HSA concurrente, ce qui pave la voie à l'obtention d'un contrôle de la coagulation sanguine, un élément déterminant pour améliorer la guérison des anévrysmes suite à une procédure médicale endovasculaire .

Contents

Acknowledgements	ii
Abstract	iv
Abrégé	vi
List of Figures	xiii
List of Tables	xix
List of Abbreviations	xx
1 Introduction	1
1.1 Motivation	1
1.2 Thesis organization	4
1.3 Objectives	4
1.4 Original contributions	6
2 Literature Review	8
2.1 Plasma surface engineering	8
2.1.1 Plasmas	8
2.1.2 Glow discharge and plasma polymer	10
2.1.3 General effects of plasma deposition parameters	11
2.2 Plasma surface functionalisation for influencing biomolecule immobilisation .	13
2.2.1 Plasma surface modification	14
2.2.2 Plasma polymerisation	14
2.3 Stability of plasma polymer coatings	17
2.4 Biomaterials in contact with blood	20
2.4.1 Platelet adhesion, activation and Fg adsorption	21

2.4.2	Competitive protein adsorption	24
2.4.3	Changes in conformation and biological properties in adsorbed proteins	26
3	Experimental Methods	28
3.1	Plasma generation	28
3.1.1	RF discharges	28
3.1.2	Experimental setup for film deposition	30
3.2	Characterisation techniques	32
3.2.1	Mass spectrometry	32
3.2.2	Fourier transform infrared spectroscopy	33
3.2.3	Optical emission spectroscopy	36
3.2.4	X-ray photoelectron spectroscopy	37
3.2.5	Chemical derivatisation with 4-trifluoromethyl benzaldehyde	38
3.2.6	Dynamic contact angle goniometry	39
3.2.7	Tribometry	40
3.2.8	Surface plasmon resonance spectroscopy	41
3.2.9	Surface plasmon fluorescence spectroscopy	43
4	A Fundamental Study of Two Distinct Methods for Synthesis of N-based Plasma Polymer Films	46
4.1	Introduction	47
4.2	Experimental section	51
4.2.1	Sample preparation and thin film characterisation	51
4.2.2	Plasma characterisation	53
4.2.2.1	FTIR	53
4.2.2.2	OES	53
4.2.2.3	MS	54
4.3	Results and discussion	54

4.4	Conclusions	75
5	Preparation of N-based Films with Optimised Amine Content and Water Stability	78
5.1	Introduction	79
5.2	Experimental section	81
5.2.1	Deposition of plasma polymer coatings	81
5.2.2	Materials characterization	83
5.3	Results and discussion	85
5.3.1	Optimisation of $[-NH_2]$ and stability	85
5.3.1.1	PPE:N vs. PPB:N - Effect of R and power	85
5.3.1.2	PCEB:N - Effect of R_{HC} , F_T and power	87
5.3.2	Regression analysis of $[N]$ and stability	91
5.3.2.1	Multivariate linear regression model for $[N]$	91
5.3.2.2	Multivariate non-linear regression model for stability	92
5.3.3	Functional group analysis	94
5.3.3.1	HR-XPS	94
5.3.3.2	FTIR	96
5.3.3.3	OES	97
5.4	Conclusions	99
6	Plasma Polymer Films to Regulate Fibrinogen Adsorption	101
6.1	Introduction	102
6.2	Experimental section	106
6.2.1	Plasma polymer deposition	106
6.2.2	Film characterisation	107
6.2.3	Protein adsorption by SPRS and SPFS	109
6.3	Results and discussion	112

6.3.1	Effect of pressure on film properties	112
6.3.2	Influence of film type on Fg adsorption	116
6.3.3	Influence of HSA on Fg adsorption	123
6.4	Conclusions	128
7	Conclusion	131
7.1	Summary	131
7.2	Limitations and future improvements	138
	References	140

List of Figures

1.1	Steps involved in the endovascular coiling treatment of an aneurysm. Upper left: Positioning of the tip of a microcatheter into the aneurysmal neck. Upper right: Introduction of a Pt coil attached to a stainless steel delivery guidewire, into the aneurysm through the microcatheter. Arrow indicates the junction between the Pt and stainless steel. Lower left: A positive direct current is applied to the guidewire and thus, Pt coil, which then attracts negatively charged cells and molecules, triggering thrombus formation. Lower right: Pt coil is detached from the guidewire due to dissolution of the stainless steel portion at the junction, by electrolysis within 4 to 12 minutes of applying the current. (Reproduced from ref. ¹⁵)	3
2.1	Classification of plasmas	9
2.2	Schematic diagram of the Rapid Step-Growth Polymerisation (RSGP) mechanism, reproduced from ref. ²⁰	11
2.3	Deposition rates as functions of gas mixture ratios, $X = NH_3/C_2H_4$ for L-PPE:N and $X = N_2/C_2H_4$ for H-PPE:N (reproduced from ref. ³¹)	17
2.4	Surface energy, γ_s , and its dispersive γ_s^d and polar γ_s^p components, as functions of the nitrogen concentrations, of a) L-PPE:N and b) H-PPE:N films (reproduced from ref. ³¹)	19
2.5	Interaction of clotting factors through a series of enzymatic activation steps leading to the production of thrombin which acts on fibrinogen, converting it into a fibrin polymer which then stabilises to form a thrombus or clot. Thrombin also acts on Factor XI as a feedback mechanism, leading to an increased production of thrombin (a redrawn version of a figure from ref. ¹).	22

2.6	Platelet response to artificial surfaces. Protein adsorption to the surface facilitates platelet adhesion, which then become activated releasing storage granule contents such as ADP, platelet factor 4 (PF4) and β -thromboglobulin (β -TG), synthesizing thromboxane A ₂ (Tx A ₂) and generating thrombin. This promotes the stimulation of other platelets, platelet aggregation and stabilisation of the platelet mass by thrombin-generated fibrin (a redrawn version of a figure from ref. ¹).	23
2.7	(a) Fg adsorption to polystyrene from normal (triangles) and afibrinogenemic (squares) plasma at different dilutions. (b) Platelet adhesion to polystyrene preadsorbed with different dilutions of normal (solid line) or afibrinogenemic (dotted line) plasma (reproduced from ref. ⁴⁷).	24
2.8	Schematic of the structure, molecular weight and concentration in blood plasma of Fg, albumin and IgG. Surface charges on Fg and albumin shown are in pH 7.4.	25
2.9	Surface chemistry dependency of selective protein adsorption from plasma to a series of hydrophilic-hydrophobic (HEMA-EMA) copolymers. Fg (solid line), IgG (— —), albumin (●) and hemoglobin (— · —) (reproduced from ref. ⁵⁴).	26
3.1	Schematic of (a) CCP and (b) ICP reactor (redrawn version from ref. ⁵⁹).	29
3.2	Schematic of the ICP experimental setup. 1-Substrate holder, 2-load-lock system, 3-pumping system, 4-water-cooled copper coil, 5-precursor inlet, 6-mass spectrometer and 7-in situ FTIR spectrometer (reproduced from ref. ⁶⁰).	31
3.3	Optical diagram of a Michelson interferometer (redrawn version from ref. ⁶⁵).	34
3.4	OES setup used in plasma diagnostics (redrawn version from ref. ¹⁷).	36
3.5	Schematic of a photoelectron emission from the 1s orbital of an atom (redrawn version from ref. ⁶⁶).	37
3.6	Reaction between a primary amine and TFBA.	39
3.7	Schematic of the tribometer setup (reproduced from ref. ⁷²).	41

3.8	(a) Schematic of sample installation in the Kretschmann configuration, (b) example of an SPR curve before and after a protein adsorption process. . . .	43
3.9	(a) Example of an SPFS signal along with the SPR curve, (b) schematic of the experimental setup of the SPRS in combination with the SPFS ((b) reproduced from ref. ⁷⁹).	44
4.1	Mass spectra of (a) AA, (b) CPA, (c) AmEt and (d) AmBu plasmas at plasma off, 30 W, 60 W and 100 W. The top spectra (plasma off) show the cracking fractions of the monomers related to their fragmentation in the ionization source of the spectrometer. The spectra of AA and CPA when plasma is on are corrected according to Equation 4.2 while spectra of AmEt and AmBu mixture are corrected according Equation 4.6. All spectra are finally normalized with respect to the total ionic current according to Equation 4.7.	58
4.2	OES spectra of AA, CPA, AmEt and AmBu plasmas in order to compare all precursors at 100 W and at similar energy invested per particle i.e. AA, CPA at 100 W, AmEt at 250 W and AmBu at 175 W.	60
4.3	FTIR spectra of (a) CPA, (b) AA, (c) AmEt and (d) AmBu plasmas. Vibrational modes indicated in black and blue (in the case of AmEt and AmBu) are those initially present in the precursor molecules and bands in red are those appearing when the discharge is switched on. For the AmEt and AmBu spectra (c and d), modes in blue are those related to ammonia and black, related to the HC molecule. ν = stretching; δ = scissoring or deformation in general; τ = twisting; ω = wagging; ρ_r = rocking	63
4.4	FTIR spectra of (a) AA, (b) CPA, (c) AmEt and (d) AmBu plasmas zoomed in the 650-1000 cm^{-1} region.	64
4.5	Zoomed in FTIR spectra of AA and CPA plasmas aligned with a spectrum of NH_3 vapour to show the generation of ammonia in both AA and CPA plasmas.	66

4.6	OES spectra of CPA, AA, AmEt and AmBu discharges at 100 W denoting the H-alpha line in the wavelength range 590 to 735 nm.	69
4.7	Effect of power on (a) N concentration, (b) $[\text{NH}_2]/[\text{N}]$ and (c) $[-\text{NH}_2]$, where $[-\text{NH}_2]$ represents all groups that react with aldehydes such as primary amines and imines, for PPFs deposited from AA, CPA, AmEt and AmBu.	70
4.8	FTIR spectra of CPA, AA, AmEt and AmBu based films at (a) 30 W, (b) 60 W and (c) 100 W, normalised to the CH_x peak (P2) height. Peak assignments are based on. ^{107,110} Peaks P1, P3 and P4 are normalised to the intensity of peak P2, in order to more easily compare FTIR spectra at different powers.	73
4.9	Comparison of the maximum intensities of P1, P3 and P4 peaks from FTIR spectra of AA, CPA, AmEt and AmBu films at 30 W, 60 W and 100W. *AmEt film is deposited at 40 W and not 30 W.	74
4.10	Deposition rates of AA, CPA and AmEt based PPFs.	75
5.1	Schematic diagram of the low-pressure, capacitively coupled r.f. PECVD reactor used for depositing thin PP films.	82
5.2	Characterisation of PPB:N (circles) and PPE:N (squares) films: (a) Deposition rate ($\text{nm}\cdot\text{min}^{-1}$) (b) % loss in thickness (c) $[\text{N}]$ (at. %) and (d) $[-\text{NH}_2]$ (%), as a function of R for different powers: 10 W (red) and 20 W (blue). F_{HC} was maintained constant at 5 sccm at 10 W and 10 sccm at 20 W.	86
5.3	PCEB:N films: (a) Deposition rate (b) % loss in thickness (c) $[\text{N}]$ and (d) $[-\text{NH}_2]$, as a function of R_{HC} for different powers: 10 W (red) and 20 W (blue). $F_T = 10$ sccm and $R = 4$	88
5.4	PCEB:N films: (a) Deposition rate (b) % loss in thickness (c) $[\text{N}]$ and (d) $[-\text{NH}_2]$, as a function of R for different F_T values: 10 sccm (circles) and 20 sccm (squares). $R_{HC} = 0.25$	89
5.5	PCEB:N films: (a) % Loss in thickness (blue) and deposition rate (green), and (b) $[\text{N}]$ (blue) and $[-\text{NH}_2]$ (green), as a function of power. $R_{HC} = R = 4$	90

5.6	High-resolution C 1s spectra for (a) PPE:N (b) PPB:N and (c) PCEB:N films, fitted with four component-peaks. fwhm 1.2 eV, peak shape GL(70). The [N] of all three films was approximately 17%.	94
5.7	Evolution of the different component-peaks of the high-resolution C 1s spectra, [N] and [-NH ₂] as a function of R for (a) PPE:N (b) PPB:N and R_{HC} for (c) PCEB:N films.	96
5.8	ATR FTIR spectra of a 17 % [N] PPE:N, PPB:N and PCEB:N film. . . .	97
5.9	Effect of power on OES spectra of a) B-A plasma and b) E-A plasma. $F_{HC} = 10$ sccm.	98
5.10	Effect of R on OES spectra of a) B-A plasma and b) E-A plasma. $F_{HC} = 10$ sccm.	99
6.1	Effect of reactor pressure on the properties of PPB:N films deposited at gas flow ratios $R=NH_3/HC=1$ to 4 (a) deposition rate, (b) N content determined by XPS, (c) nucleophile content determined by TFBA-derivatisation-XPS, (d) stability in PBS after 1 h of exposure, (e) stability in PBS after 24 h of exposure and (f) Fg adsorption determined by SPRS under continuous flow.	113
6.2	Fg adsorption on PPFs, platinum and gold determined by SPRS. (a) Thickness of the Fg layer adsorbed on all films. The R values of the PPFs are, from left to right, 1 to 4 for the four PPB:N films, 0.5 and 0.75 for the PPE:Ns, 4 for the PCEB:N and 8 for the PPE:O. Adsorption kinetics measured by minimum tracking, under continuous flow, are presented for (b) the four PPB:N films and (c) PPE:N, PCEB:N, PPEO, PPE, Pt and Au films. Each curve represent an individual experiment. All PPFs are deposited at 80 Pa.	117
6.3	Advancing and receding water contact angles (ACA and RCA) in air for all PPFs, platinum and gold. The R values of the PPFs are, from left to right, 1 to 4 for the four PPB:N films, 0.5 and 0.75 for the PPE:Ns, 4 for the PCEB:N and 8 for the PPE:O. All PPFs are deposited at 80 Pa.	119

-
- 6.4 Friction and wear tests against a HDPE counter-surface measured using tribometry. Expected Hertzian contact stress, 21.8 MPa. Figure shows images of the wear tracks obtained during profilometry of (a) PPB:N R=1, (b) PPB:N R=3, (c) PPB:N R=4, (d) PPE:N R=0.75, (e) PCEB:N and (f) PPE:O. All films are deposited at 80 Pa. 121
- 6.5 HSA adsorption on PPB:N R=1, PPB:N R=3, PPE:O and Pt coatings determined by SPRS, under static flow. (a) Thickness of HSA layer adsorbed. (b) Adsorption kinetics obtained by minimum tracking for the PPFs and time measurement for the Pt coating. The PPB:N films were deposited at 45 Pa and PPE:O at 80 Pa. 124
- 6.6 Competitive Fg adsorption from a Fg-HSA mixture, on PPB:N R=1, PPB:N R=3 and PPE:O coatings determined by SPFS. (a) Thickness of the Fg layer adsorbed from a pure Fg solution and the Fg-HSA mixture. (b) Adsorption kinetics of Fg-HSA for the PPFs. Kinetics of labelled Fg from a pure solution on PPB:N R=3 is also shown (grey line). (c) Adsorption kinetics of Fg-HSA and labelled Fg from a pure solution on the Pt coating. Kinetic experiments were done by time measurement under static flow. The PPB:N films were deposited at 45 Pa and PPE:O at 80 Pa. 126

List of Tables

4.1	Mass assignments for CPA, AA, AmEt and AmBu plasmas.	59
4.2	Observed IR frequencies assignment for AA and CPA plasmas	62
4.3	Observed IR frequencies assignment for AmEt and AmBu plasmas	65
5.1	List of regressor variables	92
5.2	Values of the significant regression coefficients ($p < 0.05$) of the nitrogen concentration model. p values are shown in parentheses.	92
5.3	Values of the significant regression coefficients ($p < 0.05$) of the water stability model. p values are shown in parentheses.	93
6.1	Surface chemistry of PPFs. Films were deposited at 80 Pa.	118
6.2	Coefficients of friction of the PPFs measured under 21.8 and 2.7 MPa Hertzian contact stresses. Films deposited at 80 Pa.	122

List of Abbreviations

AA	Allylamine
AmBu	Ammonia/1,3-Butadiene
AmEt	Ammonia/Ethylene
CPA	Cyclopropylamine
DBD	Dielectric barrier discharge
DI	Deionised
Fg	Fibrinogen
FTIR	Fourier transform infrared spectroscopy
HC	hydrocarbon
HSA	Human serum albumin
IgG	Immunoglobulin
MS	Mass spectrometry
OES	Optical emission spectroscopy
PCEB:N	N-based plasma co-polymerised ethylene butadiene film
PPB:N	N-based plasma polymerised butadiene film
PPE:N	N-based plasma polymerised ethylene film
PPE:O	O-based plasma polymerised ethylene film
PPF	Plasma polymer film
RF	Radio frequency
SPFS	Surface plasmon fluorescence spectroscopy
SPRS	Surface plasmon resonance spectroscopy
T_g , T_e	Gas temperature, electron temperature
TFBA	4-trifluoromethyl benzaldehyde
vWF	von Willebrand factor
XPS	X-ray photoelectron spectroscopy

Chapter 1

Introduction

1.1 Motivation

A biomaterial is defined as a nonviable material used in a medical device, intended to interact with biological systems.¹ The surface of a biomaterial is what comes in direct contact with the surrounding and is responsible for the proper functioning of the device. Therefore, designing a surface with optimised characteristics is a key factor in biomaterials engineering. Out of the many surface engineering techniques available, plasma-based processes are increasingly gaining interest, especially in the biomedical field, owing to reasons such as, involvement of no wet chemicals, production of no harmful by-products and the ease of controllability of the surface chemical composition.

There are two main plasma-based approaches of surface engineering for organics, namely, plasma surface modification (also known as "grafting" or "plasma treatment") and plasma polymerisation. In the first approach, macromolecules in the near-surface region of a synthetic polymer substrate are modified by the addition of new chemical functionalities via substitutive radical reactions.²⁻⁴ In the second method, a macromolecular coating, commonly referred to as a plasma polymer film, is deposited on the surface by using either a functional group based precursor gas, such as allylamine, heptylamine and ethanol, or a gas mixture containing a source of functional groups and a source of carbon to produce the polymer backbone, for example nitrogen/ethylene, ammonia/ethylene and carbon dioxide/ethylene.⁵⁻⁹ Plasma surface modification has several limitations, such as reptational movement of near-surface macromolecules on long-term storage leading to change in surface functionality,^{10,11} difficulty in achieving highly specific surface chemistries and difficulty in

achieving high nitrogen concentrations on surfaces modified with N.¹² On the other hand, plasma polymerisation allows for higher nitrogen concentrations,⁸ limited hydrophobic recovery (i.e. less reptational movement of near-surface molecules)⁵ and also more specific surface functionalities by careful choice of deposition conditions,^{5,6} thereby making plasma polymerisation the preferred technique. In the context of implementation, however, plasma polymerisation can be more complicated to implement and the choice of plasma polymerisation would depend on cost-benefit analysis.

Plasma polymers are commonly functionalised with chemical groups such as amines, carboxyl and hydroxy groups.⁵ Among these functionalities, N-based films have gained considerable interest in the biomedical field owing to chemical groups such as primary amines, secondary amines and imines that become positively charged in physiological pH media and thus, are able to attract negatively charged biomolecules such as proteins, which are responsible for mediating cell processes. Thus, the focus of this thesis is on N-based plasma polymer coatings. The development of such a coating for a specific biomedical application requires the consideration of several factors mainly, surface chemistry, aqueous stability and biological performance.

Recall, these coatings can be deposited using either a single precursor gas which contains the N functional groups, such as allylamine, or a gas mixture, such as ethylene/ammonia. A direct comparison of these two methods of producing N-rich coatings have not been studied previously and a fundamental understanding of the differences between these two approaches is lacking. Furthermore, the presence of hydrophilic surface functionalities, such as amines, can often lead to the dissolution of the plasma polymer coating when exposed to an aqueous environment. Therefore, it is vital that a compromise between the concentration of functional groups and aqueous stability is achieved, for the proper functioning of the coating.

The main function of these films is to be able to regulate the adsorption of a blood clotting protein, namely fibrinogen (Fg), which is responsible for platelet attachment and

aggregation in the blood coagulation cascade.¹³ The motivation behind this goal has been in the treatment of brain aneurysms, a localised dilatation of a blood vessel wall in the brain, which involves the insertion of platinum coils into the aneurysm as shown by the steps explained in Figure 1.1. The surface of the coil is expected to initiate a coagulation response by blood, leading to a thrombus formation, thereby sealing the aneurysm and preventing it from further expansion and rupture. The instability of the thrombus formed can lead to recanalisation and re-opening of the aneurysm in the long run,¹⁴ and the relationship between the thrombogenicity of the coil, i.e. the degree to which the coil is able to promote thrombosis, and aneurysm healing is poorly understood. Thus, in light of developing a surface engineering technique to vary the thrombogenicity of the coil surface, the long-term intention would be to coat the coils with plasma polymers with varying degrees of thrombogenicity. In this regard, to successfully regulate the adsorption of Fg is considered the first step towards the development of a series of coatings that is able to control platelet adhesion, activation and subsequently, blood coagulation.

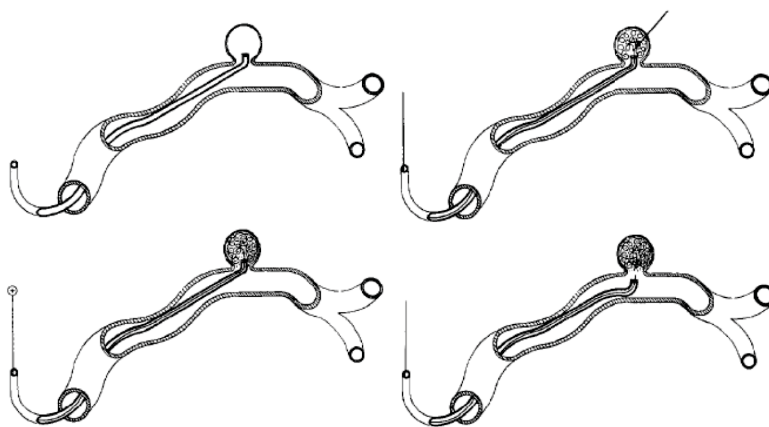


Figure 1.1: Steps involved in the endovascular coiling treatment of an aneurysm. Upper left: Positioning of the tip of a microcatheter into the aneurysmal neck. Upper right: Introduction of a Pt coil attached to a stainless steel delivery guidewire, into the aneurysm through the microcatheter. Arrow indicates the junction between the Pt and stainless steel. Lower left: A positive direct current is applied to the guidewire and thus, Pt coil, which then attracts negatively charged cells and molecules, triggering thrombus formation. Lower right: Pt coil is detached from the guidewire due to dissolution of the stainless steel portion at the junction, by electrolysis within 4 to 12 minutes of applying the current. (Reproduced from ref.¹⁵)

1.2 Thesis organization

This is a manuscript-based thesis, composed of 7 chapters, written by the author. Chapter 2 includes a thorough and relevant literature review of the work done. Chapter 3 describes and explains the experimental setup of the plasma reactor and the characterisation techniques used. Chapter 4 presents the manuscript titled "*Single source precursor vs. precursor mixture for N-rich plasma polymer deposition: Plasma diagnostics and thin film analyses*" where the first objective is fulfilled. The second objective is accomplished in Chapter 5 where the manuscript titled "*Plasma Co-polymerisation of Ethylene, 1,3-Butadiene and Ammonia Mixtures: Amine Content and Water Stability*" is presented. The final objective is achieved in Chapter 6 which presents the manuscript titled "*Plasma Polymer Films to Regulate Fibrinogen Adsorption: Effect of Pressure and Competition with Human Serum Albumin*". Chapter 7 concludes the work done, discusses limitations and provides suggestions for future work.

1.3 Objectives

1. *Investigate and compare plasma polymerisation of N based coatings using single source precursors and precursor mixtures.*

In achieving this objective, single source precursors namely, allylamine (AA) and cyclopropylamine (CPA), and precursor mixtures namely, ammonia/ethylene (AmEt) and ammonia/1,3-butadiene (AmBu) are used to deposit N-rich coatings. An N to C elemental ratio of 1 to 3 in the inlet gas stream is maintained a constant for all depositions. The plasma phase as well as the films deposited are characterised using a variety of techniques in order to elucidate the effect of different plasma species and possible plasma-phase reactions on the nature of film chemistry. Results show similar plasma-phase fragmentation patterns between these two approaches of prepar-

ing N-based films, however, with regards to the chemistry of thin films, differences such as better amine/imine selectivity, i.e. $[\text{NH}_2]/[\text{N}]$ or $[\text{C}=\text{N}]/[\text{N}]$, under mild power conditions, are observed in films deposited from the precursor mixtures.

2. *Deposition of N based coatings with optimised concentration of desirable N functional groups and aqueous stability.*

To fulfill this objective, the approach of using precursor mixtures for depositions is employed, since it allows to control the ratio of functional group to HC content in the film. As previously, the gas mixtures used are, AmEt and AmBu. The purpose of using 1,3-butadiene for comparison with previously studied ethylene, is due to the presence of two conjugated C-C double bonds in the butadiene molecule which is expected to increase the cross link density of the plasma polymer, thereby leading to an improvement in film stability, in terms of film dissolution in aqueous media. Films are deposited using ethylene and butadiene individually to give PPE:Ns and PPB:Ns, as well as, using a mixture of the two HCs to produce co-polymerised films, the PCEB:Ns. A series of films from each of the three types are deposited by varying plasma parameters such as power and ammonia to HC gas flow ratio. Surface chemistry and water stability measurements are conducted to arrive at the optimum plasma conditions required to achieve a compromise between these two conflicting film requirements. Indeed, the butadiene films show better resistance to dissolution in aqueous media compared with those deposited from ethylene, with similar amine concentrations.

3. *Characterisation of the N based coatings for regulation of Fg adsorption from a pure solution as well as a protein mixture containing Fg and human serum albumin (HSA).*

The optimised coatings found from fulfilling the previous objective, are used to study the adsorption of Fg, after a further optimisation step. In this optimisation step, the gas pressure during film deposition is varied and the optimum pressure to generate amine/imine rich films with satisfactory aqueous stability is found. Fg adsorption onto PPB:Ns, PPE:Ns and a PCEB:N show a clear trend with the increase in amine/imine

content of the films, suggesting that these plasma polymer coatings can successfully control the extent of Fg adsorption. Furthermore, Fg adsorption is also studied on an oxygen rich coating (PPE:O) and a Pt coating, where the lowest adsorption amounts are observed, with the PPE:O being the least attractive to the protein molecules. Study of Fg adsorption is then carried out in the presence of HSA, the most abundant protein in blood plasma. Regulation of Fg adsorption is still found to be successful, although with some alterations, using a combination of N-based and O-rich coatings.

1.4 Original contributions

Following are publications associated with this work, presented in Chapters 4, 5 and 6, respectively. These are either published in or to be submitted to a peer-reviewed journal.

1. **M. Buddhadasa**, C. R. Vandenabeele, R. Snyders and P. L. Girard-Lauriault. Single source precursor vs. precursor mixture for N-rich plasma polymer deposition: Plasma diagnostics and thin film analyses. *Plasma Processes and Polymers*, DOI: 10.1002/ppap.201700030, 2017.

This work was a collaboration with the University of Mons in Belgium. M. Buddhadasa performed part of the experiments, analysed the results and wrote the manuscript. C. R. Vandenabeele helped with performing the experiments, results analysis and revising the manuscript. Other authors contributed in supervising the research, discussing the results and revising the manuscript.

2. **M. Buddhadasa** and P. L. Girard-Lauriault. Plasma Co-polymerisation of Ethylene, 1,3-Butadiene and Ammonia Mixtures: Amine Content and Water Stability. *Thin Solid Films*, 591:76-85, 2015.

M. Buddhadasa performed the experiments, analysed the results and wrote the

manuscript. P. L. Girard-Lauriault contributed in supervising the research, discussing the results and revising the manuscript.

3. **M. Buddhadasa**, S. Lerouge and P. L. Girard-Lauriault. Plasma Polymer Films to Regulate Fibrinogen Adsorption: Effect of Pressure and Competition with Human Serum Albumin. *To be submitted to a peer-reviewed journal.*

M. Buddhadasa performed the experiments, analysed the results and wrote the manuscript. Other authors contributed in supervising the research, discussing the results and revising the manuscript.

Chapter 2

Literature Review

2.1 Plasma surface engineering

An interaction of a material with its surrounding environment can be described as a chemical or physical process that takes place at its surface, which forms the interface between the bulk of the material and the surrounding. Many technologies of the modern world involve such surface interactions whose efficiency depends upon the surface properties. Hence, it is vital to understand the structure and behaviour of those surfaces of interest. In general, surface engineering is the process by which surface properties are modified, in order to get the desirable interactions with the surroundings. Out of the many surface engineering techniques available, plasma techniques are considered to be effective and versatile methods which are economical as well as ecologically friendly due to the low consumption of chemicals, considering the low flow rates used (< 100 standard cubic centimetres per minute, sccm, of precursor gas, in most cases) and absence of solvents.

2.1.1 Plasmas

Plasma is commonly referred to as the fourth fundamental state of matter, and it consists of charged particles formed by the ionisation of a gas in the presence of an electric field. There are several ways in which plasmas can be classified and one of the ways is shown in Figure 2.1. High-temperature plasmas are those where more than 90% of the gas is ionised and are being researched in only a few cases, for example in nuclear fusion power generation. In these plasmas, all species are in complete thermal equilibrium. Low-temperature plasmas

are associated with a much smaller degree of ionisation, $< 1\%$. In thermal plasmas, the electrons and other heavy plasma particles are in local thermal equilibrium, i.e. $T_e \sim T_g$ in each small volume of the plasma, and the temperature of the plasma is of the order of 10^3 - 10^4 K. These plasmas are usually excited at higher gas pressures (> 10 kPa).^{16,17} In non-thermal plasmas, the electrons and the plasma species are not in thermal equilibrium, i.e. $T_e \gg T_g$, where the electron temperature is in the order of 10^4 K and the heavy particles are at a temperature of around 300 K.^{16,17} These plasmas are generated under vacuum or atmospheric conditions, examples include low-pressure glow discharge and dielectric barrier discharge (DBD).

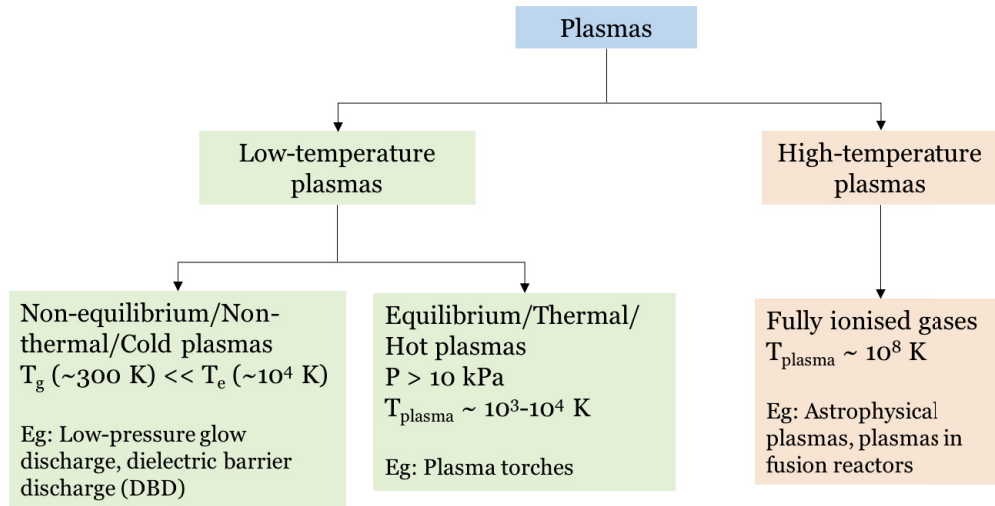


Figure 2.1: Classification of plasmas

Plasma processing technology is used in a wide variety of applications such as waste management, optics, biomedicine and automobiles, to name only a few. With regards to coating technology, both thermal and non-thermal plasmas can be utilised, depending on the type of deposition required and substrates used. In thermal plasma coating, the raw material can be metallic, ceramic or polymeric substances and can be introduced into the heat source in the form of a wire or powder, which is then melted or partially melted into finely divided

droplets to produce a coating on the substrate placed in front of the plasma jet.¹⁸ In non-thermal plasma coating, the plasma species generated from a polymerisable gas, itself, serves as the raw material for the coating deposited on the substrate. For biomedical applications, it is generally coatings produced from non-thermal plasmas that are commonly investigated to promote specific biological responses owing to their more reactive and controllable surface chemistry. Thus, the following sections and chapters will be focussed on non-thermal plasmas, unless otherwise specified.

2.1.2 Glow discharge and plasma polymer

When a certain sufficient voltage is applied across two electrodes in a chamber containing a gas, the bombardment with high energy electrons causes the ionisation of the gas creating ions, free radicals and neutral species. This transforms the gas into a plasma which then starts conducting electricity. The excitation of the gas causes it to glow and thus, it is given the name, *glow discharge*. A direct current (DC) or alternating current (AC) can be used to excite the gas molecules. When the gas is an organic molecule, then the material formed which is usually deposited as a thin film, is known as a *plasma polymer* and this process of deposition is broadly referred to as *plasma polymerisation*.

The main reactive species involved in plasma polymerisation are free radicals, that are created in the bulk of the plasma, which eventually undergo recombination with radical sites at the film, growing on the substrate. This growth mechanism is known as the Rapid Step-Growth Polymerisation (RSGP)¹⁹ and a schematic diagram of it is shown in Figure 2.2. The process gas travels through an active zone (bulk plasma) where radicals are created, and then enters a passive zone (plasma sheath and surface growth region), where recombination and deposition of stable products take place. Etching processes at the surface may also occur leading to ablation and re-deposition. Therefore, plasma polymerisation is a competition between deposition and ablation processes. Unlike in conventional polymerisation, since

plasma polymerisation is dominated by radical processes the resulting polymer is amorphous and more or less cross-linked, depending on the plasma species that participate in film growth. In the case of plasma modification or plasma treatment, gases such as Ar, N₂, O₂ and NH₃ are used to insert or substitute chemical functional groups on a substrate or to create radical sites for cross-linking or subsequent grafting. Deposition, substitution or ablation processes may dominate depending on the precursor gases used and the energy invested per particle.

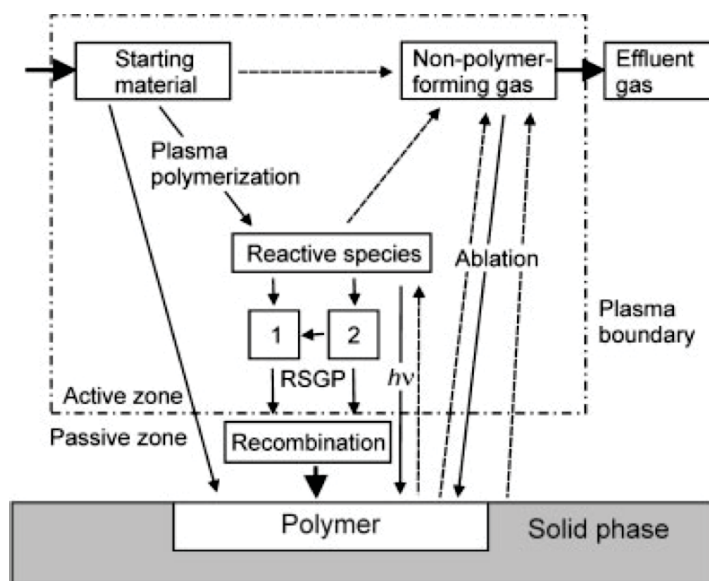


Figure 2.2: Schematic diagram of the Rapid Step-Growth Polymerisation (RSGP) mechanism, reproduced from ref.²⁰

2.1.3 General effects of plasma deposition parameters

The structure, composition, physical and chemical properties of the thin film and its deposition rate depend upon several plasma process parameters for a given gas or gas mixture. Usually the deposition rate depends on the discharge power, precursor flow rate and working gas pressure, assuming the type and size of reactor, frequency of the excitation voltage and substrate position are fixed. When the power is increased while flow rate and working pressure are maintained constant, the deposition rate also increases until all the monomer

supplied at the working pressure are completely consumed in deposition. Upon further increase in power, there will be no effect on the deposition rate. It will remain constant. The resulting deposition is a net effect of competing deposition and etching processes. Depending on the precursor gas used, for example oxygen, higher powers may cause etching to dominate leading to ablation or removal of the film.

A similar pattern is observed when the pressure is varied while the power and flow rate are kept constant. Some of the important effects of pressure include the energy invested per particle, given by the parameter W/p (power/pressure), the collision frequency, expansion/contraction of the plasma volume and the residence time. Pressure can affect the physical and chemical contributions to plasma polymerisation by greatly affecting the ion density. Generally, positive ions are accelerated in the plasma sheath and their bombardment with the substrate causes initiation or activation of the surface, which then lead to deposition or etching processes by forming chemical bonds with atoms or radicals that diffuse to and adsorb at the surface. The ions/neutrals ratio is significantly increased by reducing the pressure ($p < \sim 9$ Pa).²¹

When the flow rate is increased while the other two parameters are kept constant, the deposition rate also increases but if the flow rate is too high all the monomer will not be excited and even some which are excited will not be able to participate in the deposition due to being drawn away too quickly from the substrate. Therefore, there is a maximum flow rate the deposition can depend upon.^{22,23} The deposition rate also depends on the temperature of the substrate. It also affects the structure of the plasma polymer deposited. However, in non-thermal plasmas, as discussed in this thesis, the film forming species are at room temperature and under mild plasma powers (for example, 10 and 20 W), the temperature effects can be neglected. With a good understanding of the effects of changing the plasma deposition parameters the surface chemistry of the resulting polymer coating can be tuned satisfactorily.

2.2 Plasma surface functionalisation for influencing biomolecule immobilisation

It is well known that cell interactions with a surface are mediated via proteins. Consequently, study of protein adsorption to a biomaterial's surface can provide useful information for achieving specific cell responses. In this regard, surface chemical functional groups can significantly influence protein adsorption, where protein-surface interactions could be governed by not only Vanderwaals forces but also H-bonding, covalent bonding, dipole-dipole and electrostatic interactions. Studies have been done to show that by careful control of plasma conditions protein adsorption can either be favoured or significantly reduced (anti-fouling).^{24,25} The main chemically reactive groups involved in these interactions are considered to be amine, carboxy, hydroxy and aldehyde groups. However, it has been found that N-rich,^{2,5} mainly amine based, functional surfaces are more successful at promoting cell adhesion,^{8,12} owing to its positive charge, in aqueous media of physiologic pH, which attracts the negatively charged biomolecules, such as proteins.^{26,27} Hence, understanding the interactions of proteins with N-based surfaces is an important step.

A common approach of immobilisation is by forming interfacial amide bonds between the amine groups on the surface and carboxyl groups present on the molecules. Amine groups are normally introduced to surfaces either by plasma surface modification with ammonia or plasma polymerisation using amine based monomers or a gas mixture of a carbon source (eg. ethylene, acetylene, etc.) and N containing gas (eg. ammonia or nitrogen). Effects of plasma surface modification with a N-source gas are unsustainable due to the movement of polar groups in the treated chains into the polymer bulk, resulting in a loss of the treatment effects and return of part of the surface into its original untreated state.²⁸ This is known as ageing and is more pronounced in plasma surface modification. In this regard, plasma polymerisation is more widely used owing to its convenience in fabrication and resulting

surfaces being good platforms for covalent immobilisation of bioactive molecules such as proteins.⁵

2.2.1 Plasma surface modification

It has been reported that in plasma treatment of polymers (polyethylene²⁹ and polystyrene³⁰) in an RF glow discharge, with ammonia and hydrogen as the feed, short treatment times (in seconds), high discharge power and a high flow rate of hydrogen monomer resulted in a higher $-NH_2$ density.^{29,30} Meyer-Plath et al.³⁰ reported a maximum amino selectivity of 100% at very short NH_3 plasma treatments. This was considered to be due to amino groups being grafted faster than other nitrogen groups at the beginning, implying that ammonia promptly decomposes into $-NH_2$ or $-NH$ radicals for the creation of amino groups.³⁰ However, long treatment times (>5 minutes), low discharge power and a low flow rate of hydrogen give rise to high nitrogen contents rather than the amino selectivity. Amino selectivity is increased with the increase in hydrogen flow rate which is responsible for the reduction of other nitrogen functionalities to amino groups.²⁹ A decrease in density of grafted surface amino groups is attributed to total removal of the amino group rather than hydrogen abstraction, two processes ascribable to positive ion bombardment.

2.2.2 Plasma polymerisation

An alternative method to obtain amino functionalised surfaces is plasma polymerisation. It is a versatile and flexible method that can be used to introduce functionalities onto surfaces of different materials with different three dimensional shapes. Two approaches to produce functional plasma polymer films involve (i) use of a single, polymerizable monomer containing the functional groups and, (ii) use of a mixture of precursors, i.e. a source of nitrogen functional groups (for example, NH_3) and a source of carbon (that can produce

the polymer backbone). The second method has more flexibility in varying the ratio of the functional group to carbon containing precursors which affects the plasma film composition significantly.³¹ However, in the first method, the functional group can be more easily incorporated into the film since it is already a part of the hydrocarbon species and many have used this method to deposit N-rich films using various amino based monomers, such as allylamine,^{32,33} propargylamine,³² propylamine,³² diaminocyclohexane (DACH),³⁴ 1,3-diaminopropane,³⁵ ethylenediamine,³⁶ heptylamine³⁷ and butylamine.³³

In the first method of plasma polymerisation, the density of amine groups on the film may vary with the type of monomer as well as the plasma conditions that is used in the process. For instance, for allylamine plasma polymer films, increased discharge powers increased the number of carbon to nitrogen unsaturated bonds and for propylamine a large concentration of imine groups resulted at decreased powers. It was found that in both these plasma polymers the formation mechanism was dominated by dehydrogenation.⁶ It was observed that out of DACH, allylamine and heptylamine, the highest degree of amine groups were obtained with DACH and the lowest was in heptylamine polymers.^{37,38} This is due to the presence of two amino groups in a DACH molecule which increases the chance of amine functionalities introduced into the polymer film.³⁸ The presence of the double bond in allylamine gives rise to increased deposition rates by plasma polymerisation as well as addition polymerisation. Higher the degree of unsaturation, higher is the rate of deposition.

As explained earlier, one of the plasma parameters that influence the chemical structure of plasma polymers is the effect of discharge power. With an initial increase in discharge power, the deposition rate of the monomer also increases, until all the monomer is completely consumed at the given working pressure and gas flow rate. However, as the discharge power is increased further, the deposition rate becomes constant as it is competed by the rate of ablation. As the discharge power is continued to increase, the deposition may decrease as ablation rate begins to dominate.²² These three regions can be defined as 'monomer

sufficient', 'competition' and 'monomer deficient' regions. In the monomer sufficient region, increase in discharge power causes fragmentation of monomers which manifests as an increase in the pressure. In the monomer deficient region, there is enough power for fragmentation but due to the lack of monomers and increased etching processes with increase in energy per particle, deposition rate is decreased. It has been shown experimentally that deposition of amino groups is favoured in the power deficient (monomer sufficient) region where there is less fragmentation of monomers in the plasma.³⁸ Hence, most work that is focussed on producing chemically reactive coatings for interfacial immobilisation, is done at low discharge powers to avoid high fragmentation, in order to obtain a larger surface density of amine functionalities.

The second approach of plasma polymerisation utilising a source of carbon and a source of nitrogen, has also been widely used to produce amine based polymers with high degree of functionality.^{8,31,39,40} Truica-Marasescu et al.³¹ have compared the physico-chemical properties of N rich plasma polymerised ethylene (PPE:N) films obtained in a conventional low pressure RF glow discharge (L-PPE:N) and a DBD reactor operating at atmospheric pressure (H-PPE:N). They state that the importance of such a comparison lies on the insight that it gives in the applicability of these coatings. It is mentioned that while H-PPE:N can be deposited onto thin polymeric substrates, it cannot be deposited on three dimensional medical devices such as stent grafts. However, this is claimed to be possible with L-PPE:N, although it accounts for greater costs.³¹ It was observed that the deposition rates of both L-PPE:N and H-PPE:N decreased with increase in the gas ratio ($\text{NH}_3/\text{C}_2\text{H}_4$ and $\text{N}_2/\text{C}_2\text{H}_4$ respectively). The reason for this observation, in the case of L-PPE:N was attributed to chemical sputtering by ammonia (which acts as an etchant for organic materials) at high concentrations. In the case of H-PPE:N, gas phase reactions between various hydrocarbon and nitrogen species are believed to be favoured by atmospheric pressure, which resulted in stable gaseous compounds that are pumped out of the reactor, thereby lowering the deposition rate. However, these deposition rates for the low and high pressure films were observed to be in the range of different orders of magnitude (1 and 2 respectively). This

observation was attributed to the increased collision frequencies and reaction probabilities under high pressure and discharge power plasma conditions.³¹ This is shown in Figure 2.3. Surface analysis (using NEXAFS and chemical derivatization reactions) of PPE:N materials with similar surface nitrogen concentrations indicated that L-PPE:N materials contain a higher concentration of primary amines. In addition, both L- and H-PPE:N coatings were found to contain many functionalities, such as amines, imines, nitriles, unsaturated carbon-carbon or carbon-nitrogen bonds as well as amides, formed due to oxidation of amines in ambient air.³¹

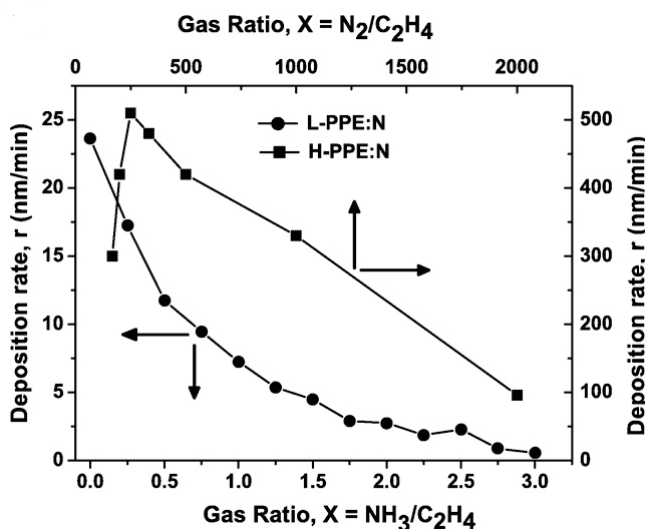


Figure 2.3: Deposition rates as functions of gas mixture ratios, $X = NH_3/C_2H_4$ for L-PPE:N and $X = N_2/C_2H_4$ for H-PPE:N (reproduced from ref.³¹)

2.3 Stability of plasma polymer coatings

In order to make use of these plasma polymerised coatings in specific applications, especially in the biomedical field, it is important to ascertain that these coatings do not eventually undergo any undesirable structural changes in aqueous media. In other words, these coatings must be stable and insoluble in water to be incorporated in a human body. For stability,

surfaces are expected to be intrinsically less energetically favourable than the bulk of the material. Higher surface energies and smaller contact angles indicate a hydrophilic surface. Generally, presence of polar groups on a polymer surface gives rise to an increase in its surface energy, γ_s , which is a measure of surface wettability of the polymer by aqueous media.^{3,4,8} It has been reported that when high amine surface concentrations are obtained by using mild plasma conditions of low discharge power and low duty cycle, then those plasma polymers may dissolve in water and other polar solvents, such as ethanol.^{26,27,41} This can be attributed to the high surface energies, resulting in a strong attraction towards polar solvents and also to reduced polymerisation and cross-linking owing to deposition under mild plasma conditions.

Truica-Marasescu et al.³¹ have tested the water solubility of L- and H-PPE:N coatings in terms of their reduction in thickness. All H-PPE:N films showed no change in thickness and hence found to be insoluble in water. On the other hand, L-PPE:N films were insoluble upto $X = 1.5$, beyond which they became partially soluble and above gas mixture ratio of 1.6, they completely dissolved in water. This can be due to the presence of high amine concentrations in L-PPE:N compared to that in H-PPE:N coatings. Figure 2.4 shows the variation of surface energy and its components with surface nitrogen concentrations for both L- and H-PPE:N films.³¹ There is a marked increase in γ_s with nitrogen concentration for both L- and H-PPE:N materials. It can be seen that the dispersive component, γ_s^d , remains almost constant in both plots, thus showing that the increase in the surface energy is due to the increase in its polar component. Another important observation is that higher surface energies were obtained for L-PPE:N than the other, under similar nitrogen concentrations.³¹ This is attributed to the presence of high primary amine concentrations in L-PPE:N films which gives rise to increased polar interactions.

Hydrophobic recovery (also known as *ageing*) is another undesirable phenomenon which plasma polymers undergo when exposed to air, in order to reduce the surface energy and its corresponding hydrophilicity or wettability. This reduction in surface energy could oc-

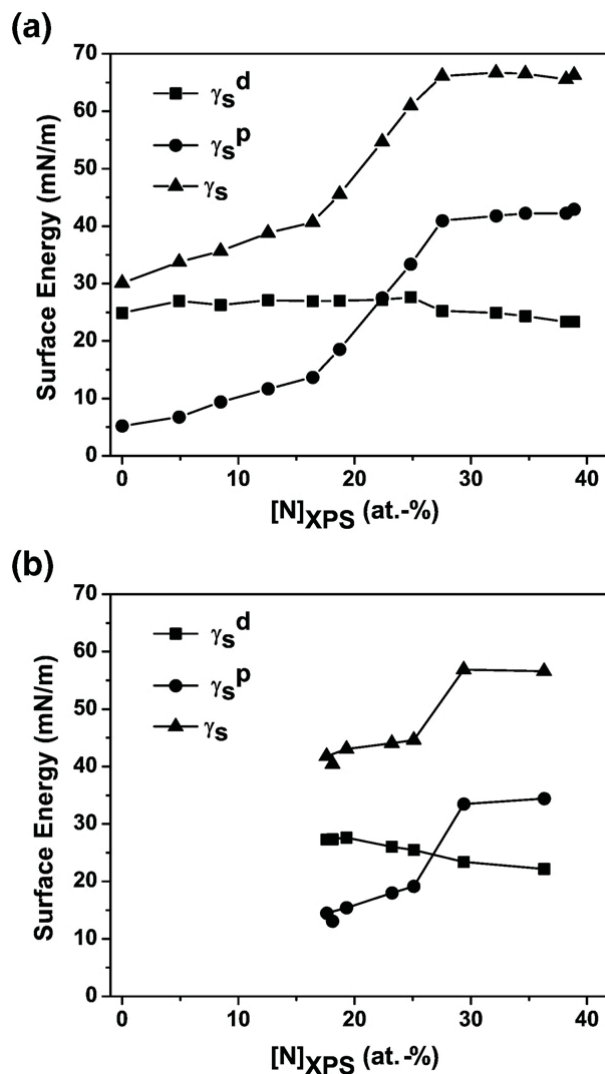


Figure 2.4: Surface energy, γ_s , and its dispersive γ_s^d and polar γ_s^p components, as functions of the nitrogen concentrations, of a) L-PPE:N and b) H-PPE:N films (reproduced from ref.³¹)

cur by oxidation of dangling bonds or unstable functional groups, reptation of low-weight oligomers out of the surface thin layer or by reorientation of near-surface chains so as to enclose the newly formed polar components.^{11,42} In contrast with plasma modified surfaces, plasma polymerised films exhibit less reptational movement and reorientation effects,⁴³ due to its highly cross linked nature and near-uniform composition across the film. Nevertheless, it has been reported that nitrogen based plasma polymerised films do undergo the same characteristics of ageing within the first two weeks of storage in air.^{35,36,44}

Based on the work done by Truica-Marasescu *et al.*,³¹ it is shown that higher the concentration of amine groups, higher is the solubility of the coating in water. This was clear by the solubility of L-PPE:N that contained a higher amine concentration, in contrast with the insolubility of the low amine containing H-PPE:N films. Therefore, this indicates that a compromise between the amine concentrations and water solubility of the coatings has to be met.

Recent work published by Dorst *et al.*⁴⁵ demonstrated that water stability of amine-containing films can be enhanced by using a vertical chemical gradient. Coatings were deposited in a low-pressure plasma using ammonia and ethylene as precursors. The chemical gradient was achieved by first depositing a more cross-linked film (using high power and low $\text{NH}_3/\text{C}_2\text{H}_4$ flow ratio), followed by a layer of less cross-linked yet more functional coating (using low power and high gas flow ratio). It was found that the coating with the gradient structure was completely stable in water up to 1 week compared to its gradient-less counterpart. The initial value of $[\text{NH}_2]/[\text{C}]$ on the surface of both types of coatings was 2 %.

2.4 Biomaterials in contact with blood

Use of synthetic materials to replace and/or support injured or diseased tissues, continues to be an accepted approach in the biomedical field mainly since non-biological materials, unlike donor tissues and organs, are not attacked by the immune system. This is due to the absence of immunologically recognizable biological features on synthetic materials. However, these materials are certainly subjected to other responses such as blood clotting and foreign-body reaction. Such responses are based on the adsorption of adhesion proteins onto the biomaterial which then interact with surrounding cells via integrin receptors present on most cells. Therefore, adhesion proteins mediate the cell responses towards a biomaterial. There are over 700 or more proteins in blood and when a biomaterial comes in contact with blood,

the proteins move on to the surface of the biomaterial via diffusion (sometimes convection) in the order of molecular weight (smaller proteins arrive before the larger ones).¹ Upon arrival at the surface, proteins may undergo various processes: they may adsorb and interact with other proteins increasing or decreasing their biological activity and may also be replaced by later arriving higher affinity proteins, a process called the Vroman effect, discussed later in section 2.4.2.

Adsorption of various clotting factors or proteins, such as Fg and von Willebrand factor (vWF), onto a foreign surface in contact with blood would trigger the blood coagulation cascade,¹ as demonstrated in Figure 2.5. This surface contact activation is called the intrinsic pathway. Clotting can also be initiated extrinsically by the action of tissue factors. Both lead to the activation of a factor X which eventually results in the formation of thrombin and a stable polymer gel called fibrin. Process of coagulation involves a series of steps where the enzymatic activation of one clotting factor leads to the enzymatic activation of another. This cascade of reactions occur quickly leading to a significant production of thrombin, fibrin formation and eventually coagulation. The clotting process is restricted only to the surface by several control mechanisms which include dilution of activated clotting factors by blood flow, presence of inhibitors of coagulation enzymes in blood plasma and so on.¹

2.4.1 Platelet adhesion, activation and Fg adsorption

As described in the previous section, clotting or coagulation is triggered by the adsorption of various clotting proteins. Platelets are blood cells that also play a vital role in blood clotting but are not necessary to cause this process. They are extremely sensitive cells that can be activated easily by a large variety of physiologic stimuli. Collagen in connective tissue, enzymes such as thrombin and trypsin, and low molecular weight compounds such as adenosine diphosphate (ADP) when present in the extracellular environment are examples of common stimuli.⁴⁶ Unactivated platelets are disk-shaped and upon activation, they become

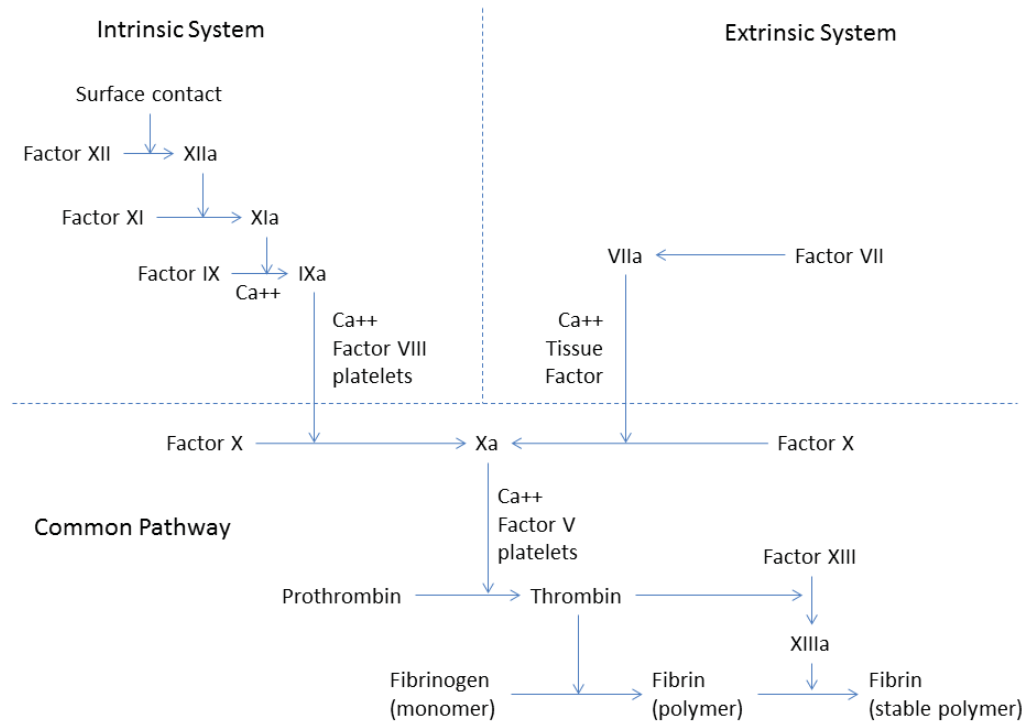


Figure 2.5: Interaction of clotting factors through a series of enzymatic activation steps leading to the production of thrombin which acts on fibrinogen, converting it into a fibrin polymer which then stabilises to form a thrombus or clot. Thrombin also acts on Factor XI as a feedback mechanism, leading to an increased production of thrombin (a redrawn version of a figure from ref.¹).

sticky and irregularly shaped with spiny pseudopods. Platelets undergo adhesion through their membrane bound receptors such as the glycoproteins (GP Ib,IIb and IIIb). Adhesion to artificial surfaces is achieved through GP IIb/IIIa and sometimes through GP Ib-vWF interaction. GP IIb/IIIa binds to surface adsorbed proteins such as Fg, vWF, fibronectin and vitronectin on activation, which leads to conformational changes in the glycoproteins. Normal unactivated platelets also adhere to surface adsorbed proteins, owing to the conformational changes that occur in those proteins upon adsorption, which makes unactivated platelet receptors to react and bind with them.¹ Such platelet adhesion, in turn, may also act as a stimuli for their activation and subsequent events leading to platelet aggregation and the formation of a fused platelet plug or thrombus (Figure 2.6).

Fg is a strong adhesion protein for platelets, yet the relationship between the amount

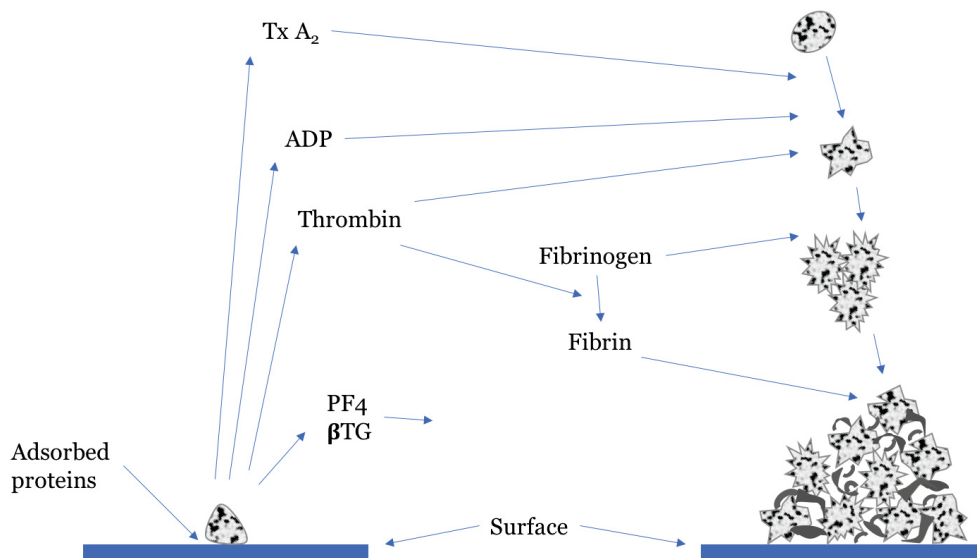


Figure 2.6: Platelet response to artificial surfaces. Protein adsorption to the surface facilitates platelet adhesion, which then become activated releasing storage granule contents such as ADP, platelet factor 4 (PF4) and β -thromboglobulin (β -TG), synthesising thromboxane A₂ (Tx A₂) and generating thrombin. This promotes the stimulation of other platelets, platelet aggregation and stabilisation of the platelet mass by thrombin-generated fibrin (a redrawn version of a figure from ref.¹).

of Fg adsorbed and the amount of platelets adhered is not necessarily proportional. For example, Tsai et al.⁴⁷ studied Fg adsorption from plasma diluted at different concentrations on to polystyrene and found an increase in Fg adsorption with increase in Fg concentration in the bulk plasma (Figure 2.7a). Nevertheless, platelet adhesion did not follow the same trend as seen in Figure 2.7b, where the number of platelets adhered increases to a maximum and then decreases with the decrease in plasma dilution, which corresponds to higher concentrations of Fg. Conformational changes in adsorbed Fg were also observed when different plasma concentrations were used. In another study,⁴⁸ platelet adhesion from a washed platelet suspension containing albumin, to plasma polymerised allylamine films were investigated. Platelet adhesion to surfaces preadsorbed with Fg-deficient plasmas was diminished, compared with normal plasmas. On the other hand, platelet adhesion to surfaces preadsorbed with vWF-deficient plasmas was comparable to that observed with normal plasma, suggesting that adsorbed Fg plays an important role in platelet adhesion.

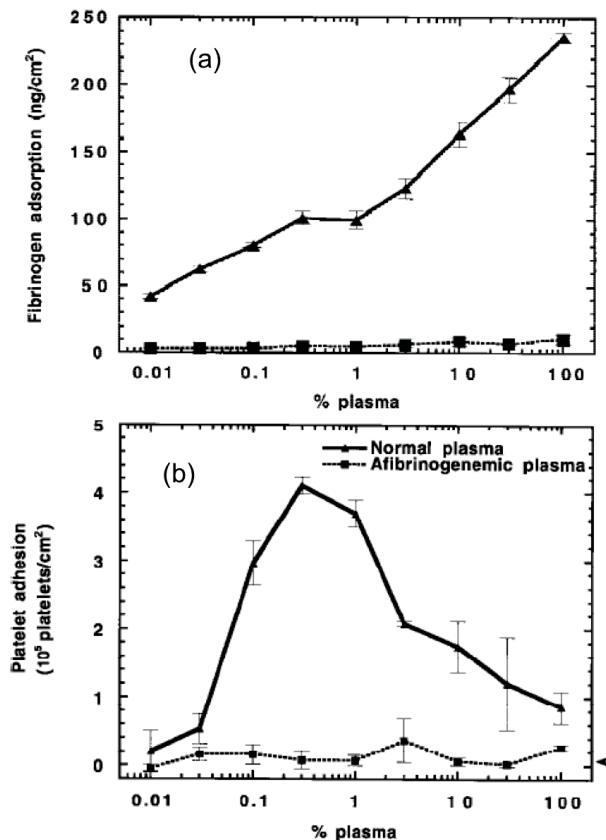


Figure 2.7: (a) Fg adsorption to polystyrene from normal (triangles) and afibrinogenemic (squares) plasma at different dilutions. (b) Platelet adhesion to polystyrene preadsorbed with different dilutions of normal (solid line) or afibrinogenemic (dotted line) plasma (reproduced from ref.⁴⁷).

2.4.2 Competitive protein adsorption

Proteins are composed of amino acids and the unique combination of amino acids define their properties and functions. The charge distribution and location of hydrophilic/hydrophobic groups on the protein can largely contribute to their affinity of adsorption to different surfaces. In a mixture of several proteins, interactions between different proteins, depending on factors such as concentration, size and structure, will affect their individual adsorption. Figure 2.8 gives general information on the structure,^{49–51} molecular weight^{1,51} and concentration^{1,52,53} of the three most abundant proteins found in blood plasma. Properties of the surface such as chemistry, energy, charge and topography may influence the adsorption from a protein mixture. As an example of the effect of surface chemistry, Figure 2.9 shows ad-

sorption of a radiolabeled protein (eg: ^{125}I -fibrinogen) from blood plasma, on to a series of polymers and copolymers of 2-hydroxyethyl methacrylate (HEMA) and ethyl methacrylate (EMA). The series ranged from hydrophilic HEMA to hydrophobic EMA. Adsorption of ^{125}I labeled proteins namely, Fg, albumin, immunoglobulin (IgG) and hemoglobin were measured individually on each surface and it is evident that each protein adsorbed differently depending on the surface chemistry of the material.

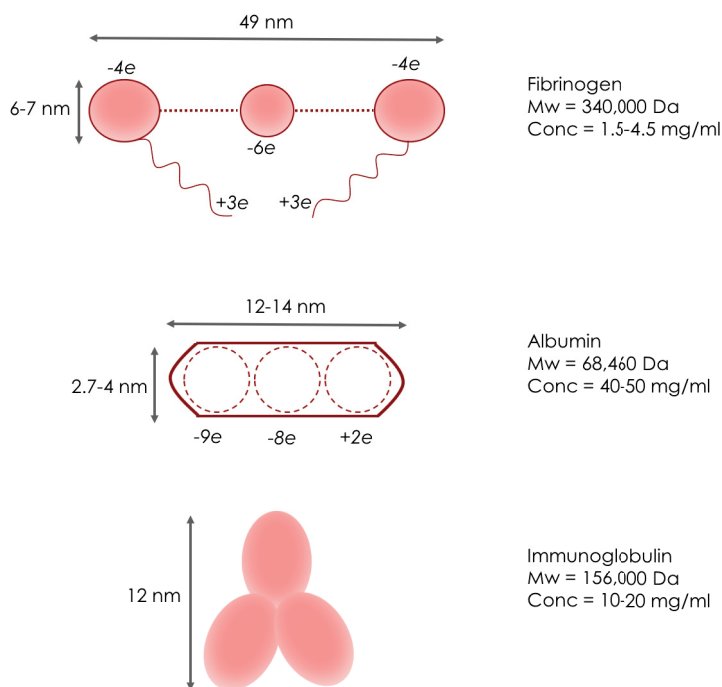


Figure 2.8: Schematic of the structure, molecular weight and concentration in blood plasma of Fg, albumin and IgG. Surface charges on Fg and albumin shown are in pH 7.4.

Competitive protein adsorption also depend upon the affinity of each protein. For example, hemoglobin is a high affinity protein and therefore despite its very low concentrations in plasma (0.01 mg/ml), it is adsorbed in amounts similar to those of other proteins with higher plasma concentrations. Similarly, Fg is also a high affinity protein and therefore, it adsorbs better than albumin and IgG, which are the two most concentrated proteins in blood plasma.^{1,34}

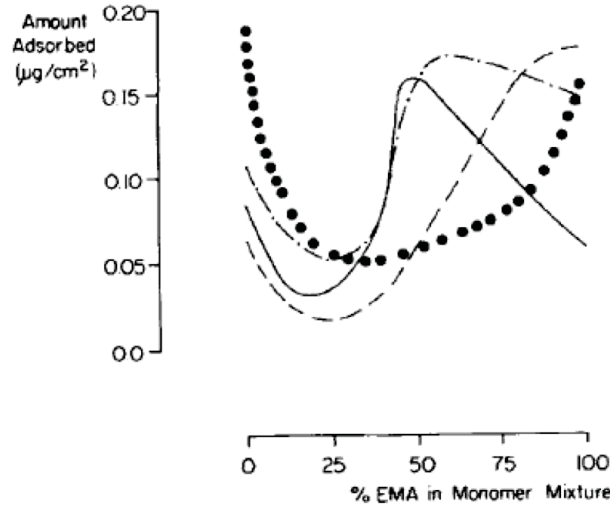


Figure 2.9: Surface chemistry dependency of selective protein adsorption from plasma to a series of hydrophilic-hydrophobic (HEMA-EMA) copolymers. Fg (solid line), IgG (— —), albumin (●) and hemoglobin (— · —) (reproduced from ref.⁵⁴).

Vroman effect. Vroman effect is the well-known process of displacement of adsorbed proteins that have higher mobility and therefore arrives first at the surface, by less mobile proteins that have a higher affinity for adsorption. This is typical for Fg where adsorption from blood plasma shows different amounts of Fg in the adsorbed layer at steady-state and transient conditions. It appears that the initially adsorbed Fg is replaced by later arriving, high affinity proteins, especially high molecular weight kininogen and with adsorption time, transitions in Fg makes it less displaceable.⁵⁵

2.4.3 Changes in conformation and biological properties in adsorbed proteins

Upon adsorption, proteins can undergo conformational or structural changes and exhibit "molecular spreading" or unfolding to form further bonds with the surface. This may affect the protein's biological activity, sometimes leading to denaturation. Proteins that have a higher tendency to undergo such changes are called "soft" proteins (eg: albumin, IgG) and those that are more stable are called "hard" proteins (eg: lysozyme).⁵⁶ Study of molecular

properties of proteins on their affinity for adsorption suggests that less structurally stable proteins are more adsorptive.⁵⁷ In the case of Fg, changes in conformation and/or orientation of the adsorbed protein can be detected by monoclonal antibody binding, which binds with only surface adsorbed Fg and not solution-phase Fg; solution-phase Fg does not compete with the adsorbed protein for binding of the antibody. Adsorbed Fg can be in different conformations on different surfaces despite adsorption in similar amounts, such as in a study of various polymethacrylates, where platelet adhesion to the different polymethacrylates was shown to correlate with antifibrinogen binding, suggesting that affinity of adsorbed Fg to bind platelets depended on the conformation of the adsorbed protein.⁵⁶

Chapter 3

Experimental Methods

This chapter is intended to provide additional information on the experimental methodology and characterisation techniques used, but are not fully explained, in the manuscripts presented in Chapters 4 to 6. Care has been taken to avoid repetition as much as possible, however, some repetition is unavoidable.

3.1 Plasma generation

Cold plasmas are usually excited by applying a DC or an AC, usually at RF or microwave frequency, to a gas.¹⁷ DC discharges are often used in the synthesis of metallic coatings via physical vapour deposition.⁵⁸ In this work, an RF discharge is used, which is the commonly implemented method for plasma polymerisation. Therefore, it is described here in detail.

3.1.1 RF discharges

To excite and sustain a DC discharge the conducting electrodes need to be placed within the reactor in contact with the plasma.¹⁷ If the plasma is of organic nature, a dielectric film will be formed (via plasma polymerisation) on the reactor walls as well as the electrodes. Thus, if a DC discharge is used, soon, the plasma will be extinguished due to recombination of electrons with available ions at the dielectric film covering the electrode. This can be avoided by alternating the polarity of the discharge. In order to sustain the AC discharge, the frequency of the alternating electric field must be high enough such that the time taken by the positive ions to move between electrodes becomes larger than half the period of the

electric field.¹⁷ Thus, frequencies used to obtain such discharges are usually in the range of radio waves and it is fixed at 13.56 MHz to avoid interference with broadcast frequencies.

The RF power generator is connected to the plasma reactor via a matching network, to make sure that the impedance of the power supply, usually 50Ω , is almost identical to that of the plasma and thereby, minimise the reflected power to the RF power generator.

RF discharges are usually generated in two ways, (i) by applying a RF voltage across two parallel plate electrodes (known as capacitively coupled plasmas, CCP) or (ii) by circulating a RF current through a coil (known as inductively coupled plasmas, ICP), placed within the plasma or placed externally to it separated by a dielectric window. A schematic of the two types of reactors is shown in Figure 3.1.

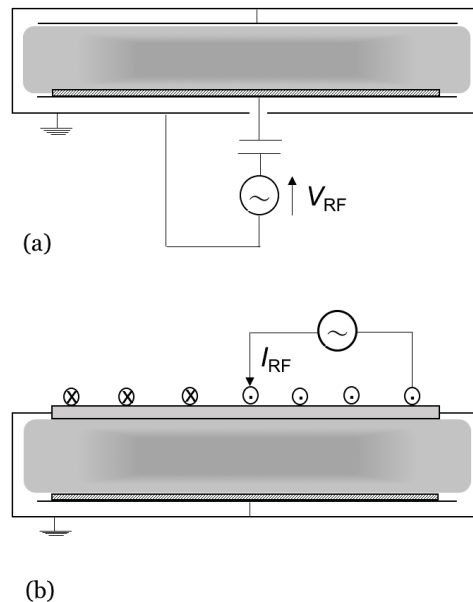


Figure 3.1: Schematic of (a) CCP and (b) ICP reactor (redrawn version from ref.⁵⁹).

Capactively coupled plasmas. A CCP design consists of two parallel electrodes, placed in contact with the plasma and separated by a distance of a few centimeters. The substrate is usually placed on the powered electrode. The plasma density in a CCP is approximately

$10^{15} - 10^{16} \text{ m}^{-3}$.⁵⁹

Inductively coupled plasmas. The RF current circulating in the coil induces a RF magnetic field in the axial direction of the coil. This, in turn, induces a RF electric field in the gas, as given by Faraday's Law,

$$\varepsilon = \frac{d\Phi_B}{dt}, \quad (3.1)$$

where $d\Phi_B/dt$ is the rate of change of the magnetic flux Φ_B induced by the RF current in the coil and ε is the resulting RF electromotive force (emf) which accelerates the free electrons in the discharge and sustains the plasma.

These two types of reactor designs are associated with two regimes, (i) E (electrostatic) mode for capacitive coupling and (ii) H (electromagnetic) mode for inductive coupling. The ICP systems usually start in the E mode and with an increase in power supplied, when the plasma density reaches a critical value ($10^{16} - 10^{18} \text{ m}^{-3}$), the discharge begins to operate in the H mode.⁵⁹

3.1.2 Experimental setup for film deposition

In this work, both CCP and ICP reactors have been used. The experimental setup for the CCP reactor is presented under the experimental section of Chapter 5, a manuscript titled, *Plasma Co-polymerisation of Ethylene, 1,3-Butadiene and Ammonia Mixtures: Amine Content and Water Stability*. Therefore, only the experimental setup of the ICP reactor, which is not described in detail, but used in the manuscript of Chapter 4, *Single Source Precursor vs Precursor Mixture for N-rich Plasma Polymer Deposition: Plasma Diagnostics and Thin Film Analyses*, is described here.

The ICP reactor, consisting of a cylindrical stainless steel vacuum chamber, 35.5 cm in diameter and 86.5 cm in length is shown in Figure 3.2. It is equipped with a turbomolecular pump, backed by a rotary pump allowing a residual pressure of 8×10^{-4} Pa to be reached before introducing the precursor gases. The water-cooled copper coil (4.5 cm internal diameter and 0.7 cm thickness) is connected to the RF generator and the distance between the coil and substrate holder is set at 10 cm. The chamber is connected to a mass spectrometer and an in situ fourier transform infra-red (FTIR) spectrometer to enable plasma diagnostics.

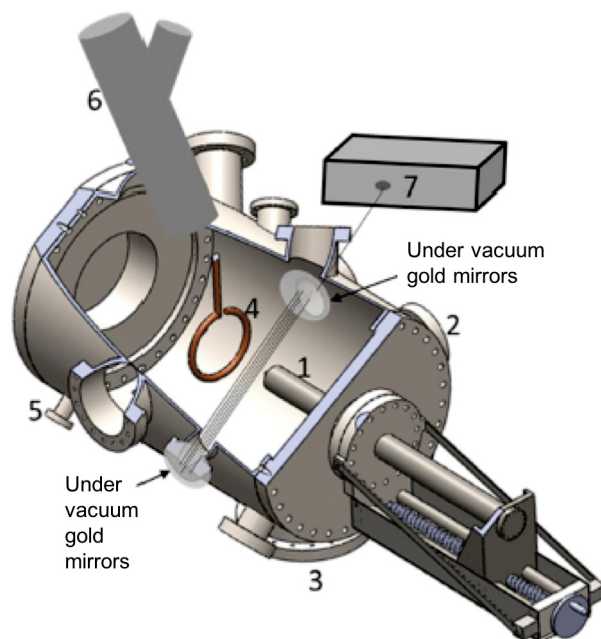


Figure 3.2: Schematic of the ICP experimental setup. 1-Substrate holder, 2-load-lock system, 3-pumping system, 4-water-cooled copper coil, 5-precursor inlet, 6-mass spectrometer and 7-in situ FTIR spectrometer (reproduced from ref.⁶⁰).

3.2 Characterisation techniques

3.2.1 Mass spectrometry

Mass spectrometry (MS) is used to analyse the plasma phase composition. It is a highly sensitive tool which can detect both ionic and neutral species. The general working principle of MS involves ionisation of a vapour from a solid, liquid or gaseous sample, and separating the charged particles (molecules, molecular fragments, atoms) according to their mass to charge (m/z) ratio, where mass is expressed in atomic mass units (a.m.u.) and the charge in elementary charge units (e).

The instrument consists of 3 main parts (i) an ionisation source, (ii) a mass analyser and (iii) a detector. The spectrometer used in this work is operated in the residual gas analysis (RGA) mode, where neutral species from the sample are ionised by electron ionisation (EI), as shown below.



The molecular ion ($M^{\bullet+}$) formed from Equation 3.2 is a radical cation with an odd number of electrons and therefore, would normally undergo fragmentation into a radical (R) and an even ion (EE) with an even number of electrons or a molecule (N) and an odd ion (OE), as shown by equations 3.3 and 3.4. Each primary product ion produced from the molecular ion can undergo further fragmentations and so on.⁶¹



or,



The ions generated are then separated using a quadrupole mass analyzer, where separation occurs based on the stability of the ion trajectories in the oscillating electric fields applied to two pairs of parallel metal rods.⁶¹

MS is widely used in plasma diagnostics to detect specific phenomena.⁶²⁻⁶⁴ For example, MS was used to demonstrate that the cyclic amine-based precursor, cyclopropylamine, was less fragmented than its linear counterpart, allylamine, below a critical mean power.⁶³ Despite its many benefits, an important limitation of MS when operating in RGA mode is that neutral species when subjected to ionisation can undergo extensive fragmentation even at low electron kinetic energies. Therefore, MS should be used in conjunction with other diagnostic tools such as FTIR and care must be taken when correcting the spectra.

In order to distinguish the contribution of fragmentation that occurs in the ionisation source from that which occurs in the plasma, the mass spectra obtained are corrected according to a method described in detail in Chapter 4.

3.2.2 Fourier transform infrared spectroscopy

FTIR spectroscopy is a useful technique to extract structural information of molecules present in a solid, liquid or gaseous sample. When a sample is irradiated with an infrared beam, vibrating molecules in the sample will absorb energy from the beam and excite to a higher vibrational level. The transmitted or absorbed light is measured by a detector as a function of the wavenumber. This method is effective only towards IR active molecules, i.e. the vibration of the molecule must yield a change in the dipole moment.

The working principle of an FTIR can be found well-explained in detail in ref.⁶⁵ It is based

on an interferometer or interference meter, which measures the interference pattern of two light beams. The most common type of interferometer used is a Michelson interferometer, as shown in Figure 3.3. An infrared light beam is passed through a beamsplitter after reflecting from a collimating mirror, which is used to make the light rays parallel. As the name suggests, the beamsplitter splits the beam into two which are made to reflect normally from two mirrors. One of the mirrors is fixed and the other is allowed to move in the direction shown in Figure 3.3. The difference in the distance of the two mirrors from the beamsplitter is called the optical path difference, δ . As the two beams travel back to the beamsplitter, they superpose to form an interference pattern whose intensity is measured by the detector as a function of δ , to produce an interferogram, i.e. a plot of intensity (arbitrary units, a.u.) vs δ (cm). This interferogram is then Fourier transformed to give an IR spectrum, which is a plot of intensity (a.u.) vs wavenumber (cm^{-1}).

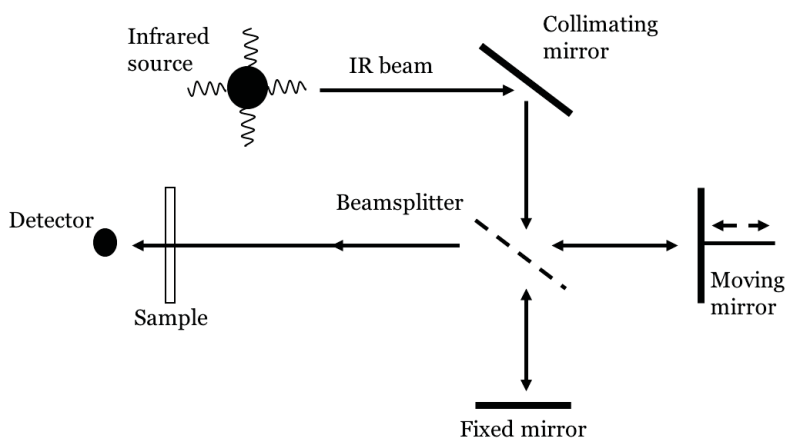


Figure 3.3: Optical diagram of a Michelson interferometer (redrawn version from ref.⁶⁵).

FTIR spectra can be plotted either in absorbance units or percent transmittance ($\%T$). Absorbance is calculated using the following equation.

$$A = \log\left(\frac{I_0}{I}\right), \quad (3.5)$$

where A is the absorbance, I_0 is the intensity of the background spectrum and I is the intensity of the sample spectrum. Absorbance is related to concentration by Beer's law,

$$A = \varepsilon lc, \quad (3.6)$$

where ε is absorptivity, l is the pathlength and c is the concentration. The height or area of a peak in the absorbance spectrum is proportional to the concentration of the corresponding molecules in the sample which can be calculated by Beer's law.

The FTIR spectrum could also be plotted in percent transmittance units on the y axis, according to the following equation.

$$\%T = 100 \times \frac{I}{I_0} \quad (3.7)$$

FTIR is useful in quantitative and qualitative analysis of the plasma phase as well as plasma polymer films where monomer dissociation, new species formation and powder formation can be detected.²² It appears to be a promising tool especially in plasma diagnostics owing to its non-intrusiveness (unlike MS) allowing for an in situ picture of the plasma-phase chemistry and the rapidity of measurement allowing for spectral acquisitions with high signal-to-noise ratios.

This technique is primarily used in Chapter 4 of this thesis, where the spectra of the plasma phase have been obtained with a resolution of 1 cm^{-1} and averaged over 50 scans and spectra of the coatings are obtained with a resolution of 4 cm^{-1} and averaged over 32 scans.

3.2.3 Optical emission spectroscopy

Optical emission spectroscopy (OES) is a popular tool used in plasma diagnostics. It is a relatively inexpensive and non-invasive technique where the experiments can be performed easily and in real-time. The setup is simple and placed external to the plasma reactor and vacuum system. It consists of an optical fibre, for light acquisition, connected to a portable spectrometer which is in turn connected to and manipulated via a computer (Figure 3.4).

The principle of OES is based on detecting the light emitted from excited species in the plasma during relaxation to the ground state or another excited state with a lower energy. By analysing the wavelengths and intensities of these emitted light rays, it is possible to identify neutral and ionic species present in the plasma and give information on physical and chemical processes occurring in the discharge. A limitation of the OES technique is that it is limited to only light-emitting species and the emission intensities are not always proportional to the concentration of the species in the plasma. It is more useful in detecting atomic and diatomic species, which give simpler and narrower spectra, rather than polyatomic species that give broader spectra or give only weak emission lines in the spectral range used by OES, which is usually 200-900 nm.¹⁷

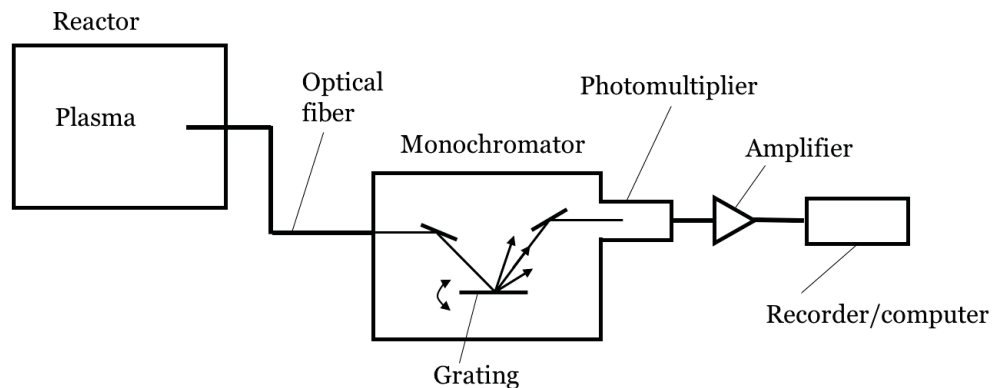


Figure 3.4: OES setup used in plasma diagnostics (redrawn version from ref.¹⁷).

3.2.4 X-ray photoelectron spectroscopy

X-ray photoelectron spectroscopy (XPS) is a highly sensitive and non-destructive technique used to determine the elemental composition and different chemical states of the detected elements in a solid sample, upto a probing depth of ~ 10 nm from the surface.

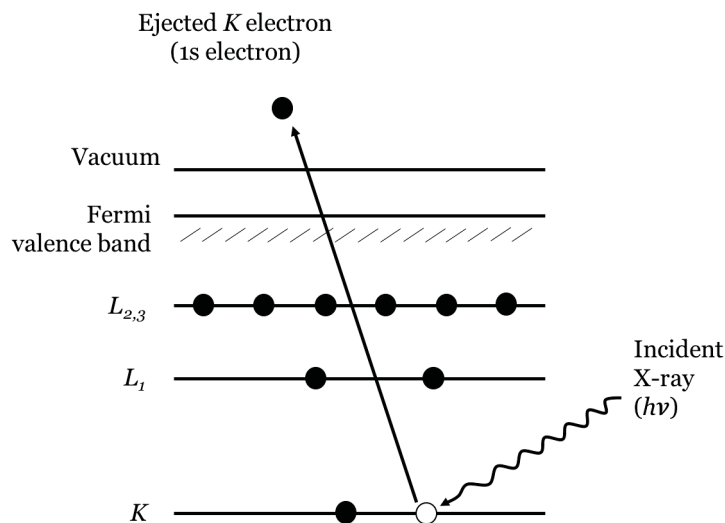


Figure 3.5: Schematic of a photoelectron emission from the 1s orbital of an atom (redrawn version from ref.⁶⁶).

The principle of XPS involves the ejection of a core level electron from an atom using an X-ray photon of energy $h\nu$. The kinetic energy of the emitted electron is then measured by an electron spectrometer and is presented as a plot of intensity (counts) vs electron energy (eV). The kinetic energy of the photoelectron depends on the energy of the X-ray photon. Using the following equation, the binding energy of the emitted electron can be calculated and thus, its parent element and atomic energy level can be identified.⁶⁶

$$E_B = h\nu - E_k - W , \quad (3.8)$$

where E_B is the binding energy of the electron, $h\nu$ is the energy of the X-ray photon, E_k

is the kinetic energy of the electron and W is the work function of the spectrometer. Once the electrons are ejected from the sample, they are made to pass through an electron energy analyser, usually operating in the constant analyser energy mode, where the electrons are made to accelerate or decelerate to a user defined energy (called the "pass energy") before reaching the detector. The level to which the electrons are accelerated or decelerated is decided such that only electrons with a particular initial kinetic energy are able to reach the detector.⁶⁶ Information on the chemical environment of the element can also be obtained by analysing any shifts observed in the binding energy of the electron, which is affected by the surrounding atoms.

3.2.5 Chemical derivatisation with 4-trifluoromethyl benzaldehyde

N functional groups such as primary amines and imines present in N-based films, under aqueous environments, play an important role in promoting biomolecule immobilisation. This is due to the electrostatic attraction between the positive charge induced on these N functional groups and the net negatively charged biomolecules. Thus, quantification of these functional groups is important when tuning the surface properties of N based films.

Chemical derivatisation with 4-trifluoromethyl benzaldehyde (TFBA) followed by XPS has been used to determine the concentration of primary amines and imines, which are the main N functional groups in N based plasma polymer films that can form stable fluorine containing products upon reaction with TFBA. Initially, it was assumed that TFBA was only selective towards primary amines (reaction shown in Figure 3.6). However, recent work published by Klages et al.^{67,68} showed that TFBA is not only selective towards primary amines but also towards imines that are likely to form in plasma processes and thus, results obtained from this derivatisation technique have been analysed accordingly.

The experimental method has been described in detail in the manuscripts presented in

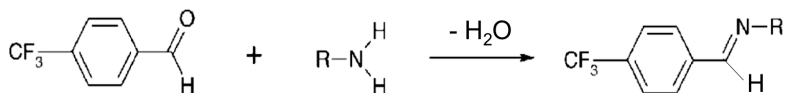


Figure 3.6: Reaction between a primary amine and TFBA.

Chapters 4 and 5. The method involves performing XPS analysis on the film before and after reaction with TFBA and calculating the concentration of the aldehyde-reactive groups, which are also "nucleophiles", as given by the following equation.⁶⁹

$$[Nu]_u = \frac{[F]_d}{3[N]_d} \times [N]_u, \quad (3.9)$$

and selectivity (in %) is calculated by,

$$\frac{[Nu]_u}{[N]_u} = \frac{[F]_d}{3[N]_d} \times 100, \quad (3.10)$$

where $[Nu]$ is the concentration of nucleophiles (in at. %), mainly primary amines and imines, $[F]$ is the concentration of fluorine (in at. %) and $[N]$ is the concentration nitrogen (in at. %). Subscripts u and d stand for underivatised and derivatised samples, respectively. Whenever the term "amine content ($[NH_2]$)" or "amine selectivity ($[NH_2]/[N]$)" is used throughout this thesis, note that it refers to all nitrogen functional groups in the film that react with TFBA, which are mostly primary amines and imines.

3.2.6 Dynamic contact angle goniometry

Wettability of a surface determines the tendency and the degree to which a liquid spreads on a solid surface. When the liquid is water, it gives the relative hydrophilicity or hydrophobicity of the surface. Wettability measurements of plasma polymers can provide useful information

since wetting properties can be used to explain the behaviour of biomolecules on a surface via hydrophilic or hydrophobic interactions. For example, modeling studies have shown that Fg binds to a $-\text{CH}_3$ terminated self assembled monolayer via hydrophobic groups present in the protein molecule, whereas a completely different orientation of the molecule was observed on a $-\text{COOH}$ terminated surface.⁷⁰

Wettability is usually measured in terms of the contact angle (CA) at a solid-liquid-gas interface. The contact angle is defined by the angle between the solid-liquid interface and the liquid-gas interface. It is known that the static CA of a certain probe liquid on a given solid surface can vary considerably. This variation is known to be between a maximum CA, known as the advancing contact angle (ACA) and a minimum CA, known as the receding contact angle (RCA). Specifically, ACA is that which is measured when the probe liquid is advanced on a previously un-wetted area and is more sensitive to the low-energy components of the surface, for example the HC fragments. RCA is measured when the liquid is receded on a previously wetted area and is more sensitive to the high-energy components of the surface, for example amines. The difference between the ACA and RCA is known as CA hysteresis. Hysteresis is zero only for ideal surfaces which are chemically homogeneous, smooth on the atomic scale and perfectly unreactive towards the liquid or gas.⁷¹ This is not the case with most surfaces and certainly not with plasma polymer films and therefore, measurement of both ACA and RCA is imperative. The experimental method used in this work has been described in detail in the manuscript presented in Chapter 6.

3.2.7 Tribometry

Tribology is the study of properties at an interface between two materials in relative motion. This includes friction, wear and lubrication testing. In this work, we have studied friction and wear properties of plasma polymer films using a tribometer in the pin-on-flat configuration, the experimental setup of which was based on that shown in Figure 3.7. Experimental details

are given in the manuscript presented in Chapter 6.

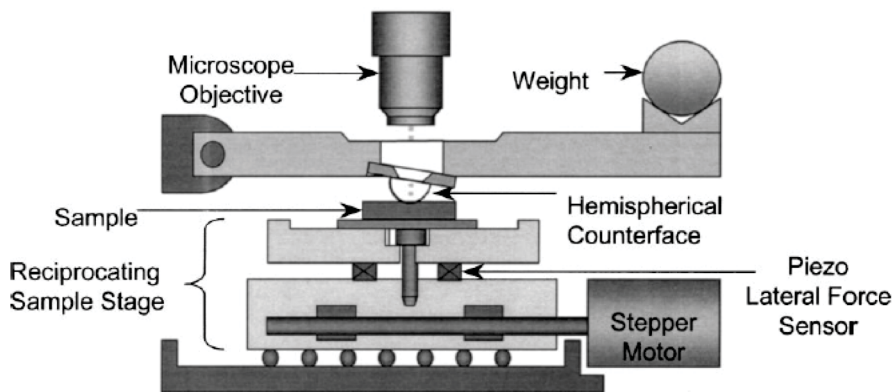


Figure 3.7: Schematic of the tribometer setup (reproduced from ref⁷²).

On a macroscopic scale, coefficient of friction is defined as the ratio of friction force to normal load applied. It is not an intrinsic material property, but rather depends on the counter-surface against which it is measured. A simple example is, the high friction experienced by a rubber against a pavement compared with that experienced by a rubber on ice. Plasma treatment, such as plasma treated rubber and deposition of plasma polymer films containing siloxane and -C-H have been shown to reduce the friction coefficient of the material.⁷³ In a biomedical point of view, oxygen plasma treatment of polyethylene has proved to decrease friction and improve lubrication with the counter-surface, in protein solutions.⁷⁴ Thus, it is important to make sure that the plasma polymer films intended for biomedical applications have satisfactory friction and wear properties.

3.2.8 Surface plasmon resonance spectroscopy

Surface plasmon resonance spectroscopy (SPRS) is an optical technique used to monitor events that occur on a surface such as adsorption of molecules, swelling and so on. Depending on the configuration of the setup it can provide real-time kinetics of the event and give information such as refractive index and thickness of the sample and adsorbed layers, if any.

A major advantage of this technique is that it allows for label-free detection of the binding events.

Surface plasmons are free electron oscillations that exist at the interface between two media with opposite dielectric constants, such as a metal (eg: gold or silver) and a dielectric medium, which could be the sample. These surface plasmons propagate in the x-direction of the interface and decays in the z-direction exponentially onto both sides of the interface. The penetration depth into the dielectric medium is 150-200 nm.⁷⁵ These surface plasmons are extremely sensitive to changes in refractive index or thickness within the penetration depth and therefore, are exploited in this technique.

The surface plasmons are excited by irradiating the interface with p-polarised (transverse magnetic) light. This is achieved by using a prism as a coupler in the Kretschmann configuration as shown in Figure 3.8a. When the intensity of the reflected light is measured as a function of incident angle, there reaches a critical angle where a maximum in reflectivity is observed and total internal reflection is achieved. As the angle is continued to increase beyond the critical angle, there will be another important angle at which the energy from the photons is transferred most efficiently to the surface plasmons and as a result, a minimum in reflectivity is observed. This phenomenon is called *surface plasmon resonance*. A typical plot of reflectivity vs incident angle is shown in Figure 3.8b. The position of the minimum angle is sensitive to any surface processes and therefore if, for example, a protein solution is passed over the sample via the flow cell, the adsorbed protein layer on the surface will be observed as a shift in the minimum angle (Figure 3.8b). By modelling the shape of the SPR curve using Fresnel's equations, the optical thickness (geometrical thickness \times refractive index) of the adsorbed layer can be determined. The kinetics of the surface process can also be monitored either by following the minimum angle with time or measuring the reflectivity at a fixed angle (usually on the linear region of the curve to the left of the minimum peak) with time.

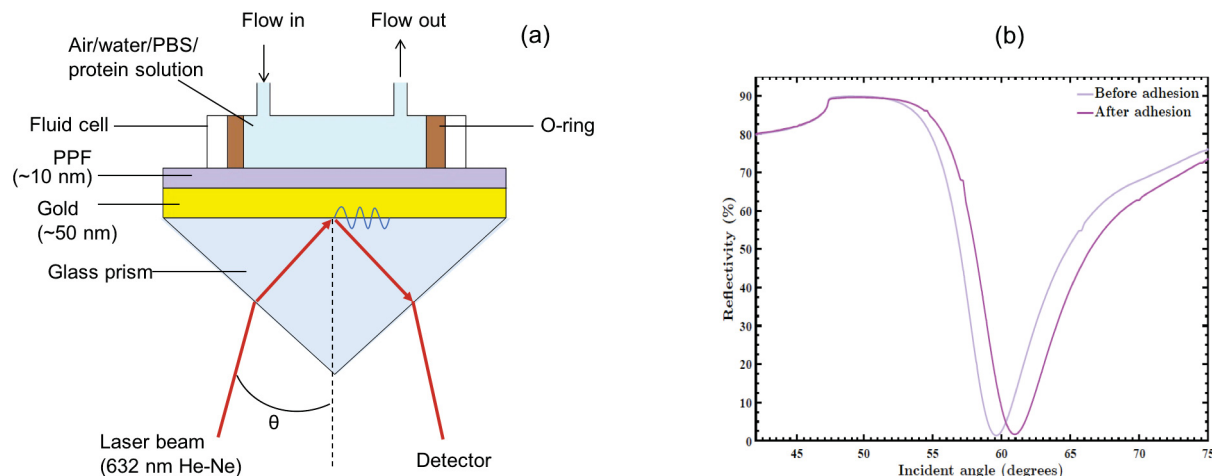


Figure 3.8: (a) Schematic of sample installation in the Kretschmann configuration, (b) example of an SPR curve before and after a protein adsorption process.

SPRS is a useful technique to monitor processes occurring in and on plasma polymer films. For example, Chen et al.²⁶ studied the stability of plasma polymerised allylamine films in buffer solution and found that films deposited at low pressure were more stable than those deposited at high pressure. Several amine based films have been studied for immobilisation of DNA strands and proteins such as fibrinogen (Fg) and albumin.^{76,77} Plasma polymer films containing ether groups have been found to show excellent anti-fouling properties above a certain value of film thickness, using this method.⁷⁸ Similarly in this work, SPRS has been used to study adsorption of Fg and albumin on the various plasma polymer films and experimental details can be found in the manuscript presented in Chapter 6.

3.2.9 Surface plasmon fluorescence spectroscopy

Surface plasmon fluorescence spectroscopy (SPFS) is an extremely sensitive tool that is especially useful in detecting angular shifts that are too low to be detected by SPRS. The technique is based on the emission of fluorescence from chromophores at the interface, upon excitation by the SPR and relaxation to the ground state. The intensity of this fluorescence

depends on the intensity of the surface plasmon excitation and the probability for the radiative decay.⁷⁹ The experimental procedure is similar to that of SPRS and involves measuring the transmitted light (instead of reflected light) as a function of incident angle (Figure 3.9a). The experimental setup of the SPRS with the addition of SPFS, used in this work, is similar to the schematic shown in Figure 3.9b.

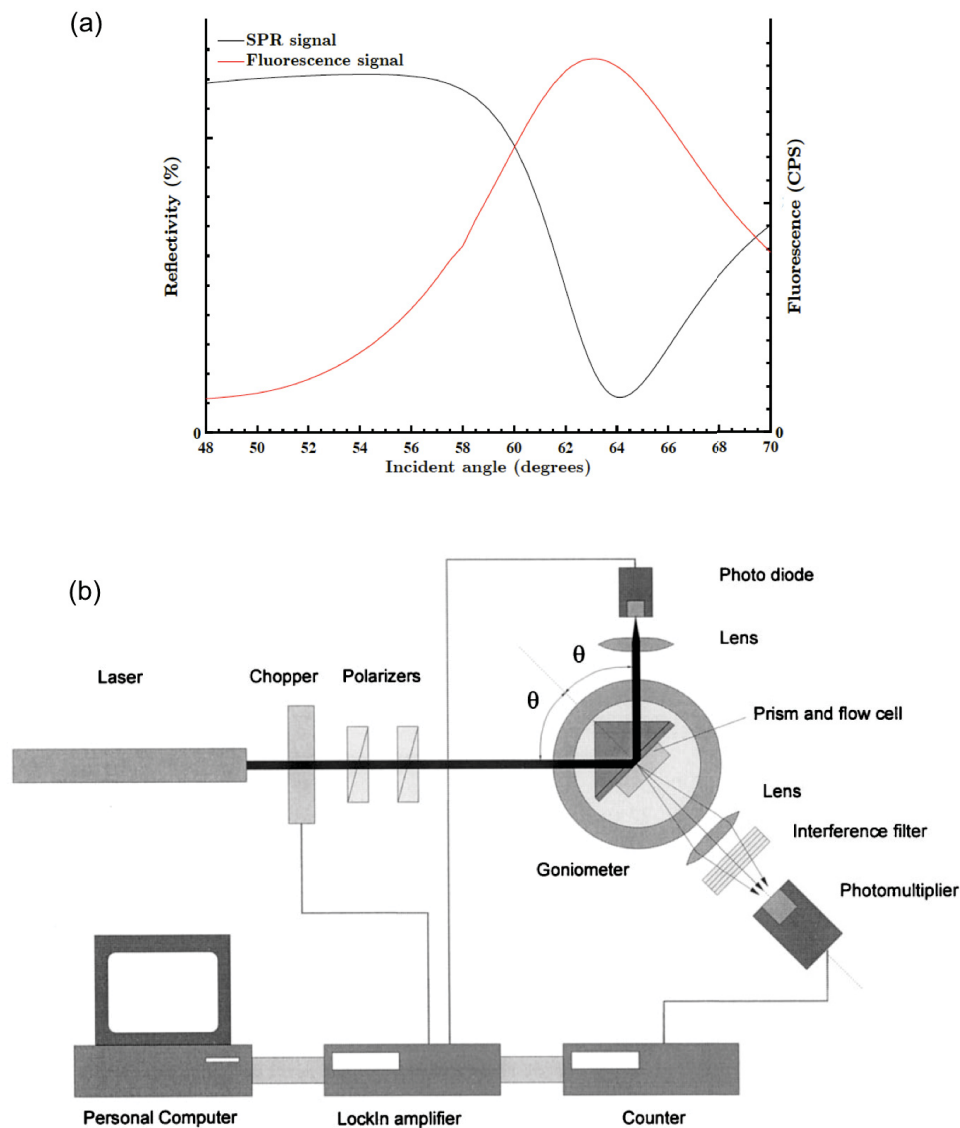


Figure 3.9: (a) Example of an SPFS signal along with the SPR curve, (b) schematic of the experimental setup of the SPRS in combination with the SPFS ((b) reproduced from ref.⁷⁹).

Important considerations of this technique include the behaviour of a chromophore at a metal surface. When the chromophore is near a metal surface (within 5 to 7 nm) the electronic coupling of the chromophore with that of the metal, results in the emitted energy from the de-excitation of the chromophore, being quenched and dissipated as heat in the metal. Therefore, it must be ensured that the chromophores are well separated from the metal, but within the decay length of the surface plasmon which is around 200 nm, beyond which no fluorescence can be observed. In addition, care must be taken to avoid saturation of the photomultiplier (PMT), used to detect the fluorescence, and make sure that the fluorescence signal is within the linear range of the PMT, in order to make reliable correlations with the SPR signal.

SPFS has been used in several studies, for example, detection of DNA hybridisation reactions⁸⁰ and binding reaction of low mass density biotinylated fluorophores to a functionalised surface, not detectable by SPR.⁷⁹ It has also been used to detect multicomponent macromolecular adsorption at the solid-liquid interface by linear correlation between SPR and SPFS signals, where SPFS gives information on the labelled component and the SPR signal gives information on the total adsorbed layer. The study involved a set of 3-component "sandwich" experiments, where layer by layer was adsorbed separately, thus allowing measurement of the unlabeled component via the difference between the two signals.⁸¹ However, if the adsorbed layer is a mixture of components, it is difficult to gain information on the unlabelled component(s) by simply subtracting the two signals, since reliable modeling of the SPR signal requires for a well-defined layered system with a known average refractive index for proper evaluation of the average layer thickness.

In this work, SPFS has been used to monitor adsorption of Fg from a mixture of labeled-Fg and albumin, in order to study the regulation of Fg adsorption by the various plasma polymer films in the presence of a second protein, albumin. Details can be found in the manuscript presented in Chapter 6.

Chapter 4

A Fundamental Study of Two Distinct Methods for Synthesis of N-based Plasma Polymer Films

This chapter presents the manuscript titled, *Single source precursor vs. precursor mixture for N-rich plasma polymer deposition: Plasma diagnostics and thin film analyses*, published in *Plasma Processes and Polymers*, where a fundamental study is conducted to compare two commonly used plasma deposition methods for producing N-rich films. The two methods differ in their choice of precursor; the first method utilising a single source precursor and the second, making use of a precursor mixture, to deposit the same type of coatings. A thorough plasma-phase analysis combined with thin film analysis has enabled to learn about the process mechanisms that govern the thin film chemistry and to compare, fundamentally, the two seemingly similar approaches to produce N-rich films. Several interesting findings on the plasma chemistry and film chemistry that differentiate between the two approaches, have resulted from this work.

Single Source Precursor vs Precursor Mixture for N-rich Plasma Polymer Deposition: Plasma Diagnostics and Thin Film Analyses

Abstract

Two distinct methods of producing N-rich films, that mainly differ in their choice of precursor are compared; the first method involves a single source precursor and the second, a mixture of precursors that consists of a heteroatom source gas and hydrocarbon (HC) gas. Plasma diagnostics and thin film chemistry of allylamine (AA), cyclopropylamine (CPA), ammonia/ethylene (AmEt) and ammonia/1,3-butadiene (AmBu) are studied, while maintaining the same N to C ratio, 1 to 3, in the gas phase. Single source precursors produce films containing higher N, whereas, precursor mixtures, owing to reduced dehydrogenation, produce films with a low nitrile content. While similarities between fragmentation patterns of single source precursors and precursor mixtures are observed in the plasma phase as the energy supplied is increased, chemical differences still exist between films produced by these two methods, within the studied range of power.

4.1 Introduction

Plasma polymer films (PPFs) are widely studied owing to their numerous potential applications mainly in the biomedical field.^{8,26,77} An important class of PPFs is the nitrogen based films which are used in, for example, influencing the differentiation of mesenchymal stem cells,⁸²⁻⁸⁴ enhancing the endothelialisation and healing around vascular grafts,⁸⁵⁻⁸⁷ serving as cardiovascular stent coatings⁸⁸ and creating non-fouling and antibacterial surfaces, where amine groups on the coating provide anchoring sites to polyethylene glycol⁸⁹ and polyvinyl

sulphonate coated silver nanoparticles,^{90,91} respectively. N-rich PPFs comprise of different N functional groups such as amines, nitriles and imines. Amine groups tend to be more beneficial since, being positively charged in aqueous environments at physiological pH values, they are able to attract negatively charged biomolecules such as proteins (for example, fibronectin and vitronectin) and in addition, they can also be used in covalent binding of proteins in aqueous environments.^{2,5} Since most cell processes are mediated via proteins, amines are the recommended N functionality for cell adhesion and growth,^{2,5,26,27,92–95} and the effective film-molecule/cell interaction for a given biological application.

The chemical composition of PPFs depends on several plasma process parameters such as power, pressure, precursor flow rates and precursor type. Precursor activation, fragmentation and dehydrogenation processes all increase with power. In the low power range, precursor activation seems to be the dominating mechanism and an increase in power leads to an increase in N while at high power, the fragmentation and dehydrogenation become dominant and an increase in power leads to depletion of N and NH₂. Similarly, pressure and precursor flow rates and/or ratios also affect the film's chemical composition.^{96,97} In this study, we focus on the effect of precursor type on the nitrogen functionalities incorporated in the film during the plasma polymerisation process. Generally, the two methods that are used to introduce the desired functionality onto the PPF include, (i) use of a single monomer molecule which already contains the desired functional group such as AA,^{98–100} heptylamine (HA),^{100,101} propylamine (PA),³² CPA^{63,102} and (ii) use of a precursor mixture consisting of a functional group monomer and a HC monomer in order to introduce the polymer backbone; for example nitrogen/ethylene, AmEt,^{96,103} AmBu⁹⁶ and ammonia/acetylene.¹⁰⁴ The first method, where the monomer already contains the amine group, allows for direct incorporation of the amine functionality into the film, whereas the second approach allows to vary the functional group to HC monomer ratio, thereby enabling fine-tuning of the film chemistry.

Thus far, plasma and thin films have been compared within these two methods, where

different aspects of the plasma polymerisation process have been addressed. For example, study of pulsed plasma polymerisation of AA and CPA by Denis et al.⁶³ showed that, even though both precursors show increased fragmentation with increase in mean power (P_{mean}), CPA is less plasma-fragmented than AA below a certain critical P_{mean} . An earlier study by Fally et al.³² showed the effect of degree of unsaturation of the precursor on the film composition. The goal was to preserve the amine functionality by choosing more unsaturated precursors which are expected to undergo less fragmentation during the plasma polymerisation process. The precursors studied were PA, AA and propargylamine. Ryssy et al.,¹⁰⁰ recently studied the plasma and thin film chemistry utilising four different monomers with different nitrogen to carbon ratios (AA, 1,2-ethylenediamine, 1,3-diaminopropane and HA) and found that the choice of precursor strongly influences the composition and stability of films, under similar energetic conditions. They concluded that it is not the N to C ratio but the molecular binding energies and stability of the resultant precursor ions and other ionic oligomeric species, being responsible for the ablation or continual growth of film, that determined the film's N functional groups. Lefohn et al.¹⁰⁵ compared N containing films deposited from acetonitrile and acrylonitrile plasmas and showed that the composition of acetonitrile based PPFs was insensitive to CW input power and duty cycle, whereas films deposited from acrylonitrile showed strong dependence on these parameters with the growth of highly conjugated imine and nitrile species. In the method 2 category, Contreras-Garcia et al.¹⁰⁴ studied films deposited from acetylene/ammonia and ethylene/ammonia and found that the former gave rise to more cross-linked but lower nitrogen and primary amine containing coatings. Similarly a previous study from our group,⁹⁶ investigated the effect of using ethylene and 1,3-butadiene as the hydrocarbon precursors along with ammonia to produce amine-rich PPFs with the aim of simultaneously improving the film's primary amine content as well as water stability.

Considering these two approaches of obtaining N rich PPFs, although the type of precursor used is clearly different at the time of introduction to the reactor, the complex plasma

polymerization process makes it difficult to define the extent to which these two methods may differ from each other. Depending on the effect of various process parameters such as power and pressure on precursor fragmentation, a wide variety of species could be generated that ultimately takes part in film deposition. Therefore, if the N to C ratio is maintained constant, although both types of precursors consist of essentially the same basic components: N-H and C-H, the degree to which these newly formed species could differ and their effect on the film composition are worthy of investigation.

A related study done by Hegemann et al.,¹⁰⁶ on acrylic acid ($\text{CH}_2=\text{CHCOOH}$) discharges showed the existence of a high energy input regime, where the plasma polymerisation of acrylic acid strongly resembles that of a $\text{CO}_2/\text{C}_2\text{H}_4$ discharge. They used a macroscopic approach, based on the concept of chemical quasi-equilibria, which involves the calculation of an apparent activation energy (E_a) required to initiate chemical reactions that give rise to the film forming species. Thus, this method is based on comparing the E_a 's of different monomer or gas mixture depositions in order to gain information on their plasma polymerisation mechanisms.

In a previous study,¹⁰⁷ we investigated PPFs produced from AmEt and CPA with the same gas-phase N to C ratio. We observed a higher N incorporation in CPA films which was attributed to the C-N bond being already present in the monomer. In addition, OES spectra of the CPA plasma showed a strong CN peak compared to that of AmEt under similar energy conditions and it was found that this was due to CN species being etched into the discharge from the surface of the growing film.

This work is a continuation of the previous study. The type of precursors that we address here are: method 1 - CPA, AA and method 2 - AmEt, AmBu. As previously, we maintain the N to C ratio as 1 to 3 in order to allow for similar elemental gas-phase compositions from both methods. We investigate the plasma-phase composition by optical emission spectroscopy (OES), fourier transform infra-red (FTIR) spectroscopy and mass

spectrometry (MS); and film composition by FTIR, x-ray photoelectron spectroscopy (XPS) and chemical derivatisation XPS with 4-trifluoromethyl benzaldehyde (TFBA). A detailed analysis of the plasma phase is intended not only to provide insight into the type of plasma species and reactions that may potentially influence the chemical composition of the films but also to certainly investigate the differences or similarities that exist between these two methods of obtaining N-rich PPFs.

4.2 Experimental section

4.2.1 Sample preparation and thin film characterisation

Plasma polymer films were prepared and characterised following the same methods and protocols described in.¹⁰⁷ Only an overview will be provided here. PPFs were deposited on silicon wafers ((100) orientation, thickness 500-550 μm) from Siltronix, which are infrared-transparent in the 1500-4000 cm^{-1} region. PPFs are synthesized from allylamine (Sigma Aldrich, purity 98%), cyclopropylamine (Alfa Aesar, purity 98%), ammonia/ethylene (Air Liquide, purity >99.9%) and ammonia/1,3-butadiene (Air Liquide, purity 99.5%) mixtures.

Depositions were done in a cylindrical stainless steel vacuum chamber wherein the plasma discharge is generated through a copper coil connected to a radio frequency power supply (13.56 MHz). Depending on the power applied, the plasma can be generated either in the capacitive or inductive mode. Power at the transition of E to H mode was between 30 and 100 W for all discharges, and was not precisely identified for all conditions. However, at 30 W, all discharges are in capacitive mode and at 100 W, they are in inductive mode. Gas flow rates are fixed at 20 sccm (standard cubic centimeters per minute) for CPA and AA, 20 sccm/30 sccm for the $\text{NH}_3/\text{C}_2\text{H}_4$ mixture and 20 sccm/15 sccm for the $\text{NH}_3/\text{C}_4\text{H}_6$ mixture, in order to have the same N/C (1/3) ratio. The flow rates were chosen such that the

elemental feed rate or the rate at which individual elements, C and N, entering the reactor, for all discharges, is constant. The working pressure is regulated at 20 mTorr (2.66 Pa). The substrates are located at 10 cm from the copper coil and are kept at the floating potential during the depositions. All films are deposited in continuous wave mode at plasma powers between 30 and 100 W.

Deposition rates are measured with a Dektak150 mechanical profilometer from Veeco, using a diamond tip with a 2.5 μm curvature radius and an applied force of 0.1 mN. PPFs of 100 nm thickness were deposited at 30, 60 and 100 W, except in the low power case of AmEt, where only a 30 nm thick coating was prepared at 40 W due to the very low deposition rate at this power. FTIR analyses of thin films are performed in transmission mode with an FTIR Bruker IFS 66V/S spectrometer. XPS analyses are performed using a PHI 5000 VersaProbe (ULVAC-PHI) hemispherical analyzer from Physical Electronics, with a highly focused (beam size 200 μm) monochromatic Al $K\alpha$ radiation (1486.6 eV, 15 kV, 50 W), at a pressure $<3 \times 10^{-7}$ Pa. FTIR and XPS analyses are performed 24 h after film deposition to allow for a consistent effect of ageing in air. The surface concentration of primary amine groups is determined using the chemical derivatization method with TFBA (Sigma Aldrich, purity 98%). Primary amine selectivity is calculated using the following equation:

$$\frac{[NH_2]_u}{[N]_u} = \frac{[F]_d}{3 \times [N]_d} \times 100 \quad (4.1)$$

where $[N]$ and $[F]$ are the relative concentration of nitrogen and fluorine, respectively, determined by XPS, and the u and d subscripts correspond to “underivatized” and “derivatized” samples, respectively. It is important to note that recent work^{67,68} suggests that TFBA is selective not only towards primary amines but also reacts with other N based groups, such as imine groups, which are usually generated during plasma polymerisation

due to high fragmentation of monomer molecules and subsequent re-arrangement that occur under high plasma powers. Since our N based monomer molecules already contain the amine functionality, chances of its incorporation and survival in the coating are considered higher, and, in order to compare with previous work, we use the symbol, $[\text{NH}_2]$, keeping in mind that it also represents other functional groups that react with aldehydes such as imines and amides which are formed on the film surface due to oxidation in air.

4.2.2 Plasma characterisation

4.2.2.1 FTIR

FTIR analyses of gas and plasma phases are performed using a Varian FTIR-670 spectrometer, whose multipass cell crosses the deposition chamber, and which is detailed in references⁶⁰ and.¹⁰⁸ Spectra are acquired using ResolutionsPro software from Agilent Technologies with a 1 cm^{-1} resolution and averaged over 50 scans.

4.2.2.2 OES

OES measurements are performed using a portable multichannel spectrometer AVS-MC2000-5 from Avantes. 5 different entrance slits allow to study the light from the plasma over 5 different wavelength ranges (200-350 nm, 330-465 nm, 440-610 nm, 590-735 nm and 720-970 nm). Light is collected through an optical fiber located at 10 cm from the coil and connected to the desired slit of the spectrometer depending on the studied wavelength range. Spectra are acquired with an integration time of 300 ms and averaged over 3 measurements.

4.2.2.3 MS

MS measurements of the gas phase are performed in residual gas analysis (RGA) mode using a quadrupole HAL EQP 1000 mass spectrometer supplied by Hiden Analytical, and connected to the deposition chamber by a 100 μm extraction orifice located at about 50 cm from the coil. Neutral species entering the mass spectrometer are ionized by electron ionization to allow their detection. The electron energy is fixed at 20 eV in the ionization source of the spectrometer in order to avoid excessive fragmentation of the precursors in the ionization chamber.

4.3 Results and discussion

Figure 4.1 shows the mass spectra of AA, CPA, AmEt and AmBu at various powers. The mass assignments to the peaks observed are given in Table 4.1. In order to distinguish the contribution of the fragmentation occurring in the ionization source of the spectrometer from that of the fragmentation that is actually taking place in the discharge, the cracking fraction of the precursor has been subtracted from the mass spectra according to the following equation proposed by Voronin et al.¹⁰⁹

$$I_c(m) = I_m(\textit{Plasma ON}) - I_m(\textit{Plasma OFF}) \cdot \frac{I_{Prec}(\textit{Plasma ON})}{I_{Prec}(\textit{Plasma OFF})} \quad (4.2)$$

where $I_c(m)$ is the corrected intensity of the peak at $m/z = m$, I_m corresponds to the experimental intensity of the peak at $m/z = m$ and I_{Prec} is the intensity of the precursor signal. Of course, this formula is not applied to the precursor peak, where m/z equal to the mass of the precursor molecule, because this peak corresponds to precursor molecules

arriving at the detector, that have not undergone any fragmentation in the ionization source of the spectrometer.

It is important to mention that this formula is only applicable if no new species having the same m/z as the precursor is created in the discharge as it is sometimes the case.⁶² Moreover, this correction only allows to subtract the cracking fraction of the precursor, without considering the cracking fraction of the new species created in the discharge. We assume that the fragmentation of the newly formed fragments/molecules in the discharge, in the ionisation source of the spectrometer is negligible since the mass of these newly formed molecules/fragments is already small. Applying this correction thus leads to a result that slightly underestimates the quantity of bigger species and overestimates the quantity of smaller ones.

For CPA and AA, Voronin's formula can simply be applied by choosing m/z 57 as the precursor signal (i.e. $I_{Prec} = I_{57}$). In the case of the two component AmEt or AmBu mixture, Voronin's formula has been adapted to account for two precursors subject to different levels of fragmentation, as follows. Taking AmEt for example, each peak (other than the two precursor peaks) of the gas-phase mass spectrum possibly being a combined result of cracking of both ammonia and ethylene in the spectrometer, it is important to determine what fraction of a peak's intensity is contributed by each precursor. The spectra of pure ammonia and ethylene gases have been used to distinguish this contribution of ammonia and ethylene to each peak of the AmEt gas phase mass spectrum according to the following equations.

$$I_m(NH_3) = \frac{I_m(Pure NH_3)}{I_m(Pure NH_3) + I_m(Pure C_2H_4)} \times I_m(AmEt) \quad (4.3)$$

$$I_m(C_2H_4) = \frac{I_m(Pure\ C_2H_4)}{I_m(Pure\ NH_3) + I_m(Pure\ C_2H_4)} \times I_m(AMEt) \quad (4.4)$$

where $I_m(NH_3)$ and $I_m(C_2H_4)$ are the intensities of the peaks at $m/z = m$ of the ammonia and ethylene spectra, respectively, reconstructed from the intensities of the peaks at $m/z = m$ of the spectra of a pure ammonia vapor $I_m(Pure\ NH_3)$, of a pure ethylene vapor $I_m(Pure\ C_2H_4)$ and of the AmEt gas mixture $I_m(AMEt)$. Thereby, for each m/z , we differentiate the contribution of the two precursors to all peaks in the spectrum of the gas mixture, i.e. when plasma is OFF. We then obtain a perfect reconstruction of the mixture signals:

$$I_m(NH_3) + I_m(C_2H_4) = I_m(AMEt) \quad (4.5)$$

The corrected intensity of a peak at $m/z = m$ in the AmEt mass spectrum when the discharge is switched on is then calculated according to:

$$I_c(m) = I_m(Plasma\ ON) - I_m(NH_3) \cdot \frac{I_{17}(Plasma\ ON)}{I_{17}(NH_3)} - I_m(C_2H_4) \cdot \frac{I_{28}(Plasma\ ON)}{I_{28}(C_2H_4)} \quad (4.6)$$

It is important to note that the right hand side of Equation 4.6, at plasma OFF, does lead to zero, as it should, due to $I_c(m)$ being the intensity of species that are produced only by the plasma. As in the case of the intensity at $m/z = 57$ for CPA and AA, the initial intensities of the two precursor peaks in the original spectra of the gas mixture plasmas are

added to the respective corrected spectra. Finally, all the spectra are normalized to the total ionic current according to:

$$I_{Norm}(i) = \frac{I}{I_{tot}} = \frac{I_c(i)}{\sum_i I_c(i)} \quad (4.7)$$

where $I_{Norm}(i)$ is the normalised intensity of the peak at $m/z = i$.

Figure 4.1 is a result of applying Equation 4.2 for CPA and AA, Equation 4.6 and its corresponding form for the AmEt and AmBu mixtures, and lastly, Equation 4.7 to all spectra. The observation that only few and weak negative peaks appear in the corrected spectra is a good indicator of the reliability of the applied corrections.

The variety of peaks seen when the plasma is switched on in the case of the single monomers compared to that of AmEt, where the spectra are limited to only 2 or 3 main peaks, or AmBu, where the new peaks appearing are relatively less intense, clearly differentiates the single monomer mass spectra from those of the gas mixtures. In AA and CPA, when plasma is off, peak at m/z 56 is the most intense, however after correction we can see that this peak completely disappears as the plasma is switched on implying that this molecule is not formed in the plasma and this might be related to the reduced stability of the precursor molecule after losing only one hydrogen atom.

Peak m/z 17 corresponding to ammonia can be seen in both CPA and AA, but more intense in AA. Moreover, peak m/z 41 is also more intense in the AA plasma than for CPA (Figure 4.1a and b). This peak mainly corresponds to $[C_3H_5]^+$ which is easily formed as a result of the removal of the NH_2 radical from the AA molecule. DFT calculations of reaction enthalpies for AA and CPA fragmentations, given by Denis et al.,⁶³ show that the energy required for the removal of NH_2 radical from AA is only 2.7 eV whereas it is 3.8 eV for CPA.

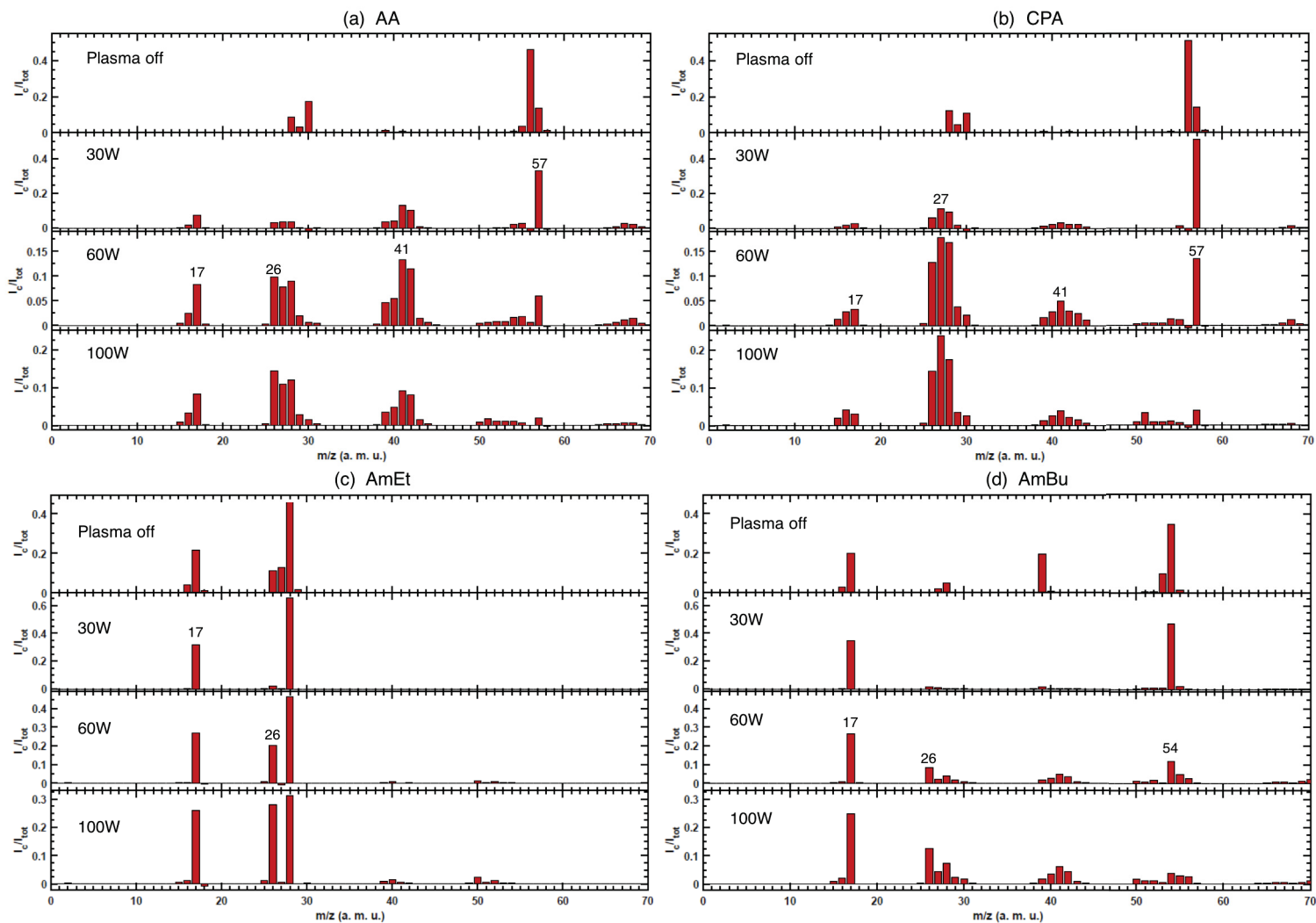


Figure 4.1: Mass spectra of (a) AA, (b) CPA, (c) AmEt and (d) AmBu plasmas at plasma off, 30 W, 60 W and 100 W. The top spectra (plasma off) show the cracking fractions of the monomers related to their fragmentation in the ionization source of the spectrometer. The spectra of AA and CPA when plasma is on are corrected according to Equation 4.2 while spectra of AmEt and AmBu mixture are corrected according Equation 4.6. All spectra are finally normalized with respect to the total ionic current according to Equation 4.7.

Table 4.1: Mass assignments for CPA, AA, AmEt and AmBu plasmas.

m/z (a. m. u.)	Assignment
15, 16	$[\text{CH}_x]^+$ $x = 3, 4$
15-17	$[\text{NH}_x]^+$ $x = 1, \dots, 3$
26-30	$[\text{H}_x\text{CN}]^+$ $x = 0, \dots, 4$
	$[\text{C}_2\text{H}_x]^+$ $x = 2, \dots, 6$
	28: $[\text{N}_2]^+$
39-44	$[\text{C}_2\text{H}_x\text{N}]^+$ $x = 1, \dots, 6$
	$[\text{C}_3\text{H}_x]^+$ $x = 3, \dots, 8$
50-55	$[\text{C}_3\text{H}_x\text{N}]^+$ $x = 0, \dots, 5$
	$[\text{C}_4\text{H}_x]^+$ $x = 2, \dots, 7$

Peak m/z 27, which may correspond to either $\text{CH}_2=\text{CH}^\cdot$ or HCN , at 100 W, is at its highest intensity in the plasma of CPA, next AA, AmBu and finally, no peak at this mass is observed in AmEt. This can be related to the OES spectra (Figure 4.2) where we can see that for 100 W, CPA has the most intense CN peak, next AA, then AmBu and finally AmEt has a very low CN peak intensity. OES spectra at 60 W show the same pattern but with less intensity and, at 30 W, almost no peaks were observed (spectra not shown). This may suggest that m/z 27 must mainly correspond to HCN . Indeed, it is possible that $\text{CH}_2=\text{CH}^\cdot$ radicals are produced in the plasma but these could undergo hydrogenation giving rise to more stable ethylene molecules given by m/z 28 or dehydrogenation, resulting in acetylene species denoted by m/z 26. The absence of a peak at m/z 27 in AmEt confirms that $\text{CH}_2=\text{CH}^\cdot$ radicals are not present in the plasma possibly due to their high instability.

Peak m/z 26 corresponds to either CN radicals or C_2H_2 . This peak tends to grow as power is increased for all four precursors, with AmEt showing the highest intensity. This relates well with the intensity of the vibrational band of CH deformation of acetylene at 729 cm^{-1} shown by plasma-phase FTIR spectra (Figure 4.3 and 4.4). Moreover, when cyanide radicals are produced in the discharge, they rapidly react with hydrogen and other radicals due to their strong reactivity, which give rise to a peak at m/z 27 corresponding to HCN , much higher in intensity, as observed in our previous work.¹⁰⁷ Hence, we can presume that the

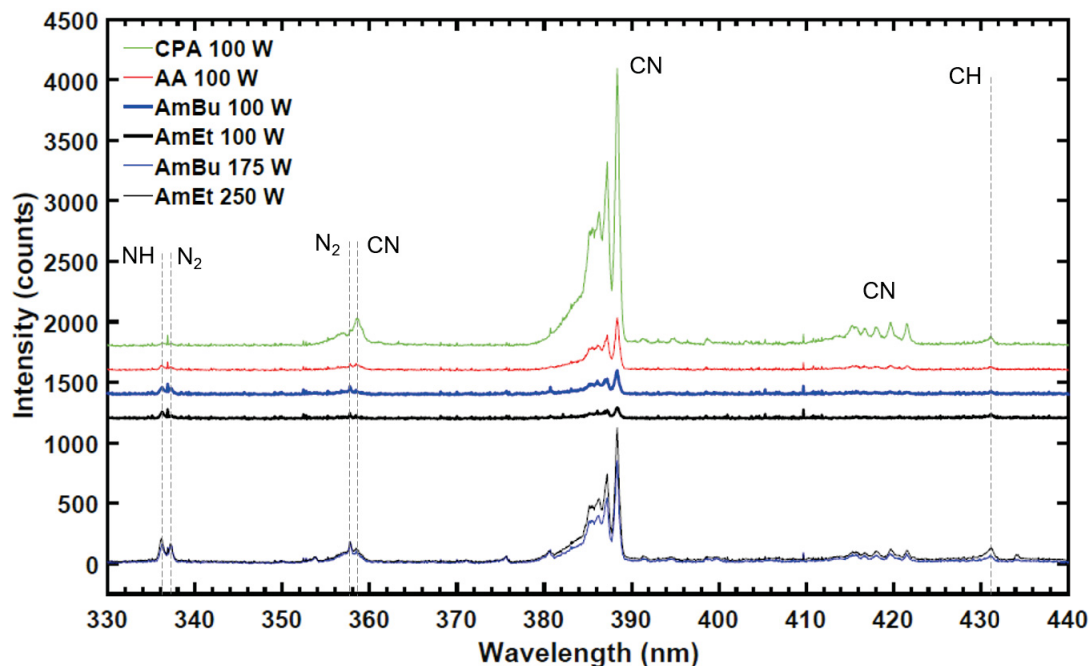


Figure 4.2: OES spectra of AA, CPA, AmEt and AmBu plasmas in order to compare all precursors at 100 W and at similar energy invested per particle i.e. AA, CPA at 100 W, AmEt at 250 W and AmBu at 175 W.

peak m/z 26 is mainly due to the formation of C_2H_2 , which is therefore the main product formed in the AmEt discharge as a result of dehydrogenation of the ethylene molecule. Acetylene fragments can also react together in the discharge or during multistep surface reactions to form bigger species such as diacetylene C_4H_2 , as evidenced by the appearance of the peak at m/z 50 which becomes the second most intense new peak at 100 W in the AmEt discharge.

Peak m/z 28 may correspond to N_2 or ethylene. However, in the OES spectra the low intensity of N_2 emission peaks implies that nitrogen is not present in significant quantities in the plasma, as nitrogen is otherwise a strongly emitting molecule in the visible range. In addition, the absence of a peak at m/z 14 in the mass spectra, re-confirms the absence of N_2 in significant quantities in the discharge. This shows that peak m/z 28 in the mass spectra must be a result of ethylene and not nitrogen.

Peak m/z 41 may correspond to $CH_2=CH-CH_2$, $CH_3C\equiv N$ or $CH\equiv CNH_2$. The high

intense peak in AA, especially at 60 W, is due to allyl $\text{CH}_2=\text{CH}-\text{CH}_2$ radicals which are easily produced by the removal of the NH_2 radical from an AA molecule. Peak at m/z 42, also of high intensity in AA plasma, can be attributed to $\text{CH}_2=\text{CH}-\text{CH}_3$ formed after hydrogenation of $\text{CH}_2=\text{CH}-\text{CH}_2$ radical. In CPA, m/z 41 is probably due to a C_3H_5 radical that forms as a result of hydrogen addition on the $-\text{NH}_2$ of the precursor molecule leading to the breaking of the C-N bond.⁶³ For AmBu, peak at m/z 41 is ascribed to $\text{CH}_2=\text{CH}-\text{CH}_2$ which can be formed via hydrogen addition to one of the C=C bonds followed by the removal of a methyl radical from the butadiene molecule. It is possible that $\text{CH}\equiv\text{CNH}_2$ is formed from a reaction between $\text{HC}\equiv\text{C}\cdot$ and NH_3 , however the absence of a peak at m/z 41 in AmEt plasma where acetylene and ammonia are present in larger quantities shows the unlikelihood of the formation of these species in all plasmas.

These MS results suggest that, in the AmEt and AmBu discharges, barely any reaction between ammonia and the HC gas, leading to the formation of CN bonds, occurs. The HCN peak, given by m/z 27, remains strong at higher powers for the single monomer plasmas and even becomes the most intense in the case of CPA at 60 W and 100 W. This implies that the fragmentation pathway of AA and CPA molecules in the discharge tends to conserve the CN bonds, even at higher powers and the increase in power leads to more and more dehydrogenation, as evidenced by the increase in the $\text{H}\alpha$ emission band near 656 nm in the OES spectra (not shown), resulting in species containing multiple CN bonds such as imines and nitrile compounds.

Unlike in AmEt, the mass spectra of AmBu show a variety of species due to increased fragmentation at higher powers. This is evident from the appearance of several peaks in each of the regions around m/z 26, 41 and 54 at 60 and 100 W of AmBu spectra. At high power, it is interesting to note that the fragmentation pattern of AmBu becomes similar to that of AA. This is likely due to structural similarities that exist between butadiene and AA molecules, such as the non-cyclic structure and the presence of at least one C=C bond.

Although fragments in the regions m/z 40 and 50 also start to appear in the AmEt plasma at 100 W, the extensive fragmentation of the already small-sized ethylene molecules reduces the possibility of formation of larger mass fragments in the discharge under current conditions of pressure.

Figure 4.3 shows FTIR spectra of AA, CPA, AmEt and AmBu plasmas at plasma off and different power conditions. Peaks assignment is shown in detail in Table 4.2 and 4.3. The decrease in intensity of the NH_2 deformation band at 1617 cm^{-1} for CPA and 1626 cm^{-1} for AA, with increase in power denotes the loss of primary amine groups in these discharges (Figure 4.3a and b). The intensities of the bands corresponding to the ring breathing and ring deformation modes of CPA at 1212 and 886 cm^{-1} , respectively, rapidly decrease when the discharge is switched on, and completely disappear at 60 W (Figure 4.3b and 4.5b). This is consistent with the DFT-calculated enthalpies of CPA reported in,⁶³ where the ring opening is reported to be the most energetically favorable fragmentation reaction that occurs in the CPA plasma, leading to the formation of highly reactive biradicals.

Table 4.2: Observed IR frequencies assignment for AA and CPA plasmas

Wavenumber (cm^{-1})		Assignment ^a	Wavenumber (cm^{-1})		Assignment ^a		
AA	AA vapour	3089	=CH ₂ asym. str.	CPA	CPA vapour	3099	CH ₂ asym. str.
		2994	=CH ₂ sym. str.			3026	CH ₂ sym. str.
		2916	-CH ₂ sym. str.			2973	CH str.
		1626	-NH ₂ deformation			1617	NH ₂ scissor.
		1418	=CH ₂ deformation			1456	CH ₂ scissor.
		1352	-CH ₂ wag.			1373	CH in-plane bend., CH ₂ scissor.
		1284	=CH bend.			1287	CH deformation
		1025	=CH ₂ twist.			1212	Ring breathing
	Plasma on	Plasma on	994		=CH ₂ twist.	1167	CH ₂ twist.
			920		=CH ₂ rock.	1019	CH ₂ asym. wag., CN str.
			782		-NH ₂ wag.	886	Ring deformation
			3333		NH str.	812	NH ₂ rock.
			3016		CH ₄ str.	761	In-phase CH ₂ sym. rock., NH ₂ wag.
			1500-900		NH rock.	3333	NH str.
949	CH ₂ wag. of C ₂ H ₄	3016	CH ₄ str.				
729	CH deformation of C ₂ H ₂	1305	CH ₄ rock.				
712	HCN deformation	1500-900	NH rock.				
		949	CH ₂ wag. of C ₂ H ₄				
		729	CH deformation of C ₂ H ₂				
		712	HCN deformation				

^aThe assignments of the FTIR absorptions are based on references.^{60, 110–117}

Figure 4.3 and 4.4 show peaks corresponding to methane ($3016, 1305\text{ cm}^{-1}$) and acety-

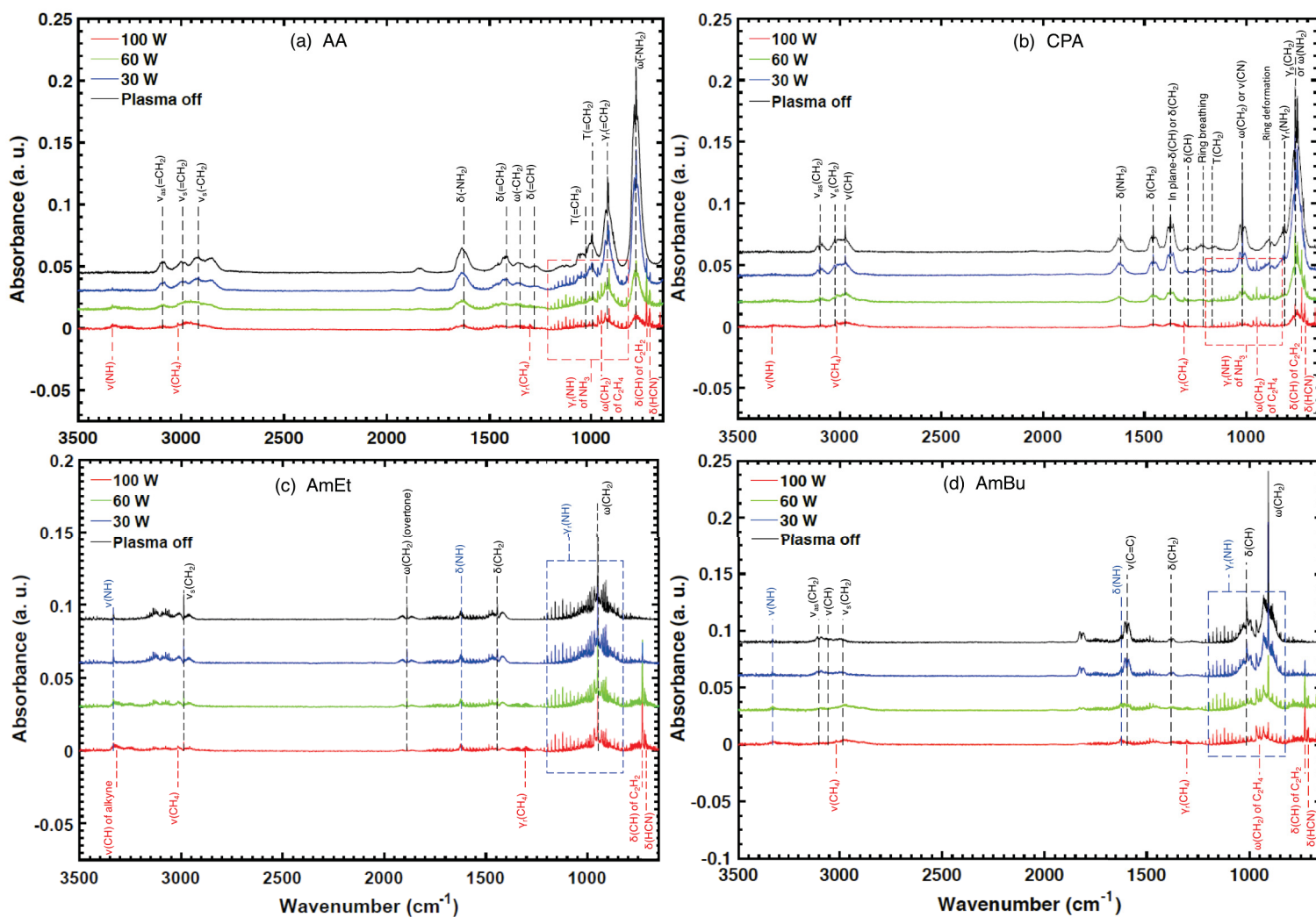


Figure 4.3: FTIR spectra of (a) CPA, (b) AA, (c) AmEt and (d) AmBu plasmas. Vibrational modes indicated in black and blue (in the case of AmEt and AmBu) are those initially present in the precursor molecules and bands in red are those appearing when the discharge is switched on. For the AmEt and AmBu spectra (c and d), modes in blue are those related to ammonia and black, related to the HC molecule. ν = stretching; δ = scissoring or deformation in general; τ = twisting; ω = wagging; ρ_r = rocking

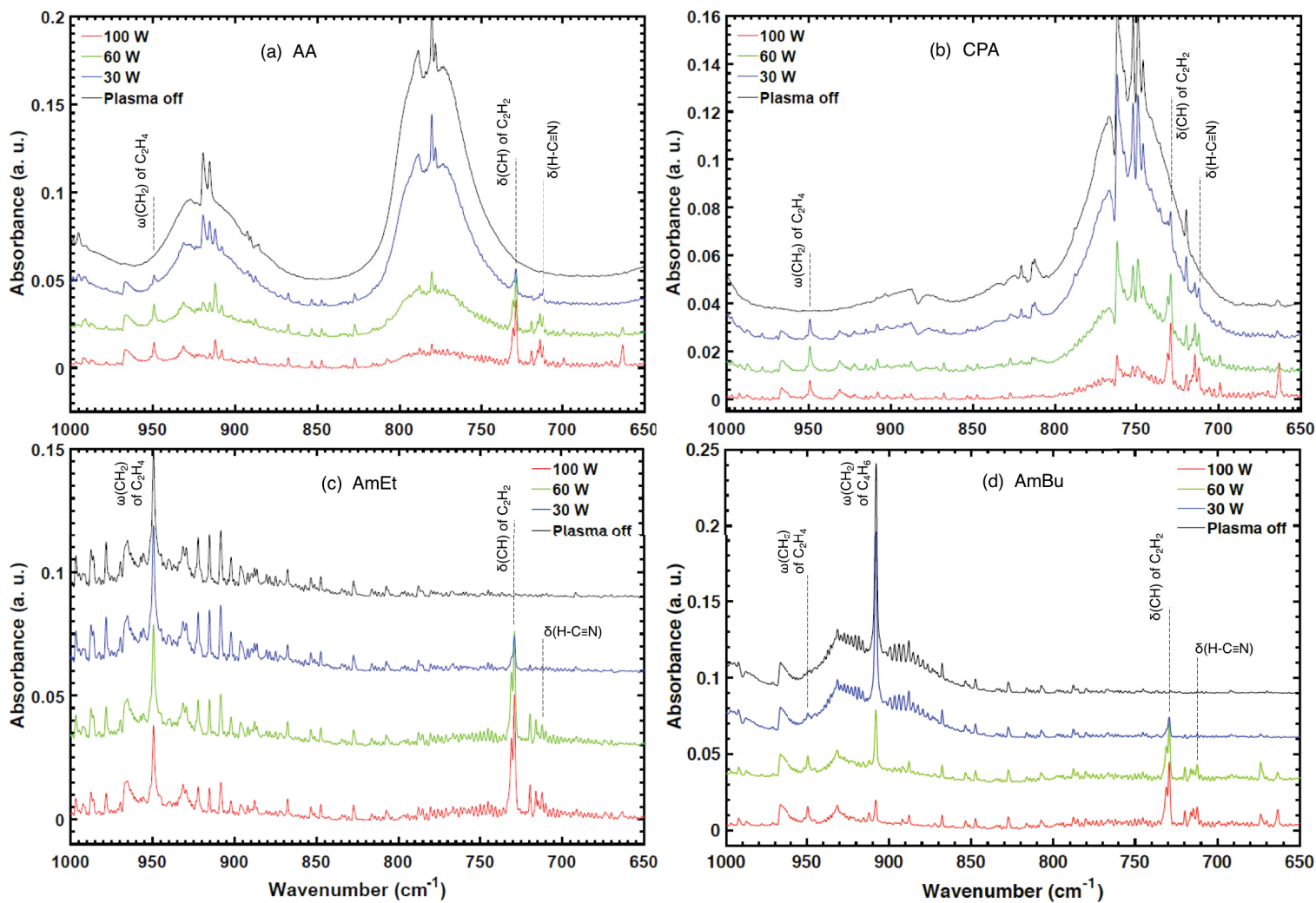


Figure 4.4: FTIR spectra of (a) AA, (b) CPA, (c) AmEt and (d) AmBu plasmas zoomed in the 650-1000 cm^{-1} region.

Table 4.3: Observed IR frequencies assignment for AmEt and AmBu plasmas

Wavenumber (cm ⁻¹)		Assignment ^a	Wavenumber (cm ⁻¹)		Assignment ^a	
AmEt	NH ₃	3333	NH str.	NH ₃	3333	NH str.
		1622	NH scissor.		1622	NH scissor.
		1200-900	NH rock.		1200-900	NH rock.
	C ₂ H ₄	2988	CH ₂ sym. str.	C ₄ H ₆	3101	CH ₂ asym. str.
		1889	CH ₂ wag. (overtone)		3055	CH str.
		1443	CH ₂ scissor.		2984	CH ₂ sym. str.
		949	CH ₂ wag.		1596	C=C str.
	Plasma on	3318	CH str. of alkynes	Plasma on	1381	CH ₂ scissor.
		3017	CH ₄ str.		1013	CH bend.
		1305	CH ₄ rock.		908	CH ₂ wag.
		729	CH deformation of C ₂ H ₂		3017	CH ₄ str.
		712	HCN deformation		1306	CH ₄ rock.

^aThe assignments of the FTIR absorptions are based on references.^{60,114-116,118}

lene (729 cm⁻¹)^{60,114} which are generated in all 4 plasmas. A peak corresponding to ethylene (949 cm⁻¹) is also found in the plasmas of AA, CPA, AmBu and can be seen in AmEt plasma even at 100 W (Figure 4.4). Figure 4.5 shows AA and CPA spectra zoomed in the 700-1300 cm⁻¹ region and aligned with a pure ammonia spectrum. This shows the appearance of NH peaks denoting the formation of ammonia in the AA and CPA plasmas, which supports MS results. The NH peaks in AA spectra are approximately 2.5 times more intense than those present in the CPA plasmas signifying greater ammonia formation in the AA plasma. This can be observed when the peak at 1120 cm⁻¹ of the AA discharge at 100 W is compared with that of CPA in Figure 4.5. This phenomenon is well explained in the work of Denis et al.⁶³ where the authors show that the hydrogen addition reaction on the nitrogen atom of the precursor molecule, leading to the formation of NH₃ after the C-N bond breaking, is more thermodynamically favorable in the case of AA than that of CPA.

Prior to obtaining FTIR spectra of the gas mixture plasmas, FTIR spectra of the pure HC gas and ammonia were taken separately (spectra not shown). No new peaks are observed for the pure ammonia FTIR spectra when the plasma is switched on. However, in the case of ethylene and butadiene, new peaks characteristic of methane and acetylene (and ethylene for AmBu) appear. The spectra of the gas mixture are close to a summation of the spectra of the individual gases. Except for a very weak band at 712 cm⁻¹, corresponding to the deformation

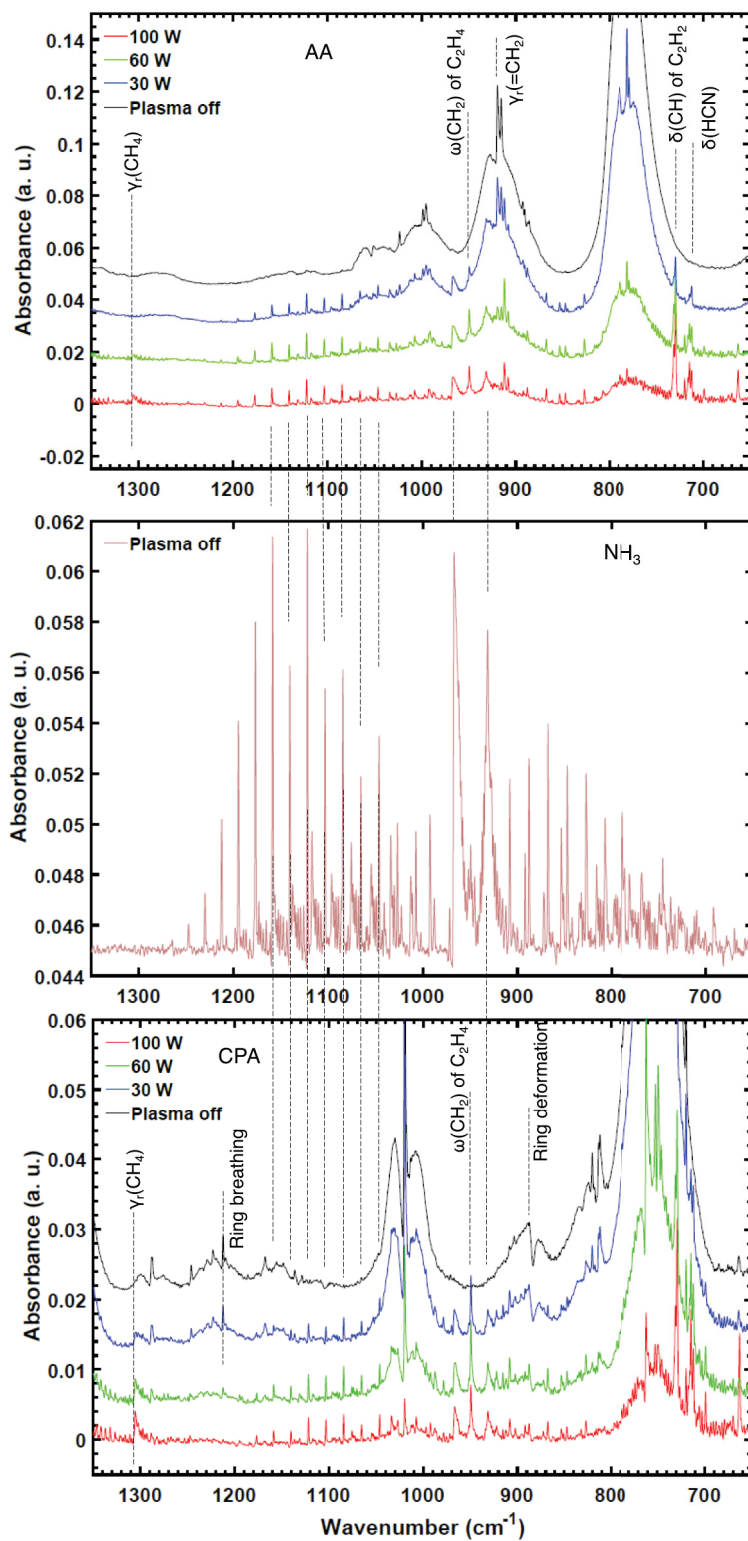


Figure 4.5: Zoomed in FTIR spectra of AA and CPA plasmas aligned with a spectrum of NH_3 vapour to show the generation of ammonia in both AA and CPA plasmas.

mode of HCN (Figure 4.4c and d), no other C-N species are seen in the discharges signifying a limited reaction between the HC gas and ammonia in the plasma phase (Figure 4.3c and d). This is also supported by the OES spectra at 100 W where the intensity of the CN band of AmEt and AmBu were much less intense compared to that of the single monomer plasmas (Figure 4.2). MS results also complement this fact where no or a less intense peak corresponding to HCN at m/z 27 is seen in AmEt and AmBu plasmas (Figure 4.1c and d). Hence, the N species found in the AmEt and AmBu based films should mainly be due to adsorption reactions of ammonia molecules and fragments occurring at the surface of the growing film.

A peak at 729 cm^{-1} corresponding to acetylene can be seen in the plasmas of all precursors (Figure 4.4) with the most intense band appearing in AmEt. The acetylene peak in the mass spectra (Figure 4.1), given by m/z 26, is also the most intense for AmEt plasma, at any given power, compared to that of other precursors.

It is noted that CN groups are not prominently seen in these spectra despite the CN peaks observed in OES spectra. This suggests that the $\text{C}\equiv\text{N}$ bonds present in the discharge must mainly stem from small species like CN radicals or HCN molecules that have, for the latter case, a notoriously weak $\text{C}\equiv\text{N}$ stretching absorption band in FTIR spectra.^{115,116} The production of hydrogen cyanide in the AA, CPA, AmEt and AmBu discharges is confirmed by a weak FTIR absorption peak at 712 cm^{-1} that corresponds to the HCN deformation band (Figure 4.4).^{114,115}

Figure 4.2 also shows OES spectra of AmEt and AmBu plasmas at 250 and 175 W respectively, which correspond to the same W/F value of $5\text{ W}\cdot\text{sccm}^{-1}$ as AA and CPA at 100 W. In our previous study,¹⁰⁷ we showed that when the deposition chamber is initially clean, there is an initial increase in the intensity of the CN peak in the OES spectra with time until it finally reaches a constant value. This was attributed to the etching of deposited species during the plasma polymerisation process, owing to events such as electron and ionic

bombardment, UV irradiation and ablation by ammonia. The CN emission band of the CPA plasma, being the most intense among all discharges under similar energy conditions, can be explained by the low cross-linking degree of CPA-based films. Indeed, the ring opening of CPA, which is the most energetically favourable fragmentation reaction,⁶³ leaves the precursor molecule with a saturated structure that gives rise to a low cross-linked plasma polymer consisting of loosely bonded oligomers which may easily be etched into the plasma. The saturated structure of the molecule also leads to a higher degree of dehydrogenation that may result in species such as HCN. The high degree of dehydrogenation for CPA is confirmed by the H α line at 656.6 nm of OES spectra being the most intense for CPA (Figure 4.6). On the other hand, AA, whose structure consists of a C=C bond would result in a more cross-linked plasma polymer leading to weaker etching and lower dehydrogenation compared to CPA. It is difficult to compare the single monomers with the gas mixtures in this regard since the presence of ammonia in AmEt and AmBu, a known etchant for organic materials,^{4,31,119} would contribute to increased etching of the PPF compared with the single monomer plasmas. Nevertheless, comparing AmEt and AmBu at the same W/F value (Figure 4.2), it is noted that the CN peak of AmBu is less intense than that of AmEt, suggesting that the more unsaturated structure of butadiene, leading to a more cross-linked PPF, results in reduced etching and dehydrogenation compared to the case of an AmEt plasma.

Figure 4.7 shows the evolution of [N], [NH₂]/[N] and [NH₂] (where [-NH₂] represents primary amines, but also all other groups that react with aldehydes) with increase in power for all 4 types of PPFs.

The noticeably low [N] values for AmEt and AmBu for all powers compared with the single monomer based films (Figure 4.7a) is attributed to the fact that AA and CPA molecules already contain the -C-N- segment. Therefore, the presence of more potentially condensable C-N containing species in the respective plasmas allows a better incorporation

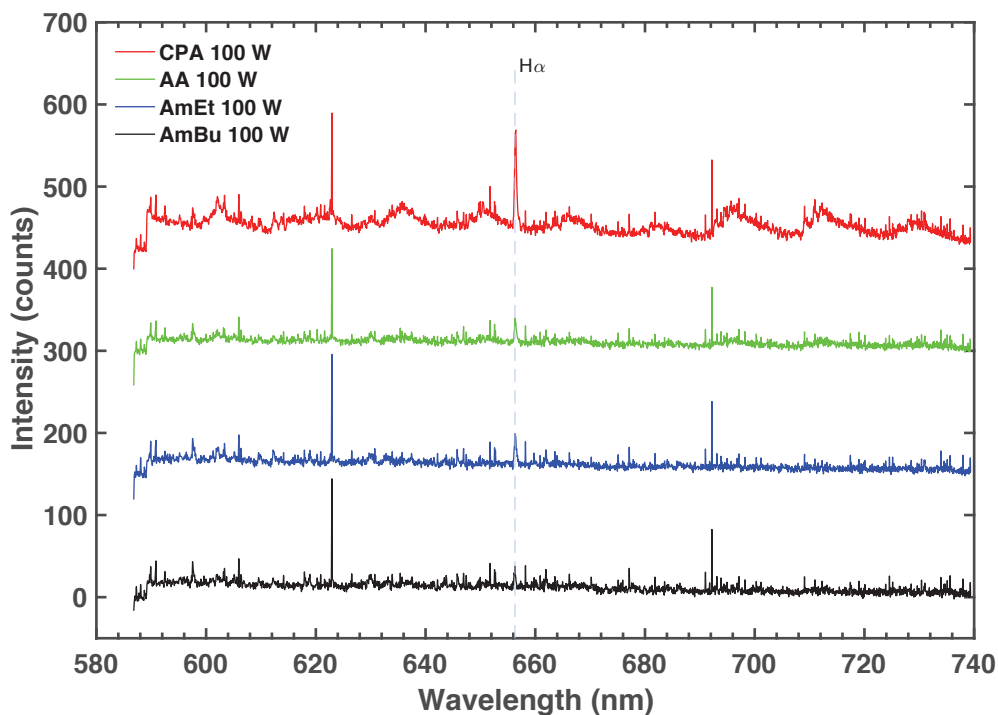


Figure 4.6: OES spectra of CPA, AA, AmEt and AmBu discharges at 100 W denoting the H-alpha line in the wavelength range 590 to 735 nm.

of N in the related films. In addition, the limited formation of C-N bonds in the AmEt and AmBu plasmas, as seen by the plasma diagnostic data, may also explain the inefficient incorporation of N in their films.

The lower [N] values of AmBu based films compared with AmEt is an observation already explained in.⁹⁶ It is attributed to the bond dissociation energy of butadiene being lower than that of ethylene. Energies required to break the C-C bond of butadiene and C=C bond of ethylene are 489 kJ/mol and 728 kJ/mol, respectively.¹²⁰ Therefore, butadiene molecules are more easily activated and fragmented than ethylene molecules, giving rise to the presence of a higher variety of carbon-containing condensable species in the AmBu discharge, and thus to a higher incorporation of carbon in the film, thereby lowering the relative [N]. This is also evidenced with the insitu FTIR spectra (Figure 4.4c and d). With the increase in power, the rapid decrease in the peak at 908 cm^{-1} denoting the CH_2 wagging

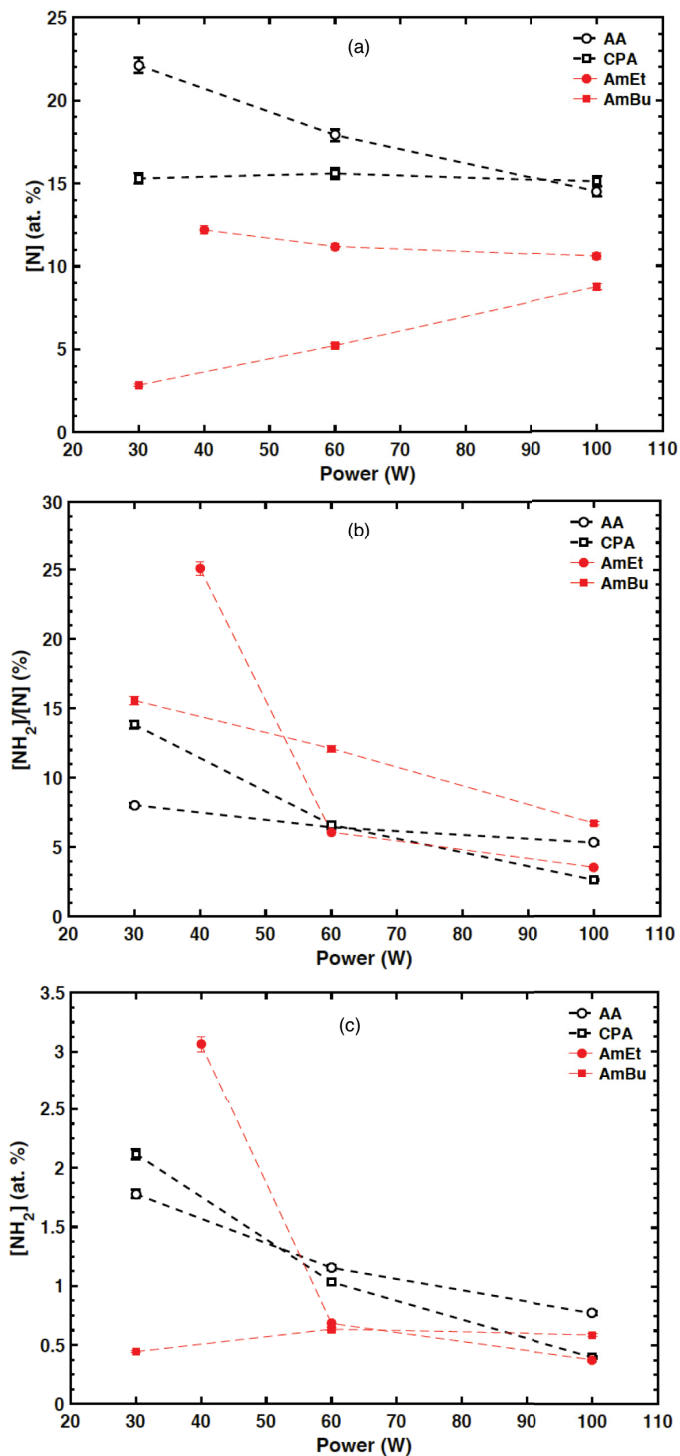


Figure 4.7: Effect of power on (a) N concentration, (b) $[NH_2]/[N]$ and (c) $[NH_2]$, where $[NH_2]$ represents all groups that react with aldehydes such as primary amines and imines, for PPFs deposited from AA, CPA, AmEt and AmBu.

of the butadiene molecule, shows that the monomer is easily fragmented into other species, whereas in the AmEt plasma, the peak at 949 cm^{-1} corresponding to the CH_2 wagging of ethylene remains strong even at 100 W.

The N incorporation in the gas mixture films is observed to decrease with power in the case of AmEt and increase in the case of AmBu. This can be explained based on the N incorporation data of AmBu, AmEt and ammonia-acetylene (AmAc) films reported in⁹⁶ and,¹⁰⁴ where it is observed that the most hindering of the relative N incorporation in the PPF occurs when the HC is butadiene and the least hindering occurs when the HC is ethylene. Accordingly, we can rank the N incorporated in the film by these plasmas under similar energy conditions and same N to C ratio, in the following order: $[\text{N}]\text{AmEt} > [\text{N}]\text{AmAc} > [\text{N}]\text{AmBu}$. Since the generation of acetylene strongly increases with power in both AmEt and AmBu plasmas, as clearly evidenced by mass spectrometry and gas phase FTIR analyses, AmEt and AmBu discharges become more and more like an AmAc discharge, leading to a decrease in [N] for AmEt-based films and an increase in [N] for AmBu-based films when the power increases.

On the other hand, for single monomers, [N] decreases with power for AA films whereas it remains almost constant for CPA films. At low power, [N] of the AA film is close to 25 %, which is the stoichiometric quantity of N in the monomer molecule, whereas in the case of the CPA film, it is less than this stoichiometric proportion of N. This suggests that AA molecule as a whole takes part in film deposition without undergoing much fragmentation, whereas the CPA molecule fragments into CN and C_2H_x species (as shown by MS peaks m/z 27 and 28 at 30 W), where the CN species get pumped out of the system in the form of HCN and the C_2H_x species condense to form the coating leading to a lesser [N] in the CPA film at low power. The decrease in [N] for AA films and the constant [N] in CPA films with power, can be attributed to the lower energy of the C-N bond in the AA molecule (2.7 eV) compared with that of a CPA molecule (3.8 eV),⁶³ which leads to a lower retention of the

CN bond in the AA discharge.

The increase in $[-\text{NH}_2]$ of AmBu based films with power, a feature not seen with other films, is probably due to the increase in $[\text{N}]$ with power which would result in more N-containing functionalities in the film that can react with aldehydes. The higher $[\text{NH}_2]/[\text{N}]$ of butadiene PPFs compared with other films suggests that butadiene undergoes lower dehydrogenation than other monomers, as supported by the least intense $\text{H}\alpha$ line in OES spectra at 100 W (Figure 4.6), leading to less nitrile species in the film.

The decrease in $[\text{NH}_2]/[\text{N}]$ with power for all precursors (Figure 4.7b) is a well discussed observation in the literature^{5,121} and is due to the high fragmentation of the monomers that leads to a loss in primary amine retention. The higher dehydrogenation of the growing PPF surface occurring at high powers, as observed in our previous work,¹⁰⁷ implies the formation of multiple CN bonds, imines first and then nitriles. This feature is well observed in Figure 4.8 and 4.9, where we can see a strong increase in intensity for peak P3, corresponding to nitriles, cumulated CN double bonds and conjugated CN multiple bonds. The overall increase in peak P4 with power observed for all films except AA should mainly be due to an increase in C=C species in the film. Since the CH stretching vibrational bands of alkenes are absent from the FTIR spectra, these C=C functional groups must be present in a tetrasubstituted fashion. However, for AmBu, the increase in P4 could also be related to the increase in N incorporation with power, which explains why the intensity of P1 and P3 also increases with power (Figure 4.9). Similarly, the decrease in $[\text{N}]$ in AA-based films with power allows to understand the strong drop in the intensities of peaks P1 and P4.

Overall, as power is increased, both XPS and film FTIR analyses show that AmEt and AmBu films become more similar in composition and the same is true for CPA and AA films. This is related to the high degree of precursor fragmentation that occurs in all discharges at high powers resulting in a loss of the initial precursor structure and thus making all discharges more and more similar to each other, as was seen by mass spectra for AA, CPA and AmBu.

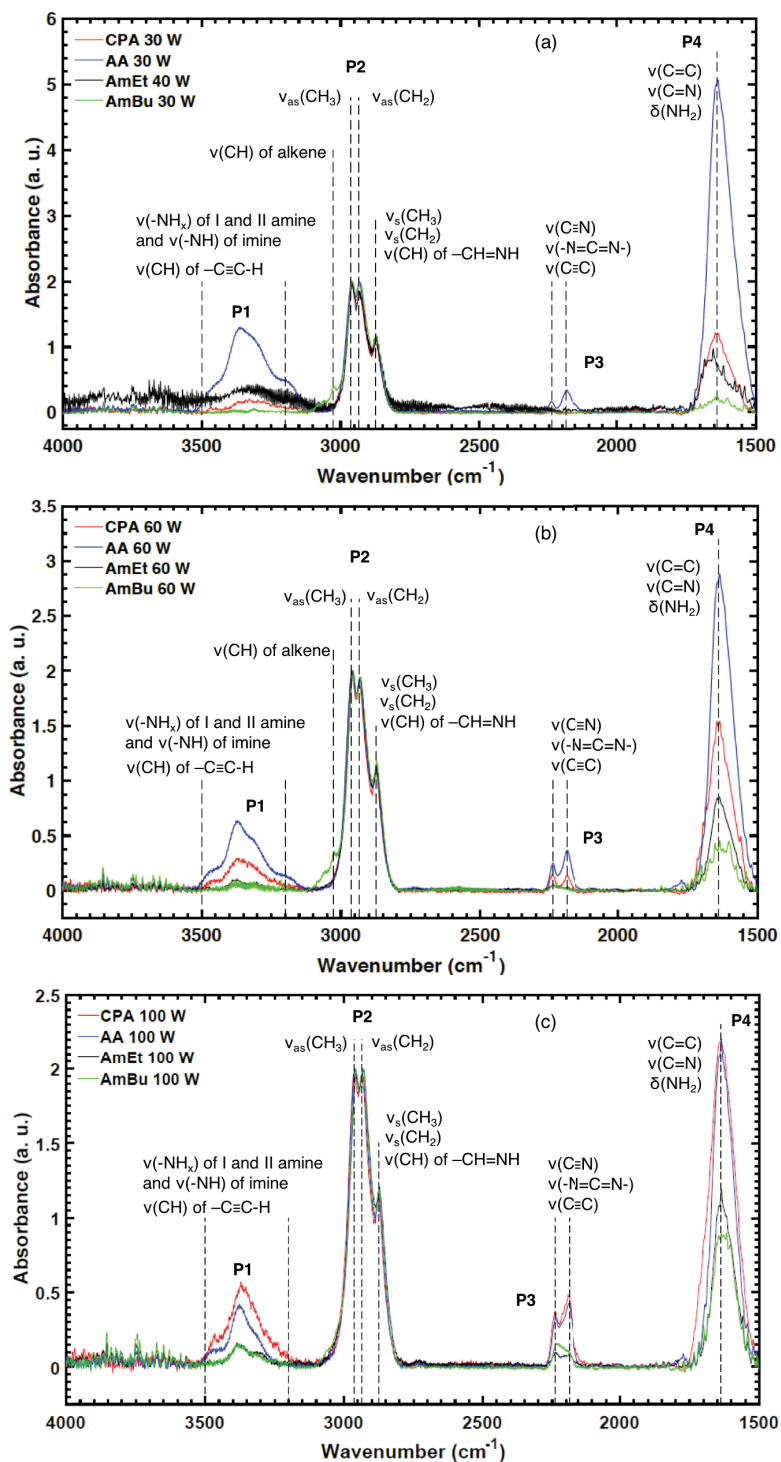


Figure 4.8: FTIR spectra of CPA, AA, AmEt and AmBu based films at (a) 30 W, (b) 60 W and (c) 100 W, normalised to the CH_x peak (P2) height. Peak assignments are based on.^{107,110} Peaks P1, P3 and P4 are normalised to the intensity of peak P2, in order to more easily compare FTIR spectra at different powers.

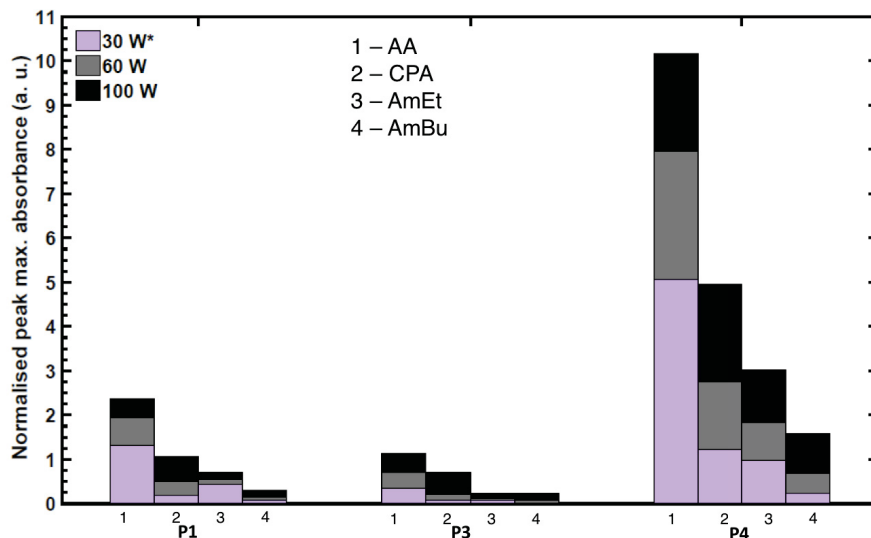


Figure 4.9: Comparison of the maximum intensities of P1, P3 and P4 peaks from FTIR spectra of AA, CPA, AmEt and AmBu films at 30 W, 60 W and 100W. *AmEt film is deposited at 40 W and not 30 W.

The different behaviour of AmEt mass spectra is probably due to the simpler structure of the starting HC molecule. Thus, the dependency of film chemistry on the starting molecule is lost in high energy conditions.

Finally, the deposition rates of the films synthesised from AA, CPA, AmEt and AmBu with respect to the power supplied are presented in Figure 4.10. CPA and AA based PPFs show faster deposition rates compared with the AmEt based film. As explained in,¹⁰⁷ it can be attributed to (i) the higher presence of larger condensing fragments in AA and CPA plasmas, even at 100 W, as seen from the MS peaks in the regions m/z 41 and 55, (ii) the higher energy supplied per molecule in AA and CPA discharges in similar power conditions, due to the lower total flow, leading to a higher activation of the molecules, and (iii) the greater presence of ammonia, an etchant, in AmEt plasma leading to competition between deposition and ablation and in turn reduced deposition rates. Interestingly, films synthesised using AmBu show a higher and sharper increase in deposition rate with the increase in power compared to all other precursors. This is attributed to the more unsaturated structure of the 1,3-butadiene molecule which consists of two conjugated C=C bonds resulting in bigger

and more active species in the plasma. The higher deposition rate of CPA films, at 100 W, compared to that of AA, could be explained by the higher generation of ammonia in AA plasmas, as evidenced by both plasma phase FTIR and MS analyses, which leads to a stronger ablation by ammonia during AA polymerisation.

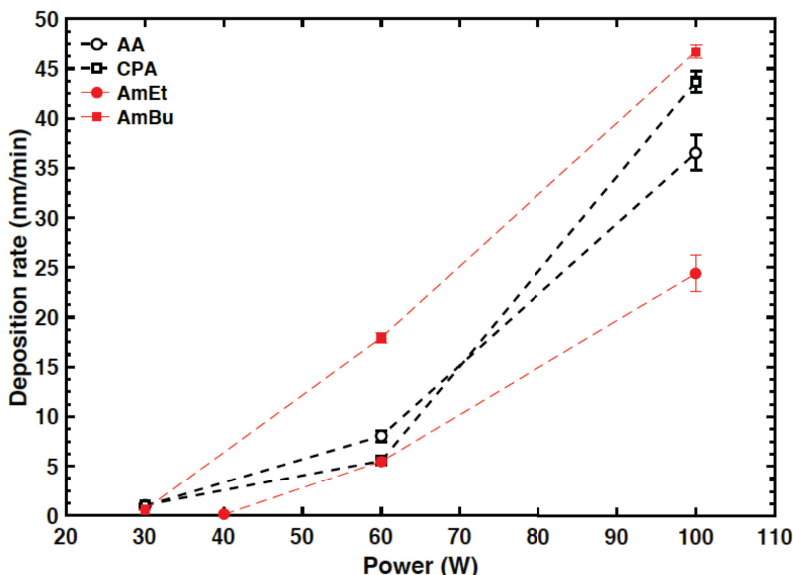


Figure 4.10: Deposition rates of AA, CPA and AmEt based PPFs.

4.4 Conclusions

In this work, we synthesised N-rich PPFs, using 2 distinct methods that differ in their choice of precursor. Films were deposited using single source precursors, CPA and AA, and precursor mixtures AmEt and AmBu. The N:C ratio was maintained 1:3 in the inlet gas streams. XPS results showed that, at the same power, films generated from the precursor mixtures contained less N compared with that deposited from the single monomers. This was attributed to the C-N bond being already present in the single monomers resulting in better N incorporation in the films. Furthermore, MS and plasma-phase FTIR showed that there was limited reaction between ammonia and the HC molecule in the gas mixture plasmas which seems to have contributed to the low [N] of these films. In spite of the lower

N content, gas mixture PPFs showed better $[\text{NH}_2]/[\text{N}]$ values at low power and AmBu film, in particular, showed better $[\text{NH}_2]/[\text{N}]$ values compared to all other films at higher powers. This was attributed to the reduced dehydrogenation in AmBu plasma, resulting in less nitrile species formed in the film. This can be considered an advantage of gas mixture based films where less unsaturated C-N species are desired and the versatility to easily vary the N to C ratio allows the synthesis of chemically well-controlled films with properties such as high water stability which is of the essence for biomedical applications. Acetylene was found to be generated in all discharges but in larger quantities in AmEt. The $[\text{N}]$ behaviour of AmEt and AmBu films was correlated to the increase in acetylene formed in the discharges with power.

OES spectra of all plasmas showed a strong CN peak which is a result of species being etched into the plasma from the growing film. The intensity of this peak is found to be correlated to the cross-link density of the PPF. CPA, after the ring opening, being a saturated molecule would give rise to a low cross-linked PPF which can be more easily dehydrogenated and etched, resulting in a stronger CN peak. The CN peak of AA, in contrast, was much less intense due to the presence of C=C bond in AA that formed a better cross-linked plasma polymer and therefore, exhibited less pronounced dehydrogenation and etching. Similarly, the CN peak of AmBu plasma was weaker than that of AmEt under similar energy conditions.

Plasma phase mass spectra showed that at increased powers AmBu, AA and CPA discharges became similar to each other in composition, with AmBu and AA being more similar in their fragmentation patterns owing to the structural similarities of these two molecules. Film FTIR results showed that the same was true between AA and CPA films and, AmEt and AmBu films, indicating that with the increase in fragmentation at higher powers, the film chemistry may no longer depend on the initial precursor molecules, however, differences in chemistry still existed between films produced from single precursor and precursor mixture plasmas.

Acknowledgements

The authors are thankful for the financial support provided by the Belgian Government (Belspo) through the "Pôle d'Attraction Interuniversitaire" (PAI, P7/34, "Plasma-Surface Interaction", ψ).

Chapter 5

Preparation of N-based Films with Optimised Amine Content and Water Stability

The manuscript titled, *Plasma Co-polymerisation of Ethylene, 1,3-Butadiene and Ammonia Mixtures: Amine Content and Water Stability*, published in *Thin Solid Films*, is presented in this chapter. This study constitutes a rigorous optimisation step to reach a compromise between the two conflicting film requirements, amine content and water stability. In doing so, several plasma deposition parameters are varied including power, gas flow ratio and total gas flow rate. A more unsaturated hydrocarbon precursor, 1,3-butadiene, is introduced to the polymerisation process, and compared with the commonly studied ethylene based coatings. It is shown that the increased unsaturation in the butadiene molecule helps enhance resistance to film dissolution in aqueous media due to increased cross-link density of the associated deposits. However, compromises are made with regards to N content in butadiene based films relative to that measured in ethylene based films. This study has led to important findings distinguishing the ethylene and butadiene based films and their individual contribution to produce films with a wider variety of properties.

Plasma Co-polymerisation of Ethylene, 1,3-Butadiene and Ammonia Mixtures: Amine Content and Water Stability

Abstract

Plasma co-polymerisation of ethylene, 1,3-butadiene and ammonia mixtures in a low pressure capacitively coupled r.f. glow discharge is investigated to produce amine-rich stable plasma polymer films for biomedical applications. Deposition kinetics, surface chemistry and water stability of films are studied as a function of r.f. power and precursor gas flow ratios. The surface primary amine content is evaluated by chemical derivatisation with 4-trifluoromethyl benzaldehyde followed by XPS; and stability by profilometric measurements of film thickness loss after 24 h of immersion in DI water. Multivariate regression analyses are used to obtain empirical models for N content and stability. Results show a clear improvement in performance in films containing butadiene as compared to the ethylene based films.

5.1 Introduction

Plasma polymerisation is a versatile and flexible method by which highly functionalised coatings can be readily deposited onto a variety of substrates with different three dimensional geometries. Owing to its several advantages such as eco-friendliness, dry process and high tunability it is now a widely studied technique. Plasma polymer coatings are investigated for use in a number of biomedical applications such as protein immobilisation, tissue engineering and cell-culture. In order for these coatings to be successful in specific end applications, it is required that certain physico-chemical properties such as chemical functionality, surface charge and roughness are carefully controlled. By doing so, it is possible to some extent

control their interaction with the biological environment and help promote the desired cell processes. Focusing on chemical functionality, there are many chemically reactive groups such as carboxy, hydroxy and amines that when present on the surface can enable the physico-chemical immobilization of biologically active molecules,⁵ an intermediate step associated with most cell processes. The focus of this study is on amine-rich coatings, an important class of functional surfaces which were found to promote cell adhesion^{8,12} and also to influence differentiation of mesenchymal stem cells.⁸²⁻⁸⁴ These effects have been attributed to amine groups that, being positively charged in aqueous environments at physiological pH values, attract negatively charged biomolecules such as proteins and DNA, and living cells.^{2,5,26,27} Moreover, amine groups can also be exploited for covalent coupling of proteins in aqueous environments^{2,5} and to enable imine or enamine coupling.⁶ Thus, having high density of primary/secondary amines on the surface of plasma polymer coatings is considered desirable for an improved interaction between the surface and the surrounding biomolecules and cells. Good physical stability of these coatings in aqueous media is also vital for most biomedical applications. It was found that amine-rich coatings have low aqueous stability owing to their high surface energy and thus, high affinity towards polar solvents.³¹ It was also shown that attempts to increase the surface concentration of amine groups, resulted in water-soluble films.^{27,122} Hence, it appears that a compromise between the requirements of high surface amine densities and good water stability must be achieved.

Two main approaches to plasma polymerisation by which N-rich coatings can be obtained are, plasma polymerisation of (i) a suitable N-based monomer gas (for example allylamine)^{5-7,27,99,101,122-125} and (ii) a gas mixture containing a hydrocarbon and N-containing gas (for example ammonia).^{8,20,39,42,43,126,127} Use of a gas mixture rather than a single amine based monomer gas allows more flexible surface chemistries to be achieved provided the monomer gas ratio and other deposition conditions are carefully tuned. In this study, we investigate a series of thin plasma polymeric coatings deposited using a mixture of ethylene, 1,3-butadiene and ammonia gases. Our main goal is to improve the optimisation of

film stability and amine content by using, 1,3-butadiene, in which the presence of two C–C double bonds is expected to facilitate the formation of a highly cross-linked, stable macromolecule. We chose to focus our study on the effect of the following plasma parameters: (i) plasma power, (ii) gas flow ratio, $R (F_{NH_3}:F_{HC})$, where HC is either ethylene, butadiene or a mixture of both and (iii) HC gas flow ratio, $R_{HC} (F_{C_4H_6}:F_{C_2H_4})$ on the co-polymerised ethylene-butadiene based films. We first present the effect of plasma parameters on the surface nitrogen concentration, $[N]$, amine concentration, $[-NH_2]$, and water stability of the coatings, which were investigated by performing XPS, chemical derivatisation XPS and immersion experiments followed by profilometric measurements of film thickness change. Next, empirical models for nitrogen content and water stability were obtained by using a multiple linear and a non-linear regression procedure based on least squares, respectively. The last part is focussed on a functional group analysis where the chemistry of the films have been discussed in-depth by using HR-XPS, ATR-FTIR and OES spectra.

The development of an empirical model for this study is intended to lead to an optimisation of a compromise between the two aforementioned key variables, amine content and water stability of the plasma polymer films.

5.2 Experimental section

5.2.1 Deposition of plasma polymer coatings

Plasma polymer films were deposited on silicon wafers using a Plasma Enhanced Chemical Vapour Deposition (PECVD) system. The substrates, 1 x 1 cm² squares of 500 μm thick (100) p-type silicon wafers (Ted Pella, Inc.) were cleaned ultrasonically first in water and then isopropanol, for 5 minutes each, prior to deposition. A cylindrical stainless steel vacuum chamber, approximately 20 cm in diameter and 50 cm in height was used to deposit the

coatings (Figure 5.1). A turbo-molecular pump, backed by a two-stage rotary vane pump was used to evacuate the chamber to high vacuum. High-purity gases (ethylene 99.999 %, 1,3-butadiene 99.8 % and ammonia 99.99 %, Megs, Inc.) were then introduced to the chamber using electronic mass flow controllers (Brooks Instrument), through a "shower head" gas distributor (~ 10 cm in diameter). The operating pressure, during plasma deposition was set constant at 80Pa by a throttling gate valve, in combination with a capacitance pressure gauge (Nor-Cal Products, Inc.). The low-pressure capacitively coupled r. f. (13.56 MHz) glow discharge was generated via an impedance matching network (Advanced Energy) connected to a 10 cm diameter powered electrode in the centre of the chamber, with the walls of the chamber acting as the grounded electrode. The distance between the bottom of the shower head and the powered electrode was ~ 4 cm.

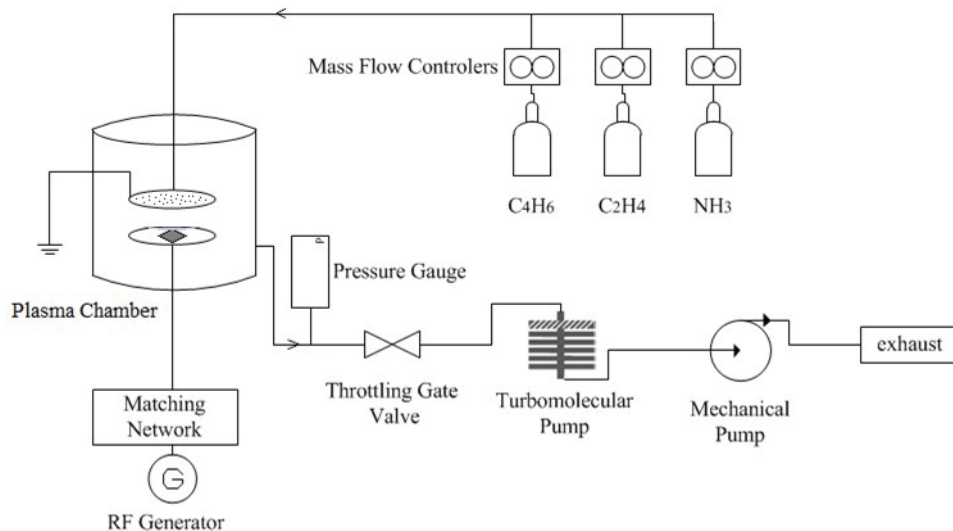


Figure 5.1: Schematic diagram of the low-pressure, capacitively coupled r.f. PECVD reactor used for depositing thin PP films.

In this work, PPE:N and PPB:N correspond to N-rich Plasma Polymerised Ethylene and Butadiene based films, respectively. Similarly, PCEB:N refers to N-rich Plasma Copolymerised Ethylene-Butadiene based films. F_T is the total flow rate of the hydrocarbon gases. All flow rates, F_x , are given in standard cubic centimeters per minute (sccm). R was always varied by varying the ammonia gas flow rate and keeping the HC gas flow rate

constant.

5.2.2 Materials characterization

X-ray Photoelectron Spectroscopy (XPS) analyses were performed 24 to 30 h after deposition in order to maintain a consistent effect of ageing, in a Thermo Scientific K-Alpha XPS instrument, using monochromated Al $K\alpha$ X-rays, producing photons of 1486 eV acquired at take-off angles (TOA) = 0° (normal to the surface). Wide scans with step size 1 eV, pass energy 160 eV, dwell time 200 ms and in the range 1200 to -10 eV were acquired for each sample. Narrow scans were also acquired for the C 1s peak with step size 0.1 eV, pass energy 20 eV, dwell time 200 ms and in the range 300 to 275 eV. The BE scale was calibrated with respect to the carbon (C 1s) peak at binding energy, BE = 285.0 eV. The relative sensitivity factors of C 1s, N 1s, O 1s and F 1s used are 1, 1.8, 2.93 and 4.43 respectively. C 1s high-resolution (HR) core-level spectra were analysed using the CasaXPS (Casa Software Ltd, <http://www.casaxps.com/>) software version 2.3.16. A few samples were also analysed by FTIR in the ATR mode, using a spectrometer (Digilab FTS7000-UMA600) equipped with a mercury cadmium telluride (MCT) detector. In addition, optical emission spectroscopy (OES) was performed to gain some insight into the interaction between the gas species in the plasma. The setup consisted of a fiber optic cable (Solarization-Resistant Multimode Patch Cables for UV, Thorlabs) connected to a portable spectrometer (OceanOptics USB2000).

Derivatization with 4-trifluoromethyl benzaldehyde (TFBA). A selective derivatization procedure with TFBA (98 % assay, Sigma Aldrich) followed by XPS analysis was performed no later than 25 h after deposition, to determine the surface concentration of primary amines. The experiment involves a gas-solid phase reaction, wherein the TFBA vapour is covalently linked with the $-NH_2$ groups at the film surface via imine bonds and the $[-NH_2]$ is calculated using the fluorine concentrations, [F], obtained by XPS, using the

following equation.⁴²

$$[-NH_2]_u = \frac{[F]_d}{3[N]_d} \times [N]_u \quad (5.1)$$

The reaction was carried out in a small glass jar wherein 4 to 5 drops of TFBA were dripped onto a ~ 1 cm thick layer of glass beads. The samples were placed on a microscope slide, which was then placed on the layer of glass beads, thereby avoiding direct contact with the TFBA liquid. The glass jar was then flushed with argon and placed in an oven at 45°C for 3 h, allowing sufficient time to convert all near-surface amine groups.^{29,42,103} It is noteworthy that recent work strongly suggests that TFBA is selective not only towards primary amines but also reacts with imine groups on the coating,⁶⁷ which are usually generated during plasma polymerisation due to high fragmentation of monomer molecules and subsequent re-arrangement that occur under high plasma powers. Surface charge studies conducted by Babaei et al.⁹ from this laboratory, show that an increase in R leads to a clear increase in positive charge on these films. Therefore, it can be assumed that amine groups being responsible for this positive charge contribute to a significant portion of N functional groups that are present on the surface.

Water stability. Stability was evaluated as the percentage loss in film thickness after immersion in DI water for 24 h. After immersion, samples were dried using a nitrogen flow and left outside for at least 10 minutes. Before and after 24 h exposure to aqueous media, the thickness of the dry samples was measured using a Dektak profilometer. The coating deposited on the silicon wafer was scratched down to the substrate using a sharp needle, and the resulting step height (thickness) was measured.

5.3 Results and discussion

5.3.1 Optimisation of [-NH₂] and stability

5.3.1.1 PPE:N vs. PPB:N - Effect of R and power

A series of PPE:N and PPB:N films deposited using mixtures of the corresponding hydrocarbon gas and ammonia were characterised in terms of the deposition rate, water stability, nitrogen and ammonia surface concentrations. The effect of power (10W and 20W) and the gas flow ratio (R) on the aforementioned film characteristics are shown in Figure 5.2. Figure 5.2a shows the film deposition rates, which decrease with the increase in R . Within the plasma zone, there exist a competition between "deposition" and "ablation" (chemical sputtering) promoted by ammonia which acts as an etchant for organic materials.^{128,129} As R is increased, "ablation" process becomes significant resulting in a decrease in deposition rate. Here, it is also apparent that the PPB:N's deposit at a faster rate than the PPE:N films. The more unsaturated structure of the butadiene molecule leads to more stable conjugated radical species in the plasma. Thus, increased active species of butadiene in the plasma results in an increased conversion of the species into a solid deposit. In addition, for a given gas flow rate, the ammonia-butadiene plasma contains more carbon than the ammonia-ethylene plasma. The high water stability of PPB:N films, as shown by Figure 5.2b, is due to a high degree of cross-linking in PPB:N films which enables most of the film thickness to be retained during exposure to water, suggesting that the PPB:N's possibly contain less loosely bound oligomers compared to PPE:N films.

The extent of conjugation in organic molecules has an effect on the energy required for electronic excitation. The electronic transition, $\pi \rightarrow \pi^*$, is the lowest and the most important transition observed in alkenes, and this transition in 1,3-butadiene requires a lower energy

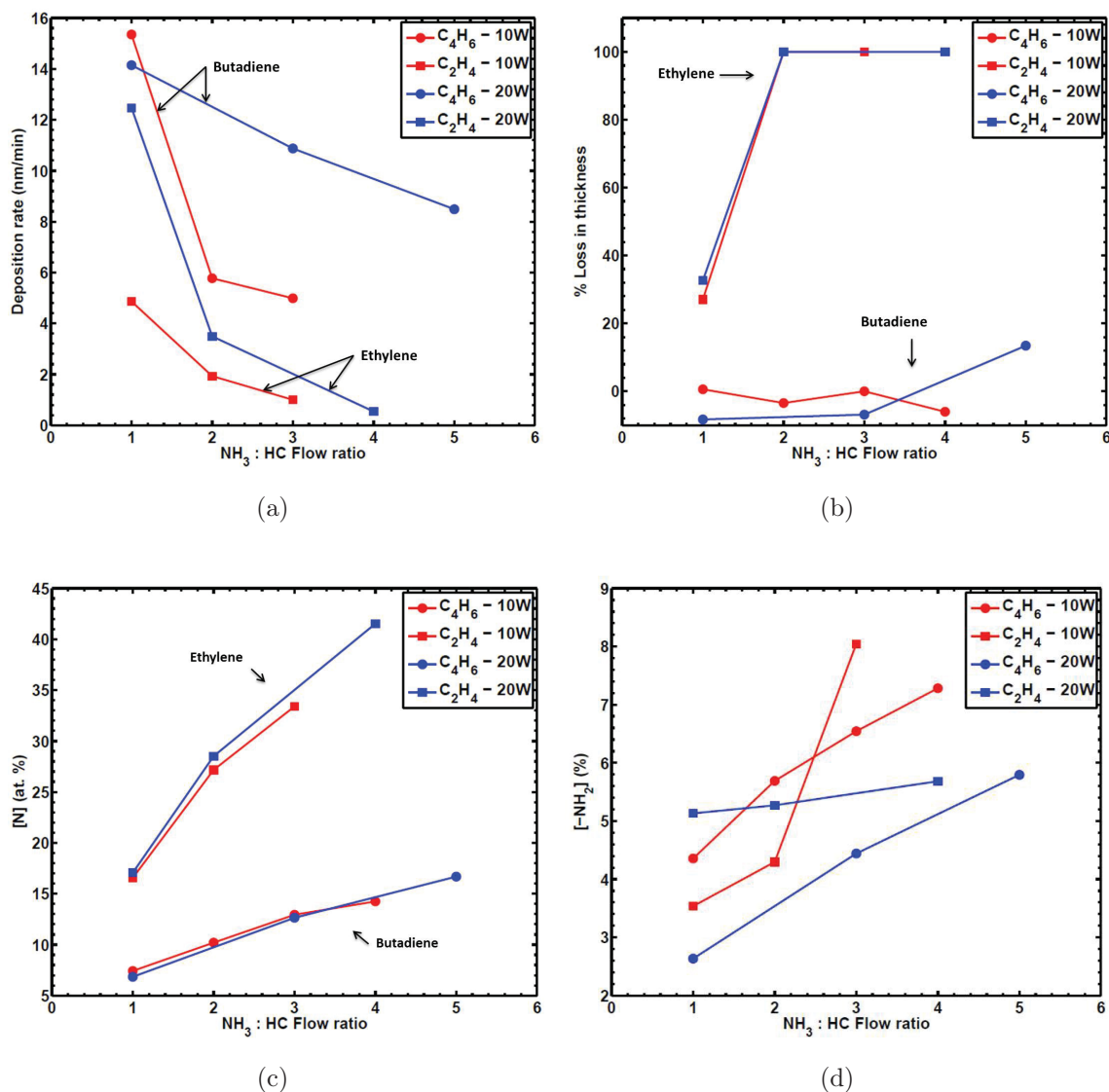


Figure 5.2: Characterisation of PPB:N (circles) and PPE:N (squares) films: (a) Deposition rate ($\text{nm}\cdot\text{min}^{-1}$) (b) % loss in thickness (c) [N] (at. %) and (d) [-NH₂] (%), as a function of R for different powers: 10 W (red) and 20 W (blue). F_{HC} was maintained constant at 5 sccm at 10 W and 10 sccm at 20 W.

than that in ethylene,¹³⁰ consequently, the bond dissociation energies for 1,3-butadiene and ethylene are known to be 418 and 682 kJ/mol, respectively.¹³¹ Hence, for the same HC gas flow rate, a higher concentration of excited butadiene species is expected to be present in the plasma than that of excited ethylene species, which in turn suggests that for the same gas flow ratio, R , the resulting PPB:N film deposited may contain a higher concentration

of carbon than that of the corresponding PPE:N film; thus, explaining the lower [N] values observed for PPB:N in this study (Figure 5.2c). Nevertheless, when PPB:N and PPE:N films with similar [-NH₂] are compared (Figure 5.2d), it can be deduced that the amine selectivity ([-NH₂]/ [N]) for PPB:N is higher than for PPE:N films. This was a motivating observation to further investigate the use of butadiene in optimising the [-NH₂] and stability of plasma polymer films.

5.3.1.2 PCEB:N - Effect of R_{HC} , F_T and power

Figure 5.3 shows results of plasma co-polymerised ethylene and butadiene based films as a functions of R_{HC} . As the concentration of butadiene in the plasma is increased the rate of film deposition and stability also increase, while the values of [N] and [-NH₂] decrease. These observations reflect the effect of butadiene in the characteristics of the resulting plasma co-polymerised films. Higher deposition rates, higher [N] and [-NH₂] are observed at 20W, showing that a higher power consumes more of the monomers available for the given pressure and gas flow rate. This can also be explained by the macroscopic approach discussed by Hegemann et al.,²⁰ where the growth mechanism during plasma polymer deposition involves reactions in an "active plasma zone", which is the bulk plasma, and a "passive zone", which is the surface growth region and the associated plasma sheath (shown in a schematic by Hegemann et al.²⁰). The gas molecules, when introduced into the chamber, are assumed to first travel through the active plasma zone where they undergo radical formation in the gas phase resulting in reactive species, which then enter the passive zone where they recombine to form a stable solid film. Based on this macroscopic approach, plasma polymerisation is governed by the energy invested per particle of the gas mixture during its flow through the active plasma zone. As the energy input per molecule is increased by increasing the plasma power, the more energetic ion bombardment leads to higher generation rate of nucleation sites on the film surface, which may explain the resulting increase in the deposition rates

and functional group incorporation.²⁰

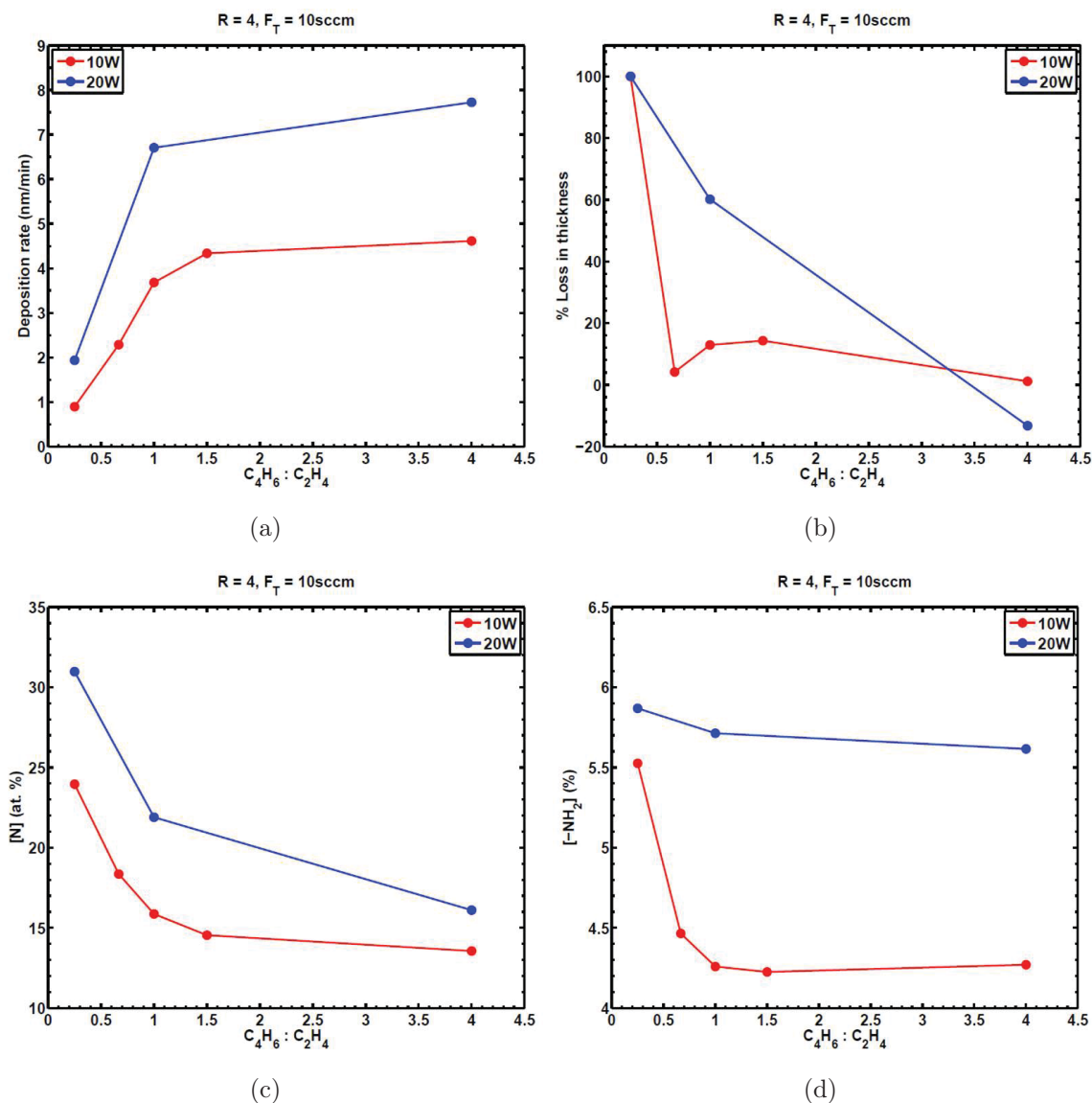


Figure 5.3: PCEB:N films: (a) Deposition rate (b) % loss in thickness (c) [N] and (d) [-NH₂], as a function of R_{HC} for different powers: 10 W (red) and 20 W (blue). $F_T = 10$ sccm and $R = 4$.

Effect of the total HC flow rate, F_T , on the properties of PCEB:N films are shown by Figure 5.4. It can be seen from Figure 5.4a that, although R_{HC} is maintained constant at 0.25, the deposition rates of PCEB:N films with $F_T = 10$ sccm (circles) are higher than that of PCEB:N's with $F_T = 20$ sccm (squares) deposited under the same power and R . This can be explained in terms of the energy supplied per molecule, where it is higher at

$F_T = 10$ sccm and as a result, higher conversion of monomer molecules into a thin film is observed at the smaller F_T value. This observation is in agreement with the work published by Hegemann et al.²⁰ Similarly, Figure 5.4c and 5.4d show that at the higher F_T value the [N] and [-NH₂] in the films were lower, for the same power. Correspondingly, films deposited with the higher F_T value show better water stability (Figure 5.4b).

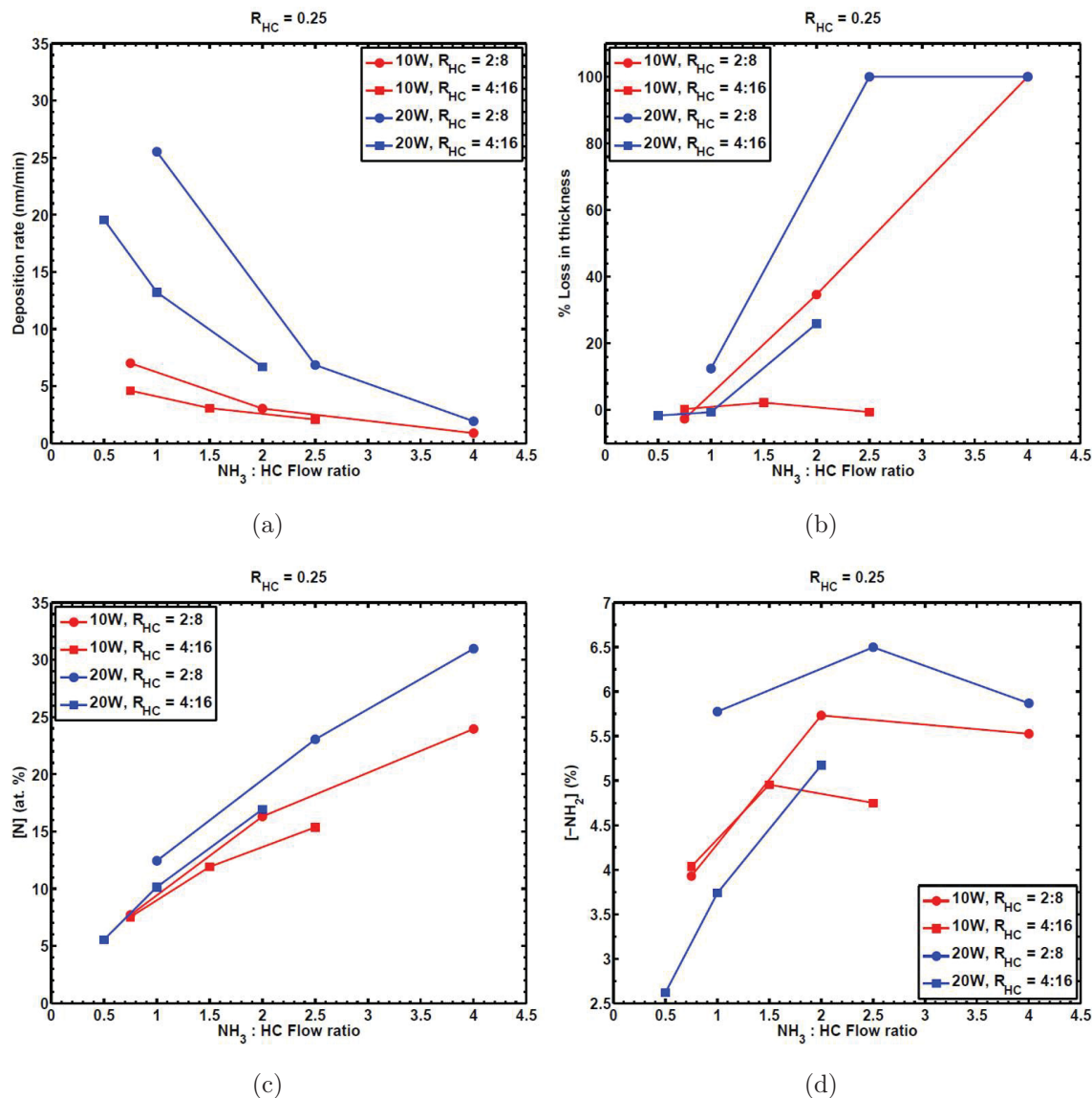


Figure 5.4: PCEB:N films: (a) Deposition rate (b) % loss in thickness (c) [N] and (d) [-NH₂], as a function of R for different F_T values: 10 sccm (circles) and 20 sccm (squares). $R_{\text{HC}} = 0.25$.

Figure 5.5 shows the effect of plasma power, ranging from 10W to 50W, on the PCEB:N

film properties. Increase in power leads to an increase in deposition rate (Figure 5.5a green squares) as well as [N] (Figure 5.5b blue circles). However, the [-NH₂] increases, reaches a maximum at 30W and drops sharply as the power is further increased up to 50W (Figure 5.5b green squares). This suggests that there exists a low power region wherein an increase in power leads to higher conversion of ammonia to amine groups in the solid deposit and a high power region wherein an increase in power leads to a high degree of fragmentation of ammonia molecules leading to a decrease in NH₂ radicals in the active plasma zone. The stability of these films, shown by Figure 5.5a (blue circles) seems to be governed by the films' [-NH₂]. The unstable nature of films deposited above 30 W may be explained by low cross-link density due to extensive monomer fragmentation that occur at high powers.

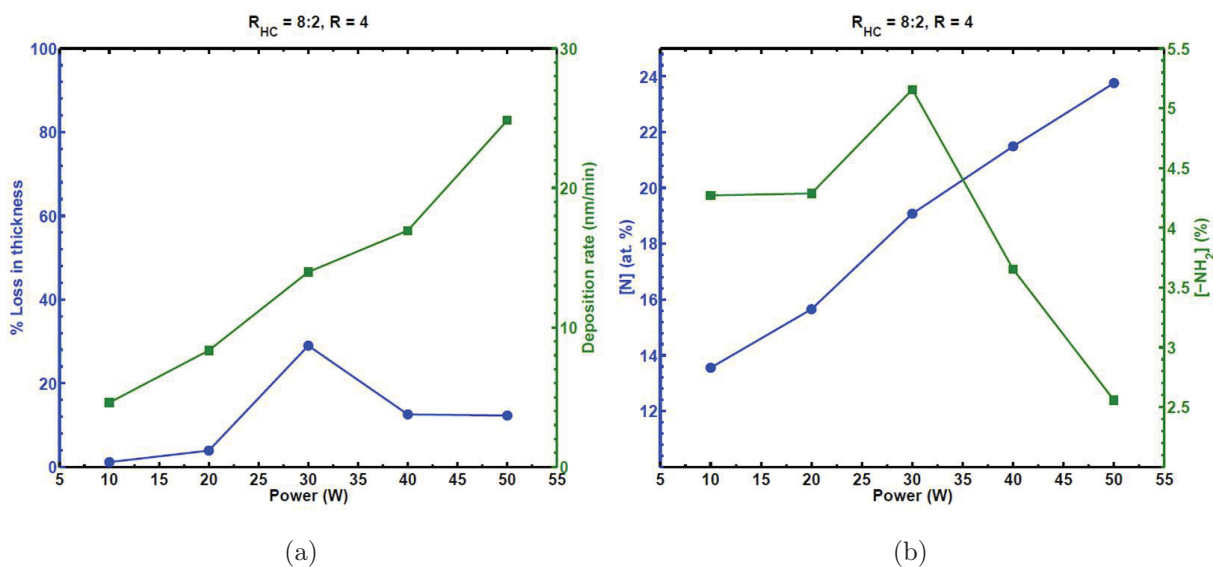


Figure 5.5: PCEB:N films: (a) % Loss in thickness (blue) and deposition rate (green), and (b) [N] (blue) and [-NH₂] (green), as a function of power. $R_{HC} = R = 4$.

5.3.2 Regression analysis of [N] and stability

5.3.2.1 Multivariate linear regression model for [N]

A multiple linear regression model has been fitted to the experimental data,¹³² using MS Excel 2010, in order to determine a relationship between the regressor variables gas flow ratio, total HC gas flow rate, power, hydrocarbon gas flow ratio; and the response variable, nitrogen concentration. From the experimental data, it is reasonable to assume a linear trend, where the interaction between the regressor variables has also been taken into account. The number of observations used were 50, 19 and 55 for modelling the PPB:N, PPE:N and PCEB:N films, respectively. The general model equation is given by Equation 5.2,

$$\hat{y} = \beta_0 + \sum_{i=1}^n \beta_i x_i \quad (5.2)$$

where \hat{y} is the [N] estimated by the model, β parameters are the regression coefficients and x_i 's are the regressor variables and their interaction factors. Parameters denoted by each regressor variable are listed in Table 5.1. An individual t-test, as mentioned in Montgomery, Runger and Hubele (2011),¹³² was performed on each regression coefficient obtained to determine the significance of the corresponding regressor variable. Regression coefficient values along with their p values corresponding to each significant regressor variable are listed in Table 5.2. The adjusted coefficients of multiple determination ($R_{adjusted}^2$) were calculated as 0.942, 0.916 and 0.958 for PCEB:N, PPB:N and PPE:N films, respectively. In order to validate the adequacy of the model, the residual plot (residuals vs. \hat{y}) of each model was examined. The residuals being evenly distributed around zero confirmed the model assumptions that the errors are uncorrelated random variables, normally distributed with mean

zero.

Table 5.1: List of regressor variables

PCEB:N	PPE:N	PPB:N
$x_1 = R$	$x_1 = R$	$x_1 = R$
$x_2 = F_T$	$x_2 = F_T$	$x_2 = F_T$
$x_3 = Power$	$x_3 = Power$	$x_3 = Power$
$x_4 = R_{HC}$	$x_4 = x_1x_2$	$x_4 = x_1x_2$
$x_5 = x_1x_2$	$x_5 = x_2x_3$	$x_5 = x_2x_3$
$x_6 = x_2x_3$	$x_6 = x_1x_3$	$x_6 = x_1x_3$
$x_7 = x_3x_4$		
$x_8 = x_1x_3$		
$x_9 = x_1x_4$		
$x_{10} = x_2x_4$		

Table 5.2: Values of the significant regression coefficients ($p < 0.05$) of the nitrogen concentration model. p values are shown in parentheses.

PCEB:N	PPE:N	PPB:N
$\beta_0 = 12.633$	$\beta_0 = 6.300$	$\beta_0 = 5.062$
$\beta_2 = -0.237 (5.423E - 5)$	$\beta_1 = 7.866 (2.577E - 12)$	$\beta_1 = 1.751 (5.180E - 17)$
$\beta_4 = -11.085 (2.272E - 2)$	$\beta_3 = 0.243 (2.485E - 2)$	$\beta_6 = 0.039 (5.121E - 11)$
$\beta_5 = 0.132 (1.127E - 4)$		
$\beta_7 = -0.074 (2.381E - 2)$		
$\beta_8 = 0.170 (3.382E - 18)$		
$\beta_9 = 2.771 (1.524E - 2)$		
$\beta_{10} = -0.194 (2.807E - 2)$		

5.3.2.2 Multivariate non-linear regression model for stability

Water stability of films, presented as a percentage of film thickness loss, is assumed to take on values from 0 to 100, with the variation of plasma parameters. Hence, an S-shaped curve, considering the interaction between parameters, was fitted to model the non-linear behaviour of film water stability, using the 'nlinfit' function of Matlab R2012b, which estimates the unknown β parameters by an iterative procedure to minimise the sum of squares of errors of prediction. The model is given by Equation 5.3,

$$\hat{y} = \frac{1}{1 + \exp[-(\beta_0 + \sum_{i=1}^n \beta_i x_i)]} \times 100 \quad (5.3)$$

where \hat{y} is the % loss in film thickness estimated by the model and, β and x are the same notations as seen in the nitrogen concentration model. A valid model could only be obtained for the PCEB:N films. For other films, it could not be obtained due to an insufficient number of unstable films in the case of PPB:N films and an insufficient number of stable films in the case of PPE:N films. The number of observations used was 55. As the model equation cannot produce negative values, all the negative values of film stability were corrected to zero. Similarly to the modelling of [N], the significance of the regression coefficients was examined by a t-test and the values of the significant regression coefficients are listed in Table 5.3, along with the respective p values. The $R^2_{adjusted}$ was calculated as 0.751. The residual plot was examined to be evenly distributed around zero which confirms the adequacy of this model.

Table 5.3: Values of the significant regression coefficients ($p < 0.05$) of the water stability model. p values are shown in parentheses.

PCEB:N
$\beta_0 = 4.505$
$\beta_3 = -0.254 (2.217E - 5)$
$\beta_5 = -0.128 (3.452E - 5)$
$\beta_7 = -0.676 (1.363E - 4)$
$\beta_8 = 0.173 (7.453E - 6)$

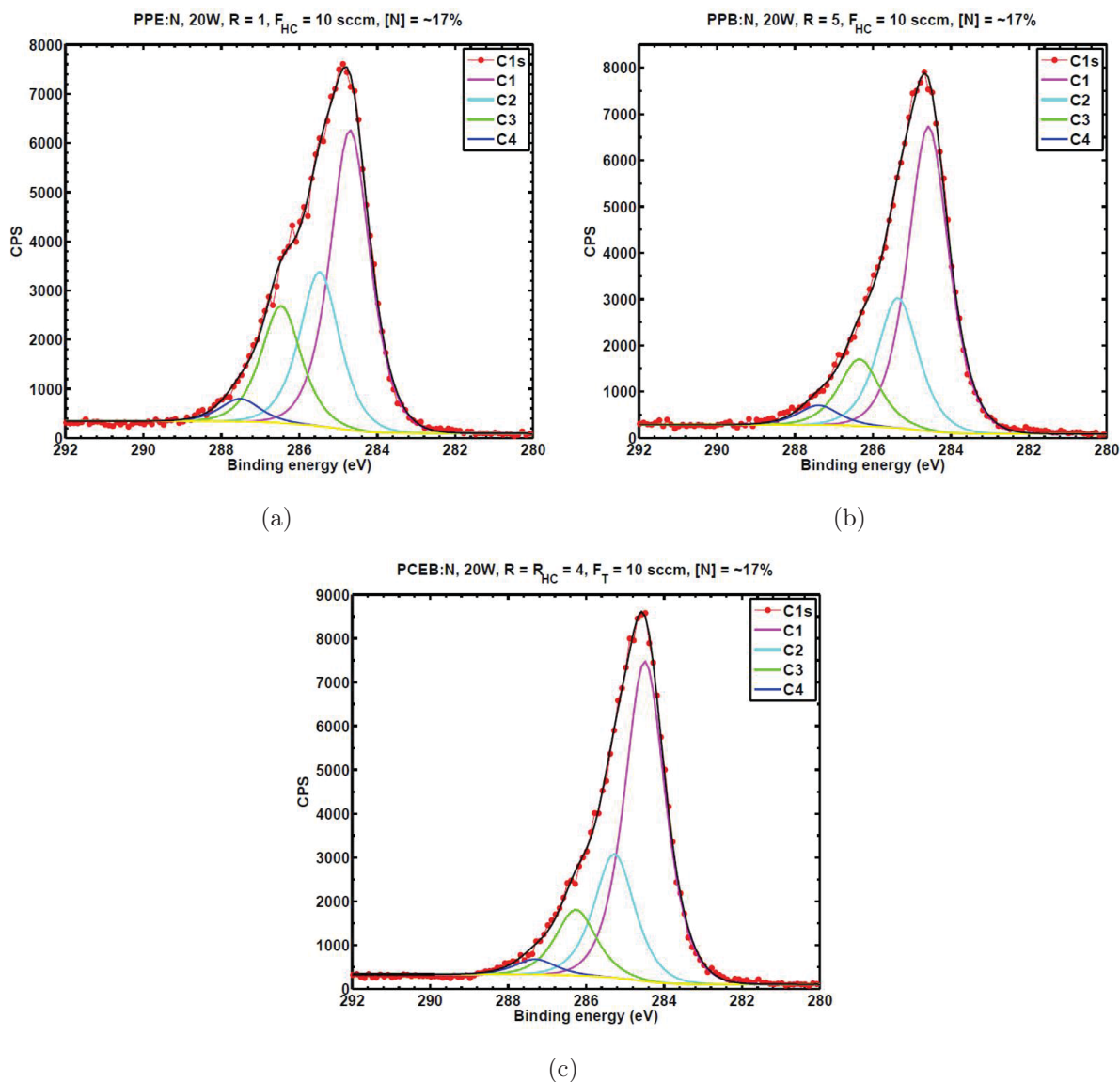


Figure 5.6: High-resolution C 1s spectra for (a) PPE:N (b) PPB:N and (c) PCEB:N films, fitted with four component-peaks. fwhm 1.2 eV, peak shape GL(70). The [N] of all three films was approximately 17%.

5.3.3 Functional group analysis

5.3.3.1 HR-XPS

The nature of chemical bonding in the plasma polymer films was investigated by performing HR-XPS. High-resolution C 1s spectra were obtained and fitted with four component peaks,

labelled C1, C2, C3 and C4. For all films, these sub-peaks were placed at fixed binding energy positions relative to the C1 peak, following a procedure reported elsewhere.¹³³ The chemical shifts of these peaks relative to C1 are: C2 at +0.78 eV, C3 at +1.77 eV and C4 at +2.82 eV. The Gaussian-Lorentzian product peak shape parameter (Casa XPS) was set at 70 to obtain the best overall fits. Due to the structural complexity of plasma polymers one cannot fully determine the exact chemical bonding states attributed to these components. Nevertheless, it can be useful in identifying the extent of different heteroatomic bonding (N and O) to the hydrocarbon backbone of the plasma polymer. Typically, the C1 peak corresponds to the lowest electronegative bonding states such as C–C, C=C and C–H; C2 to C–N (amino groups); C3 to C–O, C=N, C*–C≡N and C4 to the highest electronegative states such as C=O, N–C=O and N–C–O. The high resolution C 1s spectra of a PPE:N, PPB:N and PCEB:N film containing approximately the same [N] of 17 % are presented in Figure 5.6. It is noted that the C3 and C4 component peak areas of the PPB:N film are smaller than that observed for the PPE:N film, which implies that more carbon atoms linked to heteroatoms via sigma bonds, such as in amino groups, exist in the PPB:N film; this appears to relate well to the previously discussed higher amine selectivity of PPB:N films.

Figure 5.7 presents the evolution of the relative areas of the peak fit components of the high resolution C 1s spectra as a function of R for PPE:N and PPB:N films and R_{HC} for PCEB:N films. It is clear that the C3 and C4 component peaks are much higher in all of the PPE:N's than in PPB:N films for the same R value. This is in accordance with the [N] and [-NH₂] values where it reaffirms that PPB:N films have a higher selectivity of [-NH₂] compared to PPE:N films. Figure 5.7c further compliments this observation as it shows a net reduction in the C3 and C4 components and a net increase in the C2 component as the concentration of butadiene in the plasma is increased.

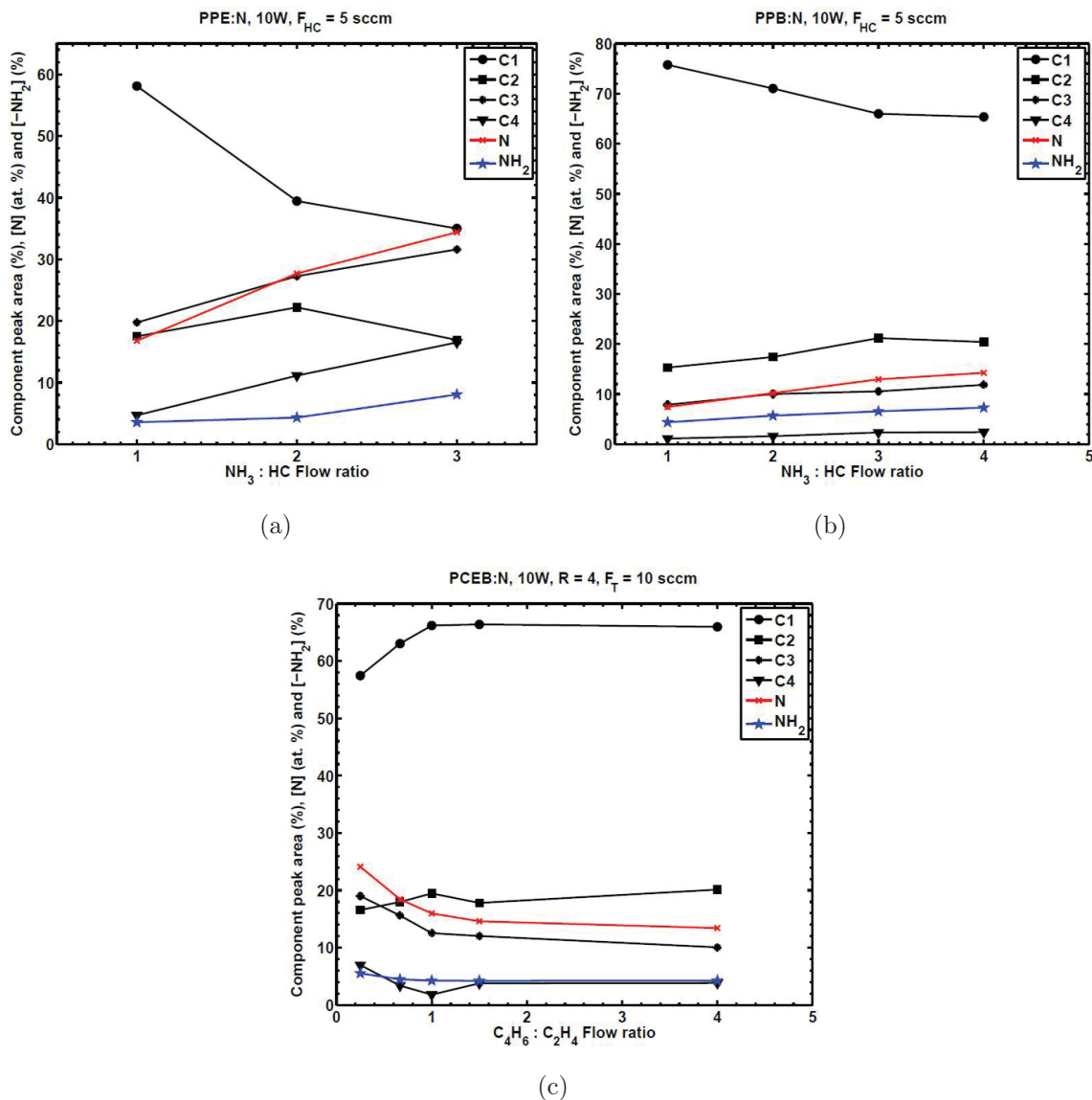


Figure 5.7: Evolution of the different component-peaks of the high-resolution C 1s spectra, [N] and [-NH₂] as a function of R for (a) PPE:N (b) PPB:N and R_{HC} for (c) PCEB:N films.

5.3.3.2 FTIR

The same PPE:N, PPB:N and PCEB:N films ($\sim 17\%$) analysed by HR-XPS (Figure 5.6) were also analysed by ATR-FTIR to confirm whether or not the type of hydrocarbon gas used affected the extent to which different functional groups were incorporated into the film (Figure 5.8). The main functional groups shown to be present are amines, nitriles and

amides. In contrast to HR-XPS data, a notable difference in the chemistry between films could not be observed by the FTIR spectra, suggesting that while some differences exist between the films, there appears to be a strong similarity in their chemical structure.

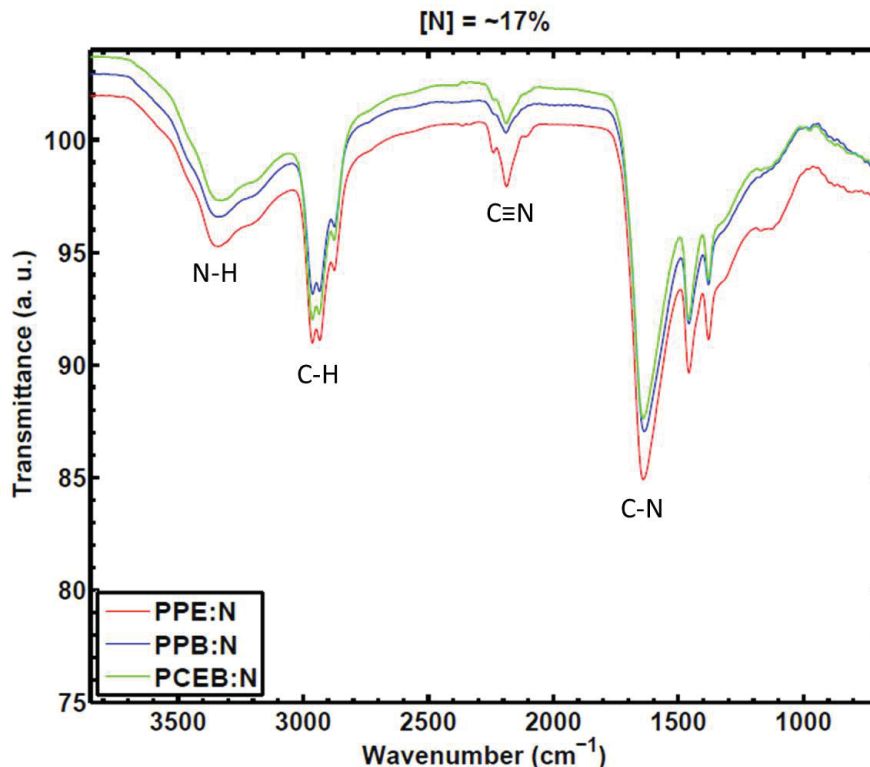


Figure 5.8: ATR FTIR spectra of a 17 % [N] PPE:N, PPB:N and PCEB:N film.

5.3.3.3 OES

The chemical species in the plasma discharge observed through optical emission spectroscopy is shown to determine the surface functionality of the plasma polymer coating.¹³⁴ Figure 5.9 shows the emission spectra for butadiene-ammonia (B-A) and ethylene-ammonia (E-A) plasmas studied at 10 W and 20 W. As a result of decomposition and recombination reactions of NH_3 , several transition peaks can be seen in the spectra. Decomposition of NH_3 under plasma conditions results in the formation of NH_2 and NH radicals with the final step being a bi-molecular recombination of NH radicals to form stable N_2 and H_2 species.^{135,136} As

the plasma power was increased from 10 W to 20 W, the intensities of N_2 (315.9, 337.1, 353.7 nm),¹³⁷ NH (336.5 nm) and CN (388.8 nm)¹³⁸ species also increased, suggesting that at higher power, the higher energy per particle results in increased reaction between the precursor gases, as well as decomposition of NH_3 yielding more stable N_2 species than the unstable and reactive NH and NH_2 species.¹³⁴ The emission line of NH at $\lambda = 336.5$ nm overlaps with that of N_2 at $\lambda = 337.1$ nm and the NH_2 spectral lines are not observed by OES which is attributed to their inherently weak intensity as compared to NH.¹³⁹

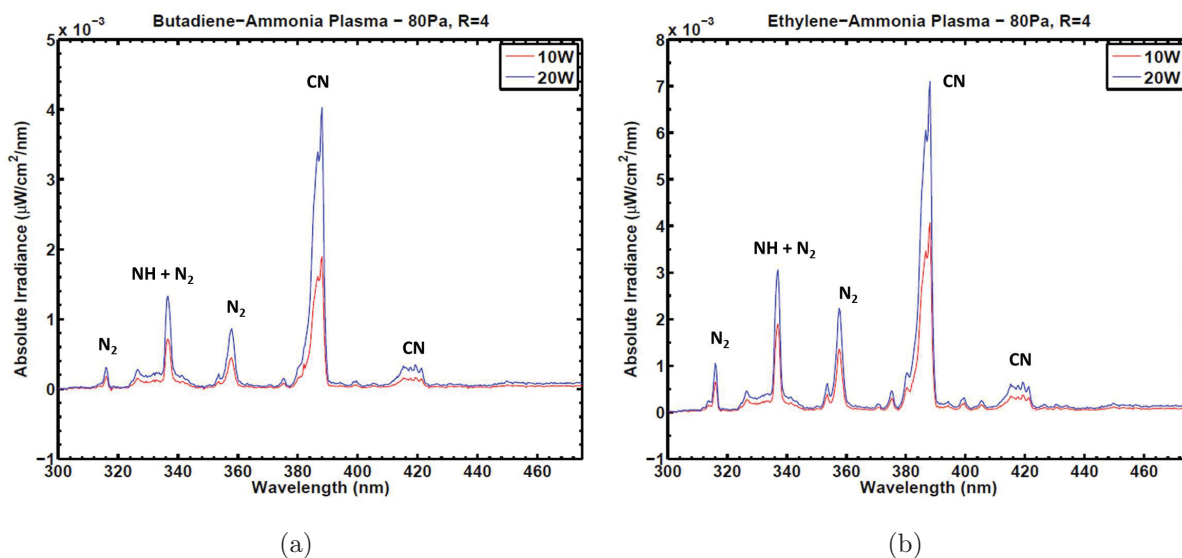


Figure 5.9: Effect of power on OES spectra of a) B-A plasma and b) E-A plasma. $F_{HC} = 10$ sccm.

Effect of R on the chemical species is shown by Figure 5.10 where it can be seen that for PPB:N films, the intensity of all peaks increase with R . However, in the case of PPE:N films, a significant drop in the CN peak at $R = 4$ is observed. From the deposition kinetics of PPE:N films discussed earlier, the very low deposition rates at $R = 4$ suggested that etching processes dominated the deposition at high gas flow ratio. Therefore, the drop in CN peak at $R = 4$ may be attributed to effects of etching where more C species may be sputtered into the plasma, reducing the probability that a C species will react with a N species. From both the Figure 5.9 and 5.10, it is apparent that the emission intensities of species in the E-A plasma were higher than that in the B-A plasma. These observations are attributed to

the complexity of the plasma process which may be explained by a combination of several reasons such as (i) the N to C ratio being higher for an ethylene-ammonia gas mixture than for a butadiene-ammonia gas mixture at the same R value, (ii) the bond dissociation energy of butadiene molecule (418 kJ/mol) being lower than that of ethylene (682 kJ/mol) as well as ammonia (435 kJ/mol), and (iii) the increased etching effects exhibited in an E-A plasma compared to a B-A plasma, as suggested by the deposition kinetics.

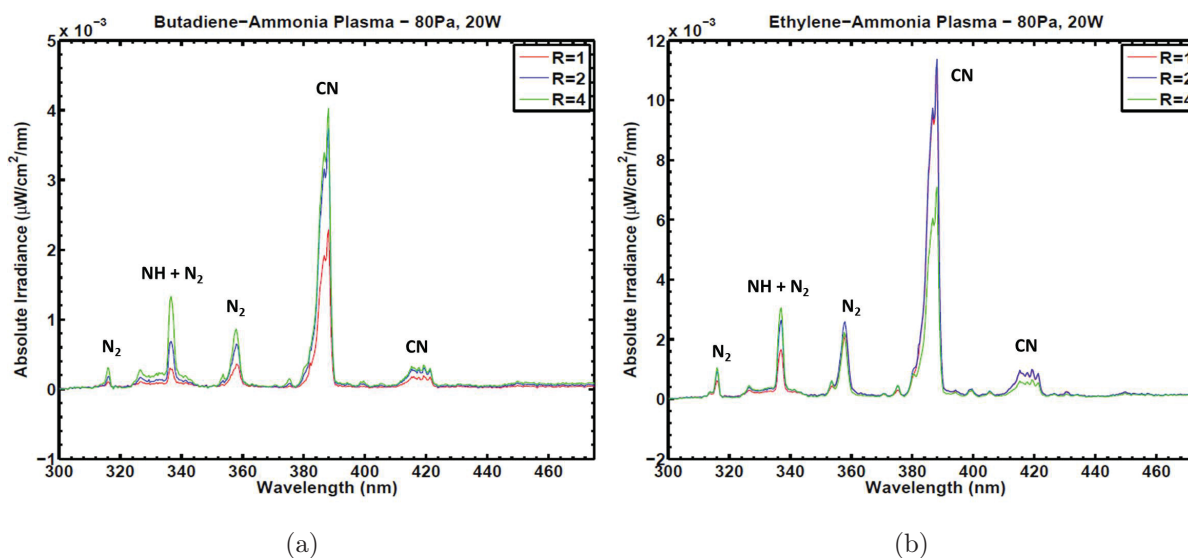


Figure 5.10: Effect of R on OES spectra of a) B-A plasma and b) E-A plasma. $F_{HC} = 10$ sccm.

5.4 Conclusions

The nature of the plasma polymer film deposited depends upon several plasma parameters, such as gas flow ratio, power, total gas flow rate and also the type of hydrocarbon gas used. Ethylene based plasma polymer films have been studied to be highly unstable in aqueous media at high amino group concentrations. The goal of this work being to study the plasma conditions to yield coatings with a maximum $[-\text{NH}_2]$ and water stability, we used 1,3-butadiene which, owing to its more unsaturated structure, could be reasonably expected

to yield highly cross-linked films with better water stability. The [N], [-NH₂] and water stability of the plasma polymer films were studied with the variation of R , power, R_{HC} , F_T and the type of HC gas used. It was found that the [N] increased with R and power but decreased with R_{HC} and F_T . The [-NH₂] was also shown to increase with R but decrease with R_{HC} and F_T . With power, the [-NH₂] increased, reached a maximum at 30W and decreased sharply. The lower [N] and [-NH₂] observed at higher F_T are attributed to the lower energy per molecule available at higher F_T value. Water stability largely depended upon the [-NH₂] of the film as well as the HC gas used. It was clear that the PPB:N films were more stable than the PPE:N films with the same [-NH₂], which is explained by the increased cross-link density in the plasma polymer deposited using butadiene. PPB:N films also showed better amine selectivity than the PPE:N films. Although the amine content values obtained were not considerably better than those previously published by Ruiz et al.,¹⁰³ it can be attributed in the well-acknowledged inter-laboratory variability in plasma related processes and analysis methods. Nevertheless, it is evident that butadiene based films performed better than the ethylene based films within the scope of our study. The distinct water stability of butadiene based films offers a good platform for the development of surfaces for biomedical applications.

Acknowledgements

The authors are grateful to Natural Sciences and Engineering Research Council of Canada (NSERC), Canada Foundation for Innovation (CFI) and the Fonds de Recherche du Québec - Nature et Technologies (FRQNT) for their financial support.

Chapter 6

Plasma Polymer Films to Regulate Fibrinogen Adsorption

This chapter presents the manuscript titled, *Plasma Polymer Films to Regulate Fibrinogen Adsorption: Effect of Pressure and Competition with Human Serum Albumin*, to be submitted to a peer-reviewed journal. It starts with a continuation of the optimisation step covered in the previous manuscript. The study involves the effect of pressure on N-plasma polymers, as pressure is an important governing parameter of the plasma polymerisation process. It yielded interesting results relating to the influence on the film amine content, aqueous stability as well as Fg adsorption. The next part of the study focuses on investigating different types of plasma polymer coatings to regulate the extent of Fg adsorption. Here, an O-rich coating and a Pt coating are also included. Finally, a subset of these coatings are chosen to investigate the influence of human serum albumin (HSA) on Fg adsorption. It is shown that, in spite of some adsorption behavioural changes observed, the coatings are able to adsorb the protein to different extents even in the presence of a high concentration of competing HSA.

Plasma Polymer Films to Regulate Fibrinogen Adsorption: Effect of Pressure and Competition with Human Serum Albumin

Abstract

Ethylene and 1,3-butadiene based plasma polymer films (PPFs) containing N- and O-groups are deposited using plasma enhanced chemical vapour deposition to regulate fibrinogen (Fg) adsorption in the presence of human serum albumin (HSA), with the long-term intention of achieving control over platelet activation. This work includes a study of the effect of pressure, in characterising the film's N content, nucleophile groups such as primary amines and imines, stability in PBS for 1 h and 24 h, and affinity for Fg adsorption. Tribometry tests against a polyethylene surface, in phosphate buffer solution, indicated that N-rich films were more susceptible to wear than the O-rich coating. Protein adsorption is monitored using surface plasmon resonance and surface plasmon fluorescence spectroscopy. HSA adsorption kinetics indicated a distinct peak in the kinetic curve which is attributed to a bilayer formation of HSA molecules owing to adsorption from a highly concentrated bulk solution. Results conclude that Fg adsorption in the presence of a high concentration of competing HSA molecules can still be regulated by the careful choice of surface chemistry in the PPFs.

6.1 Introduction

Thrombogenicity is a crucial aspect to be considered in the development of medical implants. It is broadly defined as the extent to which a device, intended for use in contact with biological tissues and fluids, causes a localised accumulation of protein and cellular blood elements leading to blood clot formation, compromising the proper functioning of the device. While

in most cases, thrombogenic devices are undesirable, in some cases, they are considered useful. This is the case in the endovascular treatment of intracranial aneurysms, a localised dilatation of a blood vessel wall in the brain. This minimally invasive treatment involves inserting small platinum coils into the aneurysm using a catheter. This method relies upon the thrombogenicity of the coils to induce a blood clot formation in the aneurysm, seal it and thereby separate it from the main blood flow, thus preventing it from further expansion and rupture. The main concern with this treatment is the instability of the thrombus formed which causes recanalisation and re-growth of the aneurysm.¹⁴ Research has been done in order to study the effects of less and more thrombogenic coils compared to Pt^{140–142} and yet, the role of the extent of coil thrombogenicity on aneurysm healing remains unclear. In light of providing a platform to achieve the long term goal of studying the effect of coil thrombogenicity on aneurysm healing, we have presented the design and characterisation of a series of functional plasma polymer coatings that render varying degrees of affinity for a blood clotting protein, fibrinogen (Fg).

Fg is a blood plasma protein that plays a vital role in the regulation of thrombosis and coagulation cascade, facilitating the attachment and aggregation of platelets to a surface.¹³ Various surface properties such as charge, morphology and chemistry could influence protein adsorption, that may in turn cause structural and functional changes in the protein molecule. Recently, Zhang et al.¹⁴³ investigated the effect of surface chemistry on adsorbed Fg conformation, orientation, fibre formation and platelet adhesion on four kinds of polymers namely, polystyrene (PS), poly(methylmethacrylate) (PMMA), polylactic acid (PLA) and poly(4-vinylpyridine) (P4VP). They observed different behaviours in Fg adsorption, more specifically, fibre formation on hydrophobic surfaces, as well as consequent platelet adhesion to these surfaces, concluding that the extent and type of Fg adsorption and tendency of adsorbed Fg to bind platelets may be manipulated by the type of surface chemistry. This implies that by modulating the Fg-coil surface interactions, it could be possible to gain some control over the extent of thrombosis, thereby paving the way to comprehend and possibly

improve aneurysm healing.

Past efforts to modify thrombogenicity of bare Pt coils involves enhancing the coil surface with bioactive components such as polyglycolic acid^{141,142} and hydrogel.^{144,145} Our approach is to use cold plasma processing, a dry (solvent-free) process, to develop functional polymeric coatings which can easily be deposited on to 3-dimensional objects and whose surface chemistry can easily be varied and controlled, in order to regulate Fg adsorption as a first step towards studying the extent of thrombogenicity of the coils on aneurysm healing. Our main focus is on N based plasma polymer films (PPFs) whose functional groups primarily include amines, imines and nitriles. Primary amines and imines are considered of high interest since, when exposed to physiological (pH 7) aqueous environments, they acquire a positive charge that aids in attracting negatively charged biological molecules such as proteins. We also consider a high oxygen based coating whose carboxylic acid groups induce a negative surface charge, when exposed to a physiological environment.

The affinity of PPFs to bind different plasma proteins such as Fg, immunoglobulin (IgG) and albumin has been investigated in literature.^{77,78} Lassen et al.³⁴ showed that competitive protein adsorption from a mixture of Fg, human serum albumin (HSA) and IgG, on a hydrophobic plasma polymerised hexamethyldisiloxane (PP-HMDSO) surface, resulted in an adsorbed layer that mostly comprised of HSA and IgG, with Fg present to a smaller extent. In contrast, the adsorbed layers on positively and negatively charged hydrophilic plasma polymerised amino and carboxy functionalised surfaces, were completely dominated by Fg with almost no HSA and very low levels of IgG present. Individually, all proteins adsorbed to all surfaces showing that apart from electrostatic attractions, hydrophobic, vander Waals and entropic interactions also contribute towards the adsorption process.

This article is organised in three sections. In the first section, the effect of deposition pressure on film properties such as surface chemistry, aqueous stability and Fg adsorption is studied. Pressure is a crucial parameter that influences the chemical and physical properties

of the PPFs. In the area of plasma diagnostics, Saboohi et al.¹⁴⁶ compared two pressure regimes namely, collision-less and collisional, where the transition from one regime to the other occurs around 6 Pa. While plasma diagnostics and polymerisation mechanisms have been studied in a wide range of pressures, from < 70 mTorr (9.33 Pa) to > 350 mTorr (47 Pa),^{21,121} the influence of pressure, treated as a deposition variable, is less commonly studied in the analysis of low-pressure PPFs, especially in the high-pressure collisional regime. Therefore, this provides the motivation for our focus in the first section, where an optimisation of the deposition pressure on the properties of PPFs is performed. In the second part of this work, the influence of the type of PPF, defined by the HC precursor used for deposition, on Fg adsorption is investigated. In addition, dynamic water contact angles are measured to understand the role of wettability in the adsorption process. Friction and wear properties of the coatings are also tested using tribometry in the context of potential use in the aforementioned biomedical application. Lastly, the impact on Fg adsorption by the presence of a competing protein is studied by monitoring Fg adsorption from a solution containing HSA, on a selected group of PPFs with varying surface chemistries. It is shown that the ability of the coatings to regulate Fg adsorption is successfully maintained despite the presence of a high concentration of the competing protein, suggesting the potential use of these coatings in achieving control over thrombosis for aneurysm healing studies upon endovascular coiling treatment. Protein adsorption is measured using surface plasmon resonance spectroscopy (SPRS) and competitive adsorption by surface plasmon fluorescence spectroscopy (SPFS).

6.2 Experimental section

6.2.1 Plasma polymer deposition

Films were deposited using a previously described⁹⁶ Plasma Enhanced Chemical Vapour Deposition (PECVD) system, on 500 μm thick (100) p-type silicon wafers cut into appropriate sizes, except for SPR and SPFS studies where gold sensors were used as the substrates. The Si wafers were cleaned ultrasonically in isopropanol and deionised (DI) water for 5 minutes in each liquid and dried with a nitrogen flow prior to film deposition. The gold sensors were cleaned by immersing in isopropanol followed by DI water for 2 minutes in each liquid and drying using a nitrogen flow. Briefly, the PECVD setup consists of a cylindrical steel vacuum chamber connected to a turbo-molecular pump, backed by a two-stage rotary vane pump. The operating pressure, during plasma deposition was varied between 15 and 80 Pa. The low-pressure capacitively coupled r. f. (13.56 MHz) glow discharge was generated via an impedance matching network connected to a 10 cm diameter powered electrode in the center of the chamber, with the walls of the chamber acting as the grounded electrode.

PPFs were deposited using a mixture of a functional group source gas, such as ammonia (99.99 %, MEGS), and a hydrocarbon (HC) gas, such as 1,3-butadiene (99.8 %, MEGS) and/or ethylene (99.999 %, MEGS). The films prepared include N-rich plasma polymerised ethylene (PPE:N) and butadiene (PPB:N) films, a co-polymerised ethylene and butadiene (PCEB:N) film, an O-rich plasma polymerised ethylene (PPE:O) film, deposited using carbon dioxide (99.99 %, MEGS) as the functional group source gas, and a pure HC film (PPE) deposited using ethylene. HC flow rates for the PPB:N, PPE:N, PPE:O and PPE films were 5, 10, 5 and 20 sccm, respectively. HC flow for PCEB:N film was 2 sccm of ethylene and 8 sccm of butadiene. These HC flow rates were maintained constant in all film depositions. Films were deposited under CW, at 10 W, except for PCEB:N and PPE:O which were

deposited at 20 W. Pressure and gas flow ratio (R, functional group gas flow:total HC gas flow) used for each film are clearly defined in the results and discussion section.

6.2.2 Film characterisation

X-ray Photoelectron Spectroscopy (XPS) analyses were performed soon after deposition, in a Thermo Scientific K-Alpha XPS instrument, using monochromated Al K α X-rays, producing photons of 1486eV. Wide scans with step size 1eV, pass energy 160eV, dwell time 200ms and in the range 1200 to -10eV were acquired for each sample.

Derivatisation with 4-Trifluoromethylbenzaldehyde (TFBA) (Sigma Aldrich, purity 98%) followed by XPS analysis was performed on N based PPFs according to the method described in our previous work.⁹⁶ Recent work,^{67,68} showed that the [-NH₂] content calculated from this method includes all N functional groups that can react with aldehydes. Since the N source gas used here is ammonia which already contains the NH₂ component, it can be assumed that most N groups incorporated into the film are NH₂ species and that they have a good chance of survival under the mild plasma deposition conditions used. Nevertheless, it is important to keep in mind that the [Nu] symbol used here is a representation of any group that can react with aldehydes such as primary amines, imines and also amides which are formed on the surface due to oxidation in air. The concentration of carboxylic acid groups in the PPE:O film was determined by derivatisation with toluidine blue as described in ref.⁹

Film stability in phosphate buffered saline (PBS, BioShop Canada) solution of pH 7.4 for 1h and 24h was measured using a Dektak profilometer and is presented as the percentage of film thickness loss after exposure to PBS. After immersion, samples were dried using a nitrogen flow and left outside for at least 10 min before measurement. The coating was deposited on a silicon wafer with a thin piece of Kapton tape, that is expected to leave no residue upon removal, to produce a step enabling thickness measurement. Approximately

100 nm thick coatings were used for the stability tests.

Dynamic water contact angle (CA) measurements were performed using a goniometer (Dataphysics OCA 15EC) with distilled water. Advancing and receding contact angles (ACA and RCA, respectively) were measured by pumping and withdrawing 8 μl of water, to and from a sessile drop of initial volume 2 μl at a rate of 0.1 $\mu\text{l/s}$. A wait time of 20 seconds was maintained between advancing and receding measurements to allow just enough time for the droplet to stabilise. All CA measurements were conducted at room temperature ranging from 20 to 25 $^{\circ}\text{C}$ and 30 to 50 % relative humidity. At least 3 measurements were taken on each sample.

Friction and wear tests were performed using two instruments, depending on the normal load exerted. The first was a custom-built pin-on-flat reciprocating *in situ* tribometer, details of which are explained elsewhere.¹⁴⁷ The static counter-surface was a ball (1/4 in. dia.) made of high density polyethylene (HDPE), a typical material used in the fabrication of micro-catheters. Tests were performed at a constant 1 mm/s sliding velocity of the flat surface, over a track length of 4 mm and for 500 cycles (total distance 4 m). The normal force applied was 0.6 N. From Hertzian contact mechanics,¹⁴⁸ this was expected to correspond to a maximum Hertzian contact pressure of 21.8 MPa and circular contact area diameter of 0.229 mm. Profilometry was conducted on these wear tracks after rinsing them with DI water to remove any residual salts from the PBS. In order to achieve a lower contact pressure, a nano-tribometer (NTR3, Anton Paar) was used which is also of a pin-on-flat configuration operated in linear reciprocating motion. A constant sliding velocity of the flat sample was maintained at 1 mm/s, over a track length of 2 mm for a total distance of 4 m. The diameter of the HDPE ball, the static counter-surface, was 6 mm. The normal force applied was 1 mN to yield a theoretical maximum Hertzian contact stress of 2.7 MPa and circular contact area diameter of 27 μm . Disregarding the end points of the wear track, an average coefficient of friction was calculated in real-time for each reciprocating cycle. Approximately 300 nm

thick films were deposited on silicon wafer substrates. All experiments were done in PBS and at room temperature ($\sim 25^\circ\text{C}$).

6.2.3 Protein adsorption by SPRS and SPFS

Fg (from bovine plasma, Sigma) adsorption was monitored using a commercial surface plasmon resonance (SPR) spectrometer (RES-TEC RT2005, Germany) where a thin noble metal layer (in this case gold), on the base of a prism is irradiated with a 632 nm He/Ne laser beam, while the reflectivity is measured, over a range of incident angles. A detailed description of the technique and its principles can be found in ref.⁷⁵ Substrates used were 25 mm \times 25 mm \times 1.5 mm LaSFN9 glass slides coated with ~ 2 nm of Cr and ~ 40 nm of Au using a NexDep e-beam evaporator (Angstrom Engineering Inc) and the test coatings (~ 15 nm) were deposited on the gold surface. Platinum coatings of ~ 7 nm thickness were deposited using a high vacuum sputter coater (Leica EM ACE600). Real-time kinetic measurements of protein adsorption were conducted using two methods. The first involved following the SPR minimum angle with time and is called "minimum tracking". In the second method, shift in the reflectivity at a fixed incident angle, typically 1° below the SPR minimum angle, was measured with time and is referred to as "time measurement". A kinetic experiment involved gently flowing PBS into the 20 μl flow cell holding the sample-prism configuration, and leaving it for 2 minutes, followed by protein solution for 10 minutes (or until equilibrium is reached), and finally PBS for another 2 min to flush any loosely attached protein molecules. Kinetic measurements were conducted under both static and continuous flow conditions. The fluids were flown using a peristaltic pump at 0.7 ml/min, which corresponds to a venous shear rate of 100 s^{-1} . During a static experiment, 15 seconds of flow was sufficient to completely fill the flow cell. Angular scans of the reflectivity were measured over a range of incident angles between 42° and 70° in PBS before and after exposure to the protein mixture. Fg solution, prepared in PBS, was of concentration 2 mg/ml, which is equivalent

to the average concentration of Fg in human blood. Similarly, individual adsorption of HSA (Sigma) to the films was also studied and the concentration of HSA in PBS was 40 mg/ml, equivalent to that in human plasma. All adsorption studies were performed within 20 minutes of exposure of the PPF to PBS and at room temperature ($\sim 25^{\circ}\text{C}$). After each protein experiment, the flow system was cleaned by passing 10% bleach solution for 2 minutes, followed by a 2 minute flow of 1% sodium dodecyl sulphate and finally rinsing with DI water for another 2 minutes.

Competitive Fg adsorption was measured using a combination of SPR and fluorescence spectroscopy, called SPFS (RES-TEC, Germany). The setup and the sample configuration is the same as that of the SPR spectrometer with the addition of a photomultiplier facing the base of the prism to detect the transmitted light. The binary mixture of proteins contained 2 mg/ml of fluorescently labelled Fg from human plasma (Alexa Fluor 647 conjugate, Fisher Scientific) and 40 mg/ml of HSA. The experiment was conducted under static flow and involved a 2 minute flow of PBS, followed by a 10 minute flow of protein mixture and finally another 2 minute flow of PBS to rinse off any loosely attached proteins. The intensities of the reflected light and transmitted light were measured over a range of incident angles between 42° and 70° in PBS before and after exposure to the protein mixture. Excitation of the fluorophores on the Fg molecules by the surface plasmon resonance results in a strong fluorescence peak about 1° below the SPR minimum angle. The fluorescence signal was normalised by the SPR signal after subtracting the SPR curve from its maximum reflectivity and shifting it horizontally to match the angular position of the fluorescence peak. The reason for this angular difference between the SPR peak and fluorescence peak is related to the resonance character of the surface plasmon excitation and is explained in detail elsewhere.⁷⁹ Real-time kinetics of the total protein binding process were obtained by conducting a time measurement on the SPR curve.

The experimental SPR curves are simulated using the WinSpall data analysis software

(Version 3.02) which uses an optical model based on solving Fresnel's equations, to determine the optical thickness of the films and the adsorbed protein layer. If the refractive index of each layer is known, the geometric thickness of the layer can be calculated. The dielectric constants of adsorbed Fg and HSA layers used here are 1.93 and 1.968, respectively. These values were chosen based on literature^{24,149} and the SPR curve fittings that assumed a monolayer packing of the protein molecules²⁷ with dimensions of HSA and Fg being in the ranges 2.7-12 nm⁴⁹ and 6-45 nm,⁵¹ respectively. The dielectric constants of the plasma polymers used were $2.5 + 0.0022i$ in air and $2.4347 + 0.0012i$ in PBS. These were an average of values measured by depositing thick plasma polymers to provide waveguides in the SPR curve and allow the simulation of both refractive index and thickness, simultaneously.

In order to convert the fluorescence signal from the Fg molecules bound at the surface during a competitive adsorption experiment, single protein experiments with fluorescently labelled Fg molecules were first conducted on one of the PPFs and the thickness of the adsorbed Fg layer was determined by simulating the shift in the SPR curve. Thus, the fluorescence signal from a competitive adsorption experiment can be used to evaluate the amount of Fg in the protein mixture layer, assuming that the fluorescence signal is a linear function of the amount of Fg adsorbed. This assumption was made possible by manually reducing the intensity of the incident laser beam to avoid saturation of the photomultiplier ($<1.5 \times 10^6$ cps). Owing to fluorescence quenching that occurs near metal surfaces, competitive protein experiments could not be successfully conducted on the Pt surface.

The thickness of the protein layer is related to the surface coverage of the protein by the Feijter equation¹⁵⁰ as shown below.

$$M = d_A \cdot \frac{n_A - n_{sol}}{\frac{dn}{dc}} \quad (6.1)$$

where M is the surface density (mass per unit area) of proteins bound to the surface,

d_A is the average thickness of the adsorbed layer, n_A is the average refractive index of the adsorbed layer, n_{sol} is the refractive index of the cover media and dn/dc is the refractive index increment of adsorbed molecules which is $0.182 \text{ cm}^3/\text{g}$, a constant for proteins. This equation is valid as long as the refractive index is a linear function of the solute concentration which is the case for proteins. According to this equation the thickness of the protein layer is directly proportional to the mass of protein per unit surface area considering that n_A is an average over all thicknesses.¹⁵⁰

All errors bars represent the standard error with experiments repeated at least three times.

6.3 Results and discussion

6.3.1 Effect of pressure on film properties

The effect of deposition pressure and gas flow ratio, $R=\text{NH}_3/\text{HC}$, on the deposition rate, surface chemistry, aqueous stability and affinity for Fg adsorption on PPB:N films is studied. Figure 6.1a shows the deposition rates of the films at 15 Pa, 45 Pa and 80 Pa and at R values from 1 to 4 for each pressure. As expected, deposition rates show an overall decreasing trend with increase in R owing to an increase in etching effect of ammonia, a known etchant for organic materials.^{4,31,119} As pressure is increased, we observe a reduction in the deposition rate at all R values. This may be explained by the lower energy per particle with increase in pressure or more specifically, the shorter average mean free path of electrons, leading to lower electron energies and thus, low plasma fragmentation resulting in less activated species that could potentially condense and contribute to film formation.

Figure 6.1b shows the films' N content with the variation of pressure and R. As expected,

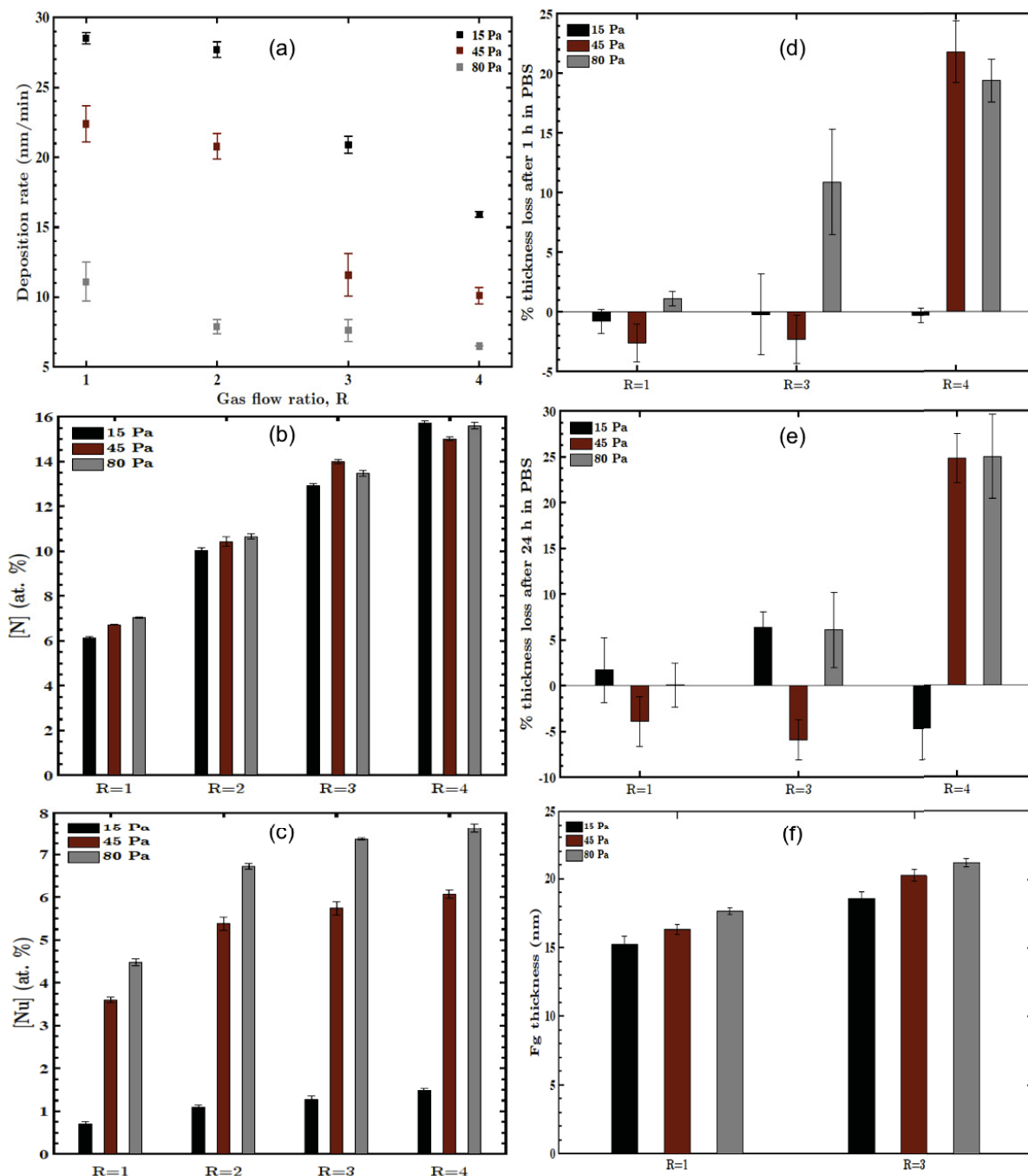


Figure 6.1: Effect of reactor pressure on the properties of PPB:N films deposited at gas flow ratios $R = \text{NH}_3/\text{HC} = 1$ to 4 (a) deposition rate, (b) N content determined by XPS, (c) nucleophile content determined by TFBA-derivatisation-XPS, (d) stability in PBS after 1 h of exposure, (e) stability in PBS after 24 h of exposure and (f) Fg adsorption determined by SPRs under continuous flow.

for all pressures, there is a clear increase in the amount of N incorporated in the films with higher values of R owing to the increase in the number of ammonia molecules in the plasma that are activated and participating in plasma polymerisation. However, increase in pressure does not seem to have a consistent effect on the N content at all R values. At lower R, we observe a slight increase in N content, despite the decrease in energy per molecule at increased pressure. This is attributed to the bond dissociation energy¹²⁰ of H-NH₂ (453 kJ/mol) being lower than that of C-C bond in butadiene (489 kJ/mol) and therefore, even at lower energies per particle, the increase in the number of molecular collisions with pressure offers a better chance of N species being activated and incorporated in the film than C-H species. At R=3, the increase and decrease in N content with pressure (and vice versa for R=4) could be explained by the net polymerisation effect of, (i) increased formation of activated N species relative to C-H species due to increase in molecular collisions and (ii) the decrease in energy per particle that leads to a decrease in activated species, with increase in pressure.

Figure 6.1c shows the content of nucleophiles [Nu], such as primary amines and imines as a function of pressure and R. As expected, similar to [N], [Nu] also increase with R. With increase in pressure, similar to [N] at low R, we observe an increase in [Nu] due to an increase in the number of molecular collisions and thus, increase in the amount of activated NH_x that are incorporated in the film. The very low [Nu] values at 15 Pa compared with 45 and 80 Pa are likely due to the fact that under these conditions of pressure, the plasma is very close to a collision-less regime wherein the high energy electrons leading to increased fragmentation of the monomer molecules and increased dehydrogenation due to more pronounced ionic bombardment, results in more unsaturated N species in the film, such as nitriles.

The percentage of thickness loss after exposure to PBS for 1 h (Figure 6.1d) and 24 h (Figure 6.1e) was measured for the R= 1, 3 and 4 coatings at all three pressures. Negative values correspond to a net effect of swelling of the coating where the polymer network has expanded due to intake of water and remained expanded upon drying, whereas positive values

denote a net effect of loss of film material due to dissolution. Thickness loss or gain within 10 % is considered stable in the context of this work. The coatings are most stable at $R=1$ and stability decreases as they lose more material at higher R values. This is to be expected since increased presence of polar nitrogen groups increases the films' affinity towards polar solvents rendering them more soluble in aqueous media. Considering the effect of pressure, 15 Pa coatings seems to be the most stable and those deposited at 80 Pa seems the least stable. One of the reasons for this observation is the presence of very low [Nu] content in the 15 Pa coatings. It is also consistent with research where diamond-like carbon thin films, characteristic of increased hardness, are usually deposited at low pressures ($\sim 1-6$ Pa).^{151, 152} This was evident with the coatings prepared with 15 Pa as it was impossible to scratch them with a needle, whereas the 80 Pa coatings were scratched very easily. It is also interesting to note that there is only a slight difference in film's aqueous stability between 1 h and 24 h measurements suggesting that the interactions between the film and the liquid leading to thickness changes occur mostly within the first hour of exposure and seem to have stabilised over the next 24 h.

Taking into account the above observations, we chose a low and high N-containing coating with acceptable [Nu] content and PBS stability, $R=1$ and $R=3$ films, to investigate Fg adsorption as a function of pressure (Figure 6.1f). Higher Fg adsorption is detected on $R=3$ coatings. This is expected owing to the higher [Nu] of these films that make them more positively charged, attracting more protein molecules which carry a net negative charge in physiological pH media.⁵⁰ There is also an increase in Fg adsorption on films with increase in deposition pressure, however this increase is small compared with the distinct increase in the films' [Nu] content with pressure (Figure 6.1c). This clearly shows that there are other factors encouraging Fg adsorption apart from the positively charged surface functional groups which may include hydrophilic, vander Waals and entropic interactions.

6.3.2 Influence of film type on Fg adsorption

We then compared Fg adsorption behaviour on PPFs that differ based on their HC precursor and surface functionality. All PPFs studied here were tested for stability and showed a thickness loss of <20 % after 24 h of exposure to DI water (results not shown). A platinum surface and the bare gold surface of a SPR sensor are used as controls. Deposition conditions and surface chemistry of the PPFs are summarised in Table 6.1. Figure 6.2(a) shows the thickness of the adsorbed Fg layer on all films. Results from static and continuous flow (0.7 ml/min) experiments are also reported and under these flow conditions, there seems to be no significant difference between them, especially in the case of the N-based films. PCEB:N film gives the highest Fg adsorption, likely due to its high [N] and [Nu] content. With the increase in R, we can observe an increasing trend in Fg adsorption in the case of PPB:N and PPE:N films and this is to be expected since, the electrostatic attraction between the negatively charged Fg molecules and the positively charged surfaces is strengthened owing to the increase in [Nu] in the films with increase in R. Comparing the PPB:N R=1 and R=3 coatings with the PPE:N coatings, despite the higher [Nu] and selectivity, [Nu]/[N], of PPB:Ns (Table 6.1), Fg adsorption between the PPB:N and PPE:N coatings is similar. This suggests that PPE:N films would have a higher affinity towards Fg compared to PPB:Ns with similar N-surface chemistry. For PPB:Ns, as R is increased from 1 to 4, there is a net decrease in the water contact angle (Figure 6.3), particularly the RCA, which is more sensitive to changes in the high energy component of the surface (N groups in this case), denoting the increase in hydrophilicity of the coatings with increase in the films' N content, which also correlates well with the increase in Fg adsorption. However, for PPE:N, the increase in the N content from R=0.5 to R=0.75 is not sufficient to bring about a significant change in its hydrophilicity, which does not seem to affect the clear increase in Fg adsorption from R=0.5 to R=0.75.

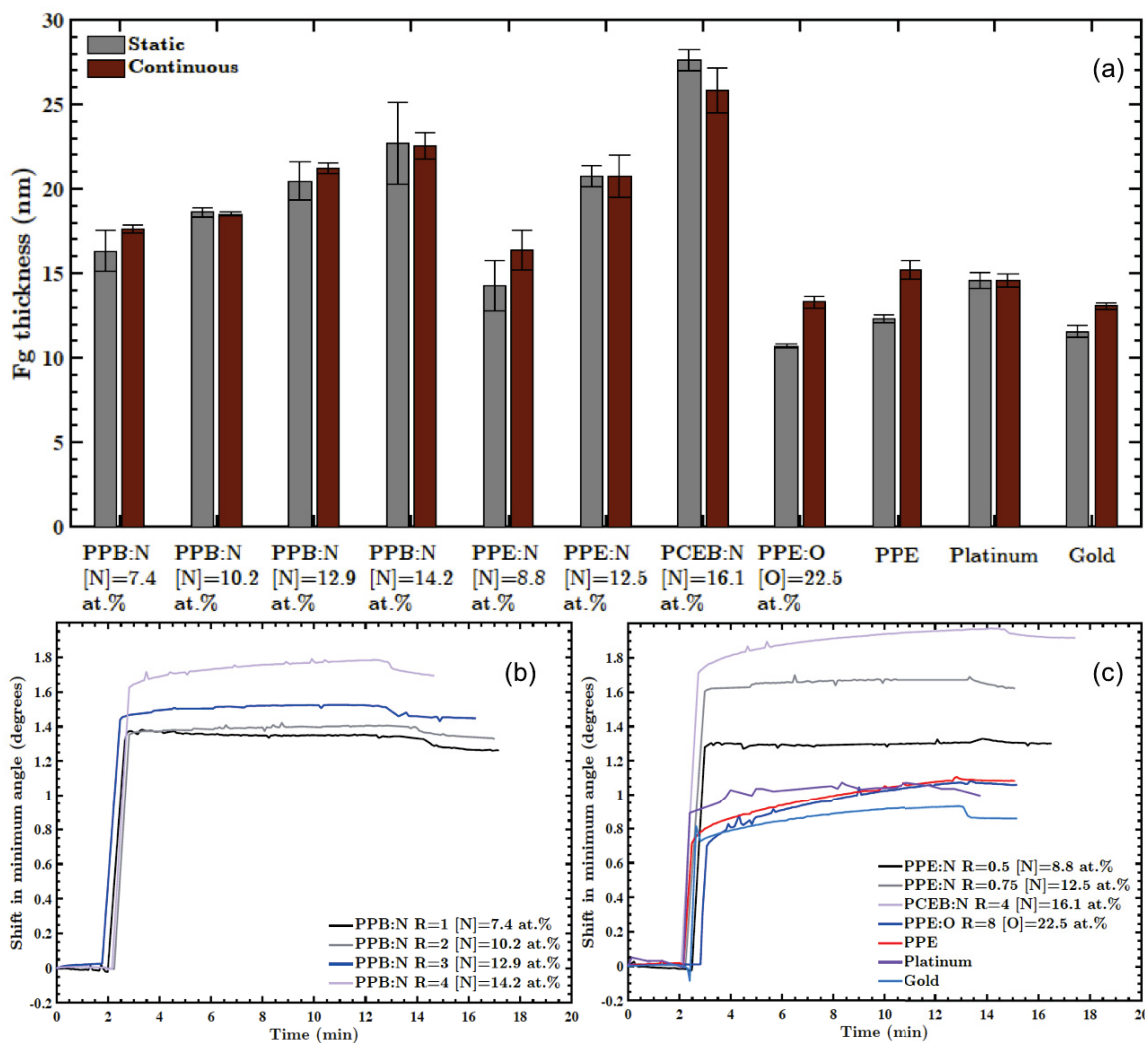


Figure 6.2: Fg adsorption on PPFs, platinum and gold determined by SPRs. (a) Thickness of the Fg layer adsorbed on all films. The R values of the PPFs are, from left to right, 1 to 4 for the four PPB:N films, 0.5 and 0.75 for the PPE:Ns, 4 for the PCEB:N and 8 for the PPE:O. Adsorption kinetics measured by minimum tracking, under continuous flow, are presented for (b) the four PPB:N films and (c) PPE:N, PCEB:N, PPEO, PPE, Pt and Au films. Each curve represent an individual experiment. All PPFs are deposited at 80 Pa.

Table 6.1: Surface chemistry of PPFs. Films were deposited at 80 Pa.

Plasma polymer	[N] (at. %)	[Nu] (at. %)	[Nu]/[N] (%)
PPB:N R=1	7.4	4.4	59.5
PPB:N R=2	10.2	5.7	55.9
PPB:N R=3	12.9	6.5	50.4
PPB:N R=4	14.2	7.3	51.4
PPE:N R=0.5	8.8	3.2	36.4
PPE:N R=0.75	12.5	4.2	33.6
PCEB:N R=4	16.1	5.6	34.8
	[O] (at. %)	[COOH] (nmol/cm ²)	
PPE:O R=8	22.5	2.0	-
PPE	-	-	-

The non-N based films namely, PPE:O, PPE, Pt and Au, show relatively lower Fg adsorption. The PPE:O, owing to its strongly negative surface charge in aqueous media (-28 mV⁹), shows the lowest affinity towards the protein molecules. However, its low RCA value, making it the most hydrophilic surface of all, is thought to support some degree of adsorption via hydrophilic interactions. Furthermore, although the overall net charge of the Fg molecule is negative, the molecule possesses an anisotropic charge distribution,⁵⁰ suggesting that the local positive charges on the molecule may also contribute to binding with the negatively charged PPE:O surface through some degree of electrostatic attraction. PPE, despite the absence of hetero-atomic functional groups, is considered to react with water or dissolved oxygen in aqueous media to form negatively charged functional groups such as alcohols and aldehydes,¹⁰³ resulting in a similar electrostatic interaction to that of PPE:O with Fg. It can be noted that PPE is the most hydrophobic surface of all and Fg adsorption on it is higher than that on the most hydrophilic PPE:O surface. This suggests that Fg molecules form stronger hydrophobic interactions with PPE than they do for hydrophilic interactions with PPE:O. Fg adsorption on charge neutral Pt and Au is likely due to Van der Waals and hydrophobic/hydrophilic interactions.

Figure 6.2b and c show the kinetics of Fg adsorption on all films, under continuous flow.

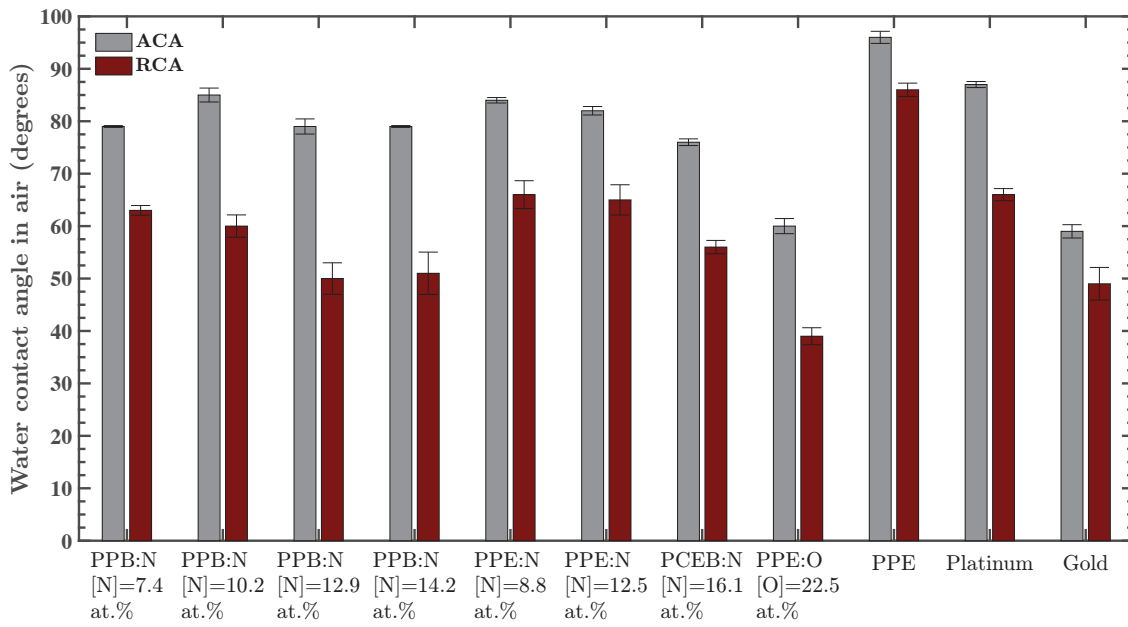


Figure 6.3: Advancing and receding water contact angles (ACA and RCA) in air for all PPFs, platinum and gold. The R values of the PPFs are, from left to right, 1 to 4 for the four PPB:N films, 0.5 and 0.75 for the PPE:Ns, 4 for the PCEB:N and 8 for the PPE:O. All PPFs are deposited at 80 Pa.

In the case of PPB:Ns (Figure 6.2b), it can be seen that the time taken to reach saturation increases from R=1 to 4. This could be explained by possible swelling of the plasma polymer with the increase in N content and thus, hydrophilicity. In Fig 6.2c, a similar observation can be made for the N-based films, where the PCEB:N with the highest N-group content undergoes some degree of swelling. It has been found that swelling of the plasma polymer results in an increase in its surface roughness,²⁷ which may favour further Fg adsorption, thereby contributing to a longer saturation time.

Longer adsorption kinetics are observed for PPE:O and PPE, as seen in Figure 6.2c. This may be due to electrostatic repulsion with the net negatively charged Fg molecules, considering that PPE could also acquire a negative charge as discussed earlier. A similar observation was made in the work of Lassen et al.,³⁴ where Fg and IgG adsorption on negatively charged carboxyl surface showed slower adsorption kinetics compared with that of positively charged amino and hydrophobic PP-HMDSO surfaces. Pt and Au seem to follow similar adsorption kinetics, although Pt is more attractive to Fg than Au. These observations show that, electrostatic attractions, when present, results in faster Fg adsorption kinetics allowing for a steady state to be reached more quickly.

The layer thickness is attributed to the orientation of the Fg molecules with which they are attached to the surface. The hydrated Fg molecule has been found to have a characteristic trinodular structure which is about 45 nm in length and 6-10 nm in width.⁵¹ Thus, the thinner layers observed with the non-N based films, where no apparent electrostatic attraction is present, can be a result of side-on adsorption of the protein molecule. Deformation or spreading of the molecule may occur depending on the hydrophobicity of the surface, leading to thicknesses of up to ~ 15 nm.¹³ The thicker layers observed with the increase in N content in the N-based films, can be attributed to an end-on adsorption of the Fg molecule, allowing for layer thicknesses ranging from ~ 15 to 45 nm, without taking into account any structural deformation.

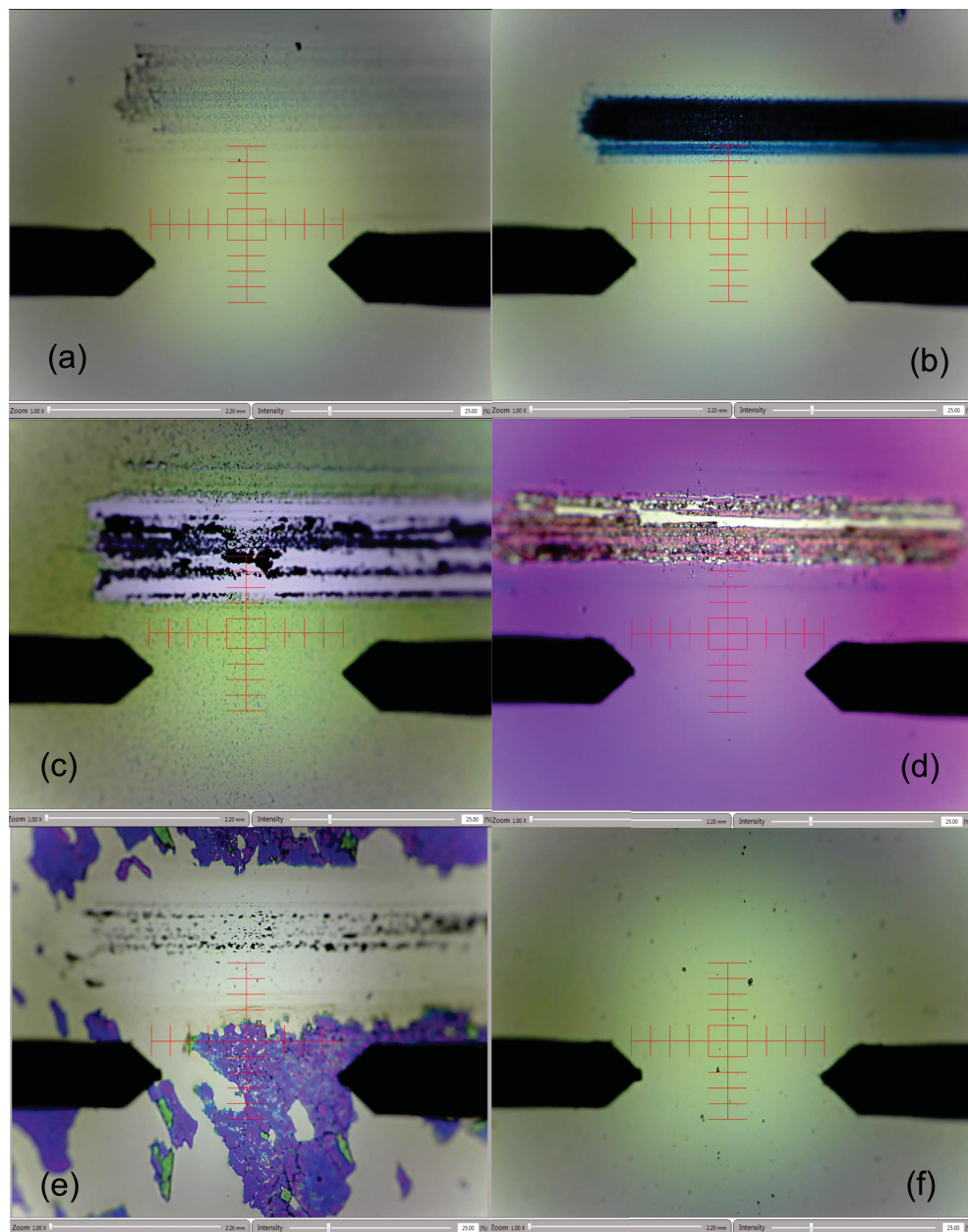


Figure 6.4: Friction and wear tests against a HDPE counter-surface measured using tribometry. Expected Hertzian contact stress, 21.8 MPa. Figure shows images of the wear tracks obtained during profilometry of (a) PPB:N R=1, (b) PPB:N R=3, (c) PPB:N R=4, (d) PPE:N R=0.75, (e) PCEB:N and (f) PPE:O. All films are deposited at 80 Pa.

Table 6.2: Coefficients of friction of the PPFs measured under 21.8 and 2.7 MPa Hertzian contact stresses. Films deposited at 80 Pa.

Plasma polymer	μ at 21.8 MPa	μ at 2.7 MPa
PPB:N R=1	0.162	0.162
PPB:N R=3	0.171	0.214
PPB:N R=4	0.191	
PPE:N R=0.75	0.170	
PCEB:N	0.151	
PPE:O	0.131	0.197

In addition to Fg adsorption, another important criteria for the development of a biomaterial for in-situ applications, would be to test for its friction and wear properties. We have measured, using a tribometer, the wear resistance of some of the above coatings and the test conditions used here are motivated by foreseeing a plasma polymer coated platinum coil being used in the endovascular treatment of brain aneurysms. Thus, good wear resistance against the inner-wall of a micro-catheter used for coil delivery is indispensable. Tests were conducted in PBS to simulate physiological conditions. First, measurements were done by applying a normal load of 0.6 N, corresponding to a Hertzian contact stress of about 22 MPa. The coefficients of friction (μ) are given in Table 6.2. These values of μ show no particular relationship with the gas flow rate or the type of precursor gases used. Images of the wear tracks taken during profilometry measurements of all samples are shown in Figure 6.4. Figures 6.4a, b and c, corresponding to PPB:N R=1, 3 and 4, show that, with increase in the film's N content, there is a clear reduction in the wear resistance of the film. These coatings were approximately 300 nm thick. The PPB:N R=1 coating is lightly scratched by the counter-surface, whereas for PPB:N R=3, the contact profile from the profilometer (not shown) indicated considerable wear of the film that reached roughly half-way into the coating. In the case of PPB:N R=4, at certain regions of the wear track, the coating is completely delaminated, as shown by the clear areas in the wear track of Figure 6.4c. Similar to PPB:N R=4, the high N PPE:N film also showed complete delamination in certain regions of its wear track (Figure 6.4d). Furthermore, the PCEB:N coating is completely delaminated

by the motion of the counterface, leaving almost no film residue in the wear track (Figure 6.4e). This is attributed to the high N content and thus, hydrophilicity of the film that causes it to undergo considerable swelling, weakening the polymer structure, allowing it to be easily removed by an external force. On the contrary, no visible wear track is observed on the PPE:O coating indicating good wear resistance to HDPE, under these test conditions (Figure 6.4f). Hence, it can be presumed that, the PPE:O coating, relative to the N-based films, is more strongly cross-linked and compact which renders it more resilient to shear stresses.

Out of the N-based coatings, PPB:N R=1 and R=3 (80 Pa) were chosen as a low and high N coating, to test for wear resistance against a reduced normal load of 1 mN, corresponding to a Hertzian contact stress of 2.7 MPa. No visible wear tracks were observed on either sample, indicating good wear resistance, under these test conditions. The coefficients of friction are given in Table 6.2. PPB:N R=1 and R=3 coatings deposited at 45 Pa also showed similarly good wear resistance under the same test conditions (results not shown).

6.3.3 Influence of HSA on Fg adsorption

Competitive protein adsorption on a surface depends strongly upon the bulk concentration of the proteins and the surface affinity of each protein which varies with the surface chemistry. Proteins upon adsorption can go through conformational changes due to their low structural stability and the tendency to undergo molecular spreading, resulting in a larger molecular footprint, allow for further bond formation with the surface. These conformational changes can affect the biological activity of the adsorbed proteins and thus, cell responses. The goal here is to investigate the influence of another protein on Fg adsorption, which can directly affect platelet adhesion and activation. It is well known that, by Vroman effect,^{153,154} surface adsorbed Fg is displaced by high molecular weight kininogen and factor XII, which are also human clotting factors as Fg. Since it is not directly involved in the coagulation cascade and

being the most abundant protein in blood plasma, we have chosen HSA as the competing protein to study Fg adsorption from a simple binary mixture of Fg and HSA. Surfaces studied include a low-N, high-N, O-rich and a Pt surface. PPB:N R=1 and R=3 coatings deposited at 45 Pa were chosen as the low- and high-N films since they demonstrated the optimum compromise between stability in PBS, wear resistance and nucleophile content. The O-rich film is the same PPE:O coating discussed previously.

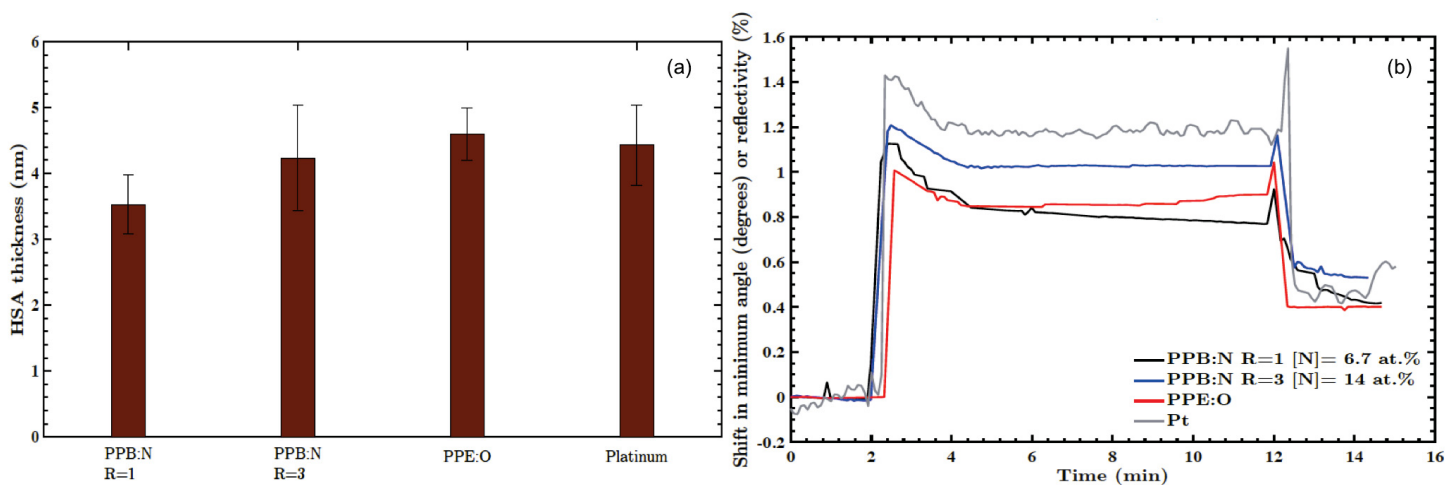


Figure 6.5: HSA adsorption on PPB:N R=1, PPB:N R=3, PPE:O and Pt coatings determined by SPRS, under static flow. (a) Thickness of HSA layer adsorbed. (b) Adsorption kinetics obtained by minimum tracking for the PPFs and time measurement for the Pt coating. The PPB:N films were deposited at 45 Pa and PPE:O at 80 Pa.

As the first step, HSA adsorption on these films from a pure HSA solution is studied using SPRS and results are shown in Figure 6.5. HSA adsorption on all four films seems to show no particular relationship with film type. A similar observation was made with bovine serum albumin where it showed no clear difference in adsorption between a positively charged plasma polymerised allylamine and a negatively charged maleic anhydride film.⁷⁷ A HSA molecule is usually ellipsoidal in shape with a length of 12-14.1 nm and width of 2.7-4.1 nm.⁴⁹ It carries a $-9e$ and $+2e$ charge on each end and a $-8e$ charge at the centre, thus bearing an overall net $-15e$ charge. Therefore, its interaction with the positively charged PPB:N films is probably mainly due to electrostatic attractions. It may also adsorb on the

negatively charged PPE:O film via the $+2e$ charge present at one of its ends. The fact that HSA adsorption on the PPE:O coating is higher than that on the PPB:N R=1 coating could be due to the protein molecule being attached in a more upright orientation on the PPE:O surface, via the positive end of the molecule, allowing for a slightly thicker protein layer. The more hydrophilic nature of the PPE:O coating may also lead to stronger hydrophilic interactions with the protein.

Figure 6.5b shows the adsorption kinetics of HSA on the four types of films. Unlike with Fg, we observe a peak in the kinetic curve of HSA, soon after protein injection. This could be related to the high HSA bulk concentration used here, unlike in other studies concerning HSA adsorption^{49,155–157} where the concentrations were 2 to 3 orders of magnitude smaller. Due to the high bulk concentration, 40 mg/ml, a large quantity of protein is driven to the surface by mass transfer laws and it is possible that albumin gets adsorbed in multilayers as was observed on positively charged surfaces terminating with polyallylamine.⁴⁹ They proposed two mechanisms one of which is the formation of an organised layer of end-on adsorbed HSA molecules, exposing their positive ends on the top, that would in turn attract more proteins, thereby leading to the building up of a multilayer. As the thickness of the multilayer increases, the less organisation of the protein layers at the top would cause this building-up process to stop.

A similar mechanism is proposed here. The fact that the final thickness of the HSA layers on all films are thin, shows that despite the differences in the surface charge of the films, the protein has undergone a more side-on adsorption, unlike in the mechanism proposed in ref.⁴⁹ This causes the molecules to be less regularly packed due to their shape and uneven charge distribution. The SPR minimum shift at the initial peak after protein injection, corresponds to a layer thickness of about 10 nm which we propose to be a bilayer, instead of a closely packed monolayer of end-on adsorbed proteins. This supports the fact that half the thickness is lost upon flushing with PBS, as the irregularly and loosely bound proteins to each other on

the top layer are detached, leaving behind just the layer of proteins that are attached to the surface. The reason for this kind of adsorption is most likely due to the high concentration of HSA in the bulk and the fact that HSA is already a low affinity protein, compared to others such as Fg and haemoglobin,¹ resulting in a less organised protein layer on the surface.

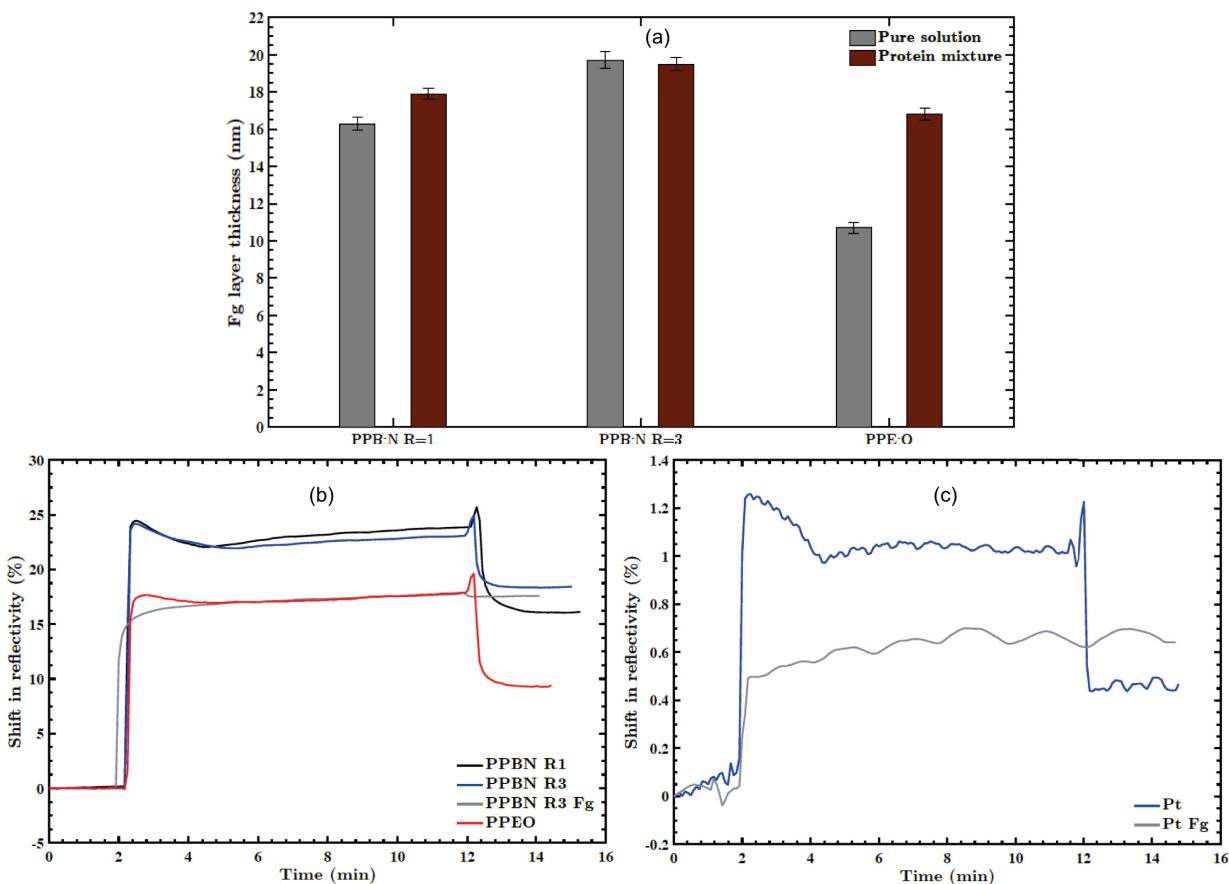


Figure 6.6: Competitive Fg adsorption from a Fg-HSA mixture, on PPB:N R=1, PPB:N R=3 and PPE:O coatings determined by SPFS. (a) Thickness of the Fg layer adsorbed from a pure Fg solution and the Fg-HSA mixture. (b) Adsorption kinetics of Fg-HSA for the PPFs. Kinetics of labelled Fg from a pure solution on PPB:N R=3 is also shown (grey line). (c) Adsorption kinetics of Fg-HSA and labelled Fg from a pure solution on the Pt coating. Kinetic experiments were done by time measurement under static flow. The PPB:N films were deposited at 45 Pa and PPE:O at 80 Pa.

Having studied the adsorption behaviour of HSA molecules, the next step is to investigate whether Fg adsorption on these surfaces would be affected by the presence of HSA. Figure 6.6a shows the thickness of the Fg layers adsorbed from a pure solution and the Fg-HSA

mixture. It must be noted that, due to the nature of the measurement, the thickness of the Fg layer adsorbed under the competitive environment is not the actual Fg layer thickness present in the layer, but rather the equivalent thickness of a closely packed monolayer of Fg. This is because the fluorescence signal measured is directly proportional to the amount of Fg molecules present in the layer, which can be converted to a monolayer thickness via the Feijter equation, however this does not give information about the true orientation with which the Fg molecules are attached in the layer. Consequently, results in Figure 6.6a are interpreted on a comparative basis for the amount of Fg adsorbed with and without the presence of HSA.

It can be seen from Figure 6.6a that there is an enhancement of Fg adsorption to PPB:N R=1 and PPE:O and no change in Fg adsorption to PPB:N R=3. A similar observation was made by Lassen et al.³⁴ where an enhancement of Fg adsorption on positively charged amino-based surface was seen in the presence of HSA. Studies conducted with fibronectin showed that the ability of the protein to promote cell spreading on the protein-adsorbed surfaces was enhanced by the addition of albumin to the fibronectin solution. This was thought to be due to the adsorption of albumin alongside fibronectin, occupying surface sites near fibronectin and preventing it from undergoing molecular spreading (thereby structural changes) over the adjacent surface sites, that would otherwise be empty in the absence of albumin.¹ Likewise, it is possible that limited molecular spreading may have occurred in the adsorbed Fg molecules in the presence of HSA, leading to an increase in Fg adsorbed on some of the films.

Figure 6.6b and c show the kinetics of the total protein adsorption on the three PPFs and Pt. Kinetics of Fg adsorption alone is also shown for PPB:N R=3 and Pt surfaces. The same initial peak, soon after protein injection, that appears in the case of pure HSA adsorption, is also observed with the Fg-HSA experiments. Moreover, this initial peak is not seen in the case of pure Fg adsorption on either PPB:N R=3 or Pt, confirming that this behaviour in the kinetic curves is related to the adsorption of HSA. Another interesting point to note is

the sharp drop in the signal upon flushing with PBS, in the case of Fg-HSA, as opposed to the slight drop in the signal with the pure Fg experiments. For PPE:O and Pt, this drop is almost half of that of the plateau, similar to that observed with the pure HSA experiments. These curves were obtained by a time measurement of the SPR signal and it is important to mention that information on the total adsorbed protein layer cannot be gained by fitting the SPR curve after protein adsorption, because, the refractive index, n_{mix} , of the protein mixture layer, which considers the relative proportions of the two proteins, is unknown. However, by repeating similar experiments with fluorescently labelled HSA, the total and individual surface densities of Fg and HSA in the adsorbed layer can be determined, from which n_{mix} can be calculated and consequently, by fitting the SPR curve, the total average thickness of the protein mixture layer can also be evaluated.

6.4 Conclusions

In this work, we have characterised plasma polymer films with N- and O- groups, deposited using PECVD, to study adsorption of Fg, a vital plasma protein responsible for platelet adhesion and activation, as a first step towards thrombogenicity testing of PPFs, for the application of endovascular coiling for aneurysm treatment. The goal of this study was to be able to regulate the extent of Fg adsorption in the presence of a competing protein such as HSA, with the intention to later provide some control over thrombosis.

As a part of initial film characterisation, we have investigated the effect of pressure on the properties of N-based PPFs, an area that has not been studied widely. At the low pressure 15 Pa, the nucleophile content in the films is noticeably lower than that observed at higher pressures. Nevertheless, the increase in Fg adsorption to films deposited at increased pressures was comparatively small, implying that protein adsorption is not only a result of electrostatic attraction between the negatively charged proteins and positively charged films,

but also significantly influenced by other factors such as hydrophobic and Van der Waals interactions.

Study of Fg adsorption on film types that differed based on the HC precursor used implied that PPE:N films exhibit higher affinity for Fg adsorption than the PPB:Ns with similar surface chemistry. Fg adsorption was observed on both N- and O-rich surfaces, but to a much lower extent on the O-rich coating owing to its strongly negative surface charge. Fastest adsorption kinetics were observed with the N-based positively charged coatings and slowest kinetics were seen with the films that carried a negative charge, i.e. PPE:O and PPE. Study of wear resistance of the PPFs against HDPE, in PBS, showed a decrease in resilience of N-based films with an increase in the N content, whereas, the O-rich coating showed no visible wear at the higher contact pressure exerted, suggesting a strong cross-linking and compact nature of the O-rich film that makes it more tolerant towards shearing forces.

Pure HSA adsorption on low-N, high-N, high-O PPFs and Pt surfaces showed no particular relationship between the film types. A thin layer, corresponding to more side-on adsorbed HSA molecules was detected on all surfaces. HSA adsorption kinetics show a rather distinct peak soon after protein injection. This is likely due to a bilayer formation of HSA molecules owing to the large concentration used (40 mg/ml) which is 2 to 3 orders of magnitude higher than the typically used values in other studies concerning HSA. The same behaviour was observed with kinetics of the protein mixture but not with pure Fg adsorption, confirming that this behaviour of the kinetic curve is related to binding of HSA molecules to the surface. This may suggest that the absolute concentrations used in competitive protein adsorption studies could influence the results obtained at different levels of dilution.

Lastly, presence of HSA caused an enhancement of Fg adsorption on both low-N and O-rich coatings, with a more pronounced increase on the O-rich surface. No change was observed for the high-N coating. Results suggest that regulation of Fg adsorption can be achieved by the careful choice of surface chemistry of the PPFs even in the presence of

an abundance of competing HSA. The successful regulation of Fg by the present coatings suggests the possibility of triggering thrombosis to different extents, thereby providing a basis for studying the effect of the degree of coil thrombogenicity on aneurysm healing. Although in the present context, Fg being the protein of interest and the goal has been to study Fg adsorption regulation in the presence of HSA, carrying out a similar set of experiments to monitor HSA adsorption under the influence of Fg, would certainly be a complement. Thus, this would be the next step of this study, followed by platelet adhesion experiments to provide insight into the control of thrombosis, thereby helping to improve aneurysm healing following an endovascular coiling procedure.

Acknowledgements

The authors are thankful to Yinyin Zhang, Ph.D., Richard Chromik, Ph.D. and Anton Paar for their kind support with the tribometry measurements. This work was funded by the Natural Sciences and Engineering Research Council of Canada (NSERC) (418117-12), Canada Foundation for Innovation (CFI) (30264) and the Fonds de Recherche du Québec — Nature et Technologies (FRQNT).

Chapter 7

Conclusion

7.1 Summary

Plasma deposited organic coatings are increasingly being investigated for biomedical applications. It is the wide variety of functional groups that can easily be introduced to the film using dry processes, the structurally homogeneous nature and the ease of deposition onto 3-dimensional geometries without apparent alteration of the bulk material, that make plasma polymer coatings very attractive. In this thesis, a surface engineering technique based on depositing plasma polymer films with varying surface chemistries and satisfactory aqueous stability, was developed to achieve regulation of Fg adsorption, with the long-term intention of gaining control over thrombosis, a concept that could improve the endovascular treatment of brain aneurysms. In designing these coatings several steps were to be followed starting from the optimisation of the plasma polymerisation process, which involved a fundamental study of comparing two different approaches for depositing N-rich coatings, followed by a rigorous characterisation step of film properties to achieve a compromise between the desired N functional group content and aqueous stability. These coatings were then characterised for their friction and wear resistance and their capacity for regulation of Fg with and without the presence of a competing protein, in the context of potential use in the aforementioned biomedical application. The steps leading to the development of these coatings are highlighted by the three main objectives which were stated in Chapter 1 and are revisited below.

1. *Investigate and compare plasma polymerisation of N based coatings using single source precursors and precursor mixtures.*

In the field of plasma polymerisation researchers use two main approaches to produce

plasma polymerised coatings. The discharge can be generated using single source precursors such as AA, CPA or propylamine, wherein the functional group and HC group are contained in a single molecule. The advantage of this method is in the fact that the N-group is already bonded with the HC group and therefore, it could be more easily incorporated in the film. It is also useful that the amine group, one of the main functional groups aiding biomolecule immobilisation, is already present in the precursor molecule. Nevertheless, the main disadvantage of this method is the limited possibility of varying the HC to heteroatom ratio which restrains the composition of the deposited coating. Therefore, in order to gain more flexibility over the surface chemistry of the coatings researchers adopt a second approach of plasma polymerisation. This method involves the use of a mixture of precursors such as AmEt, AmBu or nitrogen/ethylene, wherein the HC group and the functional group sources are contained in two separate molecules. This approach allows to vary the amount of HC and functional group containing molecules entering the discharge by simply varying the flow rates of the individual gases. However, the disadvantage of this method is that the functional group requires to be created during the process unlike in the case of single source precursors. Since there has been no direct comparison of these two approaches in the past it was unclear as to what similarities or dissimilarities would the complex plasma polymerisation process bring to coatings deposited from these two types of precursors. Therefore, this question was addressed in the first objective of this thesis.

In investigating the two distinct methods of preparing N-based coatings, the first method involved deposition using the single precursor monomers, AA and CPA, whereas the second involved using the precursor mixtures, AmEt and AmBu. Plasma diagnostics and film analyses were conducted in order to elucidate the main differences, if any, between these two well-known methods of preparing N-rich films. This was done while maintaining the N:C ratio at 1:3 in all inlet gas streams to ensure a similar elemental gas phase composition for all discharges. Film analyses showed that coatings

deposited from the first method contained a high amount of N but also a high content of nitriles. In contrast, under mild power conditions, the second method produced films with lower N content but relatively higher amine/imine selectivity, especially in the case of AmBu. These results were complemented by the plasma-phase analyses which revealed almost no C-N bond formation in precursor mixture discharges, explaining the corresponding lower N content in the films. The relatively less dehydrogenation in those discharges, corresponded to the better selectivity values of less unsaturated N species in the associated films. The extent of HCN etched into the discharge from the growing plasma polymer films was attributed to the degree of cross-linking in the film. The more unsaturated precursors yielded better cross-linked films, thereby leading to lower dehydrogenation. The increase in the N content in AmBu films and decrease of same in AmEt films with power, was attributed to the increased formation of acetylene species in the discharges with power. From the current results combined with those from literature, it was deduced that the ability of the discharge for N incorporation in films followed the trend AmEt>AmAc>AmBu under similar energy conditions. Thus, owing to the AmEt and AmBu discharges being more and more acetylene-like with increase in power, a decrease and an increase in the N content in the respective films were observed with increase in power. As a result of increased fragmentation with power, both plasma diagnostics and film analyses suggested that these two methods became increasingly similar to each other in the plasma phase as well as the solid phase. However, the precursor size may play an important role as was observed in the case of AmEt, wherein the mass spectra of this discharge showed a much lower degree of fragmentation possibly due to the smaller size of the ethylene molecule compared with the rest of the precursors.

The originality of this part of the thesis is in the direct comparison of the two different approaches of producing N based plasma polymer films, involving both plasma-phase and film composition analyses, to provide a better understanding of the plasma

processes that lead to films with different surface chemistries.

2. *Deposition of N based coatings with optimised concentration of desirable N functional groups and aqueous stability.*

In this thesis, the main functional group that was used to control protein adsorption was amines, the reason being the positive charge induced by these groups on the surface under aqueous media that aids in electrostatically attracting the negatively charged protein molecules. Therefore, a high concentration of amine groups on the coating were desired. However, the polar nature of amines render a high surface energy which makes the coating more susceptible to dissolution in aqueous biological media, which is undesirable for biomedical applications. Thus, ensuring the stability of the coatings in physiologic environments is an important step. Due to the conflicting nature of these two criteria, high amine concentration and high aqueous stability, a compromise needed to be reached. This part of the thesis focussed upon optimising the plasma deposition parameters to yield coatings with a high amine content as well as satisfactory aqueous stability.

The second method from the previous objective, deposition using a mixture of precursors, was adopted to synthesise N containing films owing to the better controllability of the N to C ratio in the gas phase and thus, in the films deposited. The HC gases utilised were ethylene and 1,3-butadiene. Film properties, namely, deposition rate, aqueous stability, N content and amine content were studied as a function of the plasma parameters such as power, gas flow ratio and total gas flow rate. Butadiene, owing to its conjugated C-C double bonds and therefore, the formation of more reactive species in the plasma, resulted in coatings with higher deposition rates. The more unsaturated nature of the molecule also led to better cross-linked films that were more resistant to film dissolution. However, the nitrogen incorporation in the butadiene based films were found to be lower compared with the ethylene based counterparts under similar energy conditions. Nevertheless, butadiene based coatings showed better amine selectivities

due to lower dehydrogenation as explained in the first part of the thesis. The effect of co-polymerisation of these two HCs rendered coatings whose properties followed the expected trends with the plasma parameters as with non-copolymerised ethylene or butadiene films. A better compromise between amine content and aqueous stability was achieved by using 1,3-butadiene as the HC precursor. A regression analysis was performed to develop a mathematical model which best fits the experimental data. This was performed for stability and nitrogen concentration results. First, the experimental data trend for both N concentration and stability with the plasma parameters was directly observed and it was assumed that N concentration followed a linear and stability followed a sigmoidal trend with the different parameters. In order to test these assumptions as well as find a mathematical relationship between these parameters, a linear and sigmoidal multivariate regression model for the two dependant variables, N concentration and stability, were numerically fitted and the adequacy of the models were validated. Thus, such models could be used to find an unknown plasma parameter value, provided the others are fixed, to produce a coating with the desired nitrogen content or aqueous stability.

The originality of this section of the thesis lies in the preparation of plasma polymer coatings using 1,3-butadiene to produce N based films that achieve a better compromise between amine/imine group content and aqueous stability, compared with the commonly investigated ethylene based counterparts and in the numerical modelling of the nitrogen content and aqueous stability of these films.

3. *Characterisation of the N based coatings for regulation of Fg adsorption from a pure solution as well as a protein mixture containing Fg and HSA.*

Fibrinogen is a blood protein that plays a vital role in the adhesion and aggregation of platelets. Therefore, in order to control thrombosis as the long-term goal, regulation of Fg adsorption was considered the first step. Fg or protein adsorption onto a biomaterial, in general, depends on a variety of factors including surface chemistry, surface

morphology, protein concentration in the media, competition with other proteins and so on. As explained in the earlier section, we exploited the presence of amine groups on the coatings to attract Fg and control its adsorption. Competition with other proteins can influence the conformation, orientation and thus, the activity of the Fg adsorbed on the surface. Thus, in this section a set of plasma polymer coatings with optimised properties were designed to study Fg adsorption with and without the presence of a competing protein, HSA. The protein concentrations used were representative of those present in human blood plasma.

Firstly, the optimised films produced while fulfilling the previous objective, were optimised one step further by investigating the effect of pressure on the film amine content, aqueous stability as well as Fg adsorption. A sharp increase in the amine content was observed with increase in pressure from 15 to 45 to 80 Pa. However, the increase in Fg adsorption with this increase in pressure was relatively small, suggesting that amine functionalities alone do not control Fg adsorption but other factors such as hydrophilic interactions and van der Waals forces also play a vital role. An increasing trend in Fg adsorption was observed with the increase in amine content for both PPB:Ns and PPE:Ns. However, despite the higher amine content and selectivity of PPB:N films compared with that of the corresponding PPE:Ns, Fg adsorption on both film types were found to be similar. As expected, Fg adsorption on Pt and O-rich PPE:O surfaces was lower compared with that observed on the N based coatings, with adsorption on PPE:O being the lowest due to electrostatic repulsion. Good wear resistance against polyethylene in aqueous media was observed for all coatings at the lower contact pressure applied. Pure HSA adsorption experiments on a high-N, low-N, high-O and Pt surfaces revealed no difference in the adsorbed amounts. HSA adsorption kinetics were clearly differentiated from that of Fg adsorption by the presence of a sharp peak on the kinetic curve at the time of HSA injection. The shape of the kinetic curves of pure HSA adsorption suggested an initial bilayer formation on the surfaces that was

reduced to a monolayer upon rinsing with PBS. Influence of HSA on Fg adsorption was indicated by an increase in Fg on the low-N and high-O surfaces, with the increase on the high-O surface being much more pronounced. No effect was observed on the high-N coating. Despite these changes, there were still significant differences in the amount of Fg adsorbed on the various coatings. Thus, within the scope of this study, regulation of Fg adsorption was successfully achieved by the designed plasma polymer coatings, with and without the influence of a competing protein.

The originality of this part of the thesis includes: the study of the effect of deposition pressure on film composition in association with Fg adsorption, the study of Fg adsorption on a Pt surface by SPRS, the study of the effect of different HC based film types on Fg adsorption and indeed, the development of a surface engineering technique geared towards the potential use in studying the effect of the degree of coil thrombogenicity on aneurysm healing.

Development of plasma polymer coatings for a specific biomedical application requires that several factors, from the type of plasma process, precursor types, process conditions to film stability, chemical and mechanical characterisation, biological testing and implementation, are considered. This thesis has attempted to cover several of these factors where the series of coatings developed, through various optimisation and characterisation procedures, were found to be suitable for successful regulation of Fg and therefore, could potentially be used to study the effect of the degree of coil thrombogenicity in brain aneurysm healing succeeding an endovascular coiling treatment. In this regard, the next steps would be to perform an in-depth study of these coatings on the biological response i.e. blood coagulation, mechanical properties and implementation on the bare Pt coils. Some limitations and suggestions for improvements and future work are presented in the following section.

7.2 Limitations and future improvements

In the study of single source precursors and precursor mixtures, calculations based on density functional theory (DFT) could provide a clearer picture of the precursor fragmentation pathways and estimate the Gibbs free enthalpies of the reactions.

In the protein adsorption study from a mixture of Fg and HSA, only Fg adsorption was measured since this was the protein of interest. It could be interesting to know if the amount of HSA adsorbed was altered in any way during the competitive process. Unfortunately, obtaining information on the total protein adsorbed from the SPR curve is difficult since modelling of the SPR curve requires for well-defined layers with well-defined refractive indices. However, by repeating similar experiments with fluorescently labelled HSA, the total and individual surface densities of Fg and HSA in the adsorbed layer can be determined, from which refractive index of the mixture layer can be calculated, thereby also allowing for the evaluation of the total adsorbed layer thickness by fitting of the SPR curve.

Studying the influence of other plasma proteins such as immunoglobulin on regulation of Fg adsorption using plasma polymer coatings could also be interesting. In addition, regulating the adsorption of other platelet adhesive proteins such as fibronectin, vitronectin and Von Willebrand factor, and clotting factors such as Factor XII may also provide insight into controlling thrombosis and blood coagulation. However, a limitation of these experiments is that proteins, especially with fluorescent labelling, are expensive and therefore, conducting experiments at relevant protein concentrations and flow conditions could be difficult.

One of the assumptions made during protein adsorption experiments was the refractive index of the protein layers. It might be useful to measure the refractive index of same to validate this assumption. This could be done by measuring protein adsorption on a thick plasma polymer coating so as to provide waveguide modes in the SPR curve. The shift in

the waveguide modes due to protein adsorption could be fitted to provide the thickness and refractive index of the protein layer, simultaneously.

The overall intention of this study was to lay the foundation for the development of plasma polymer coated Pt coils to study aneurysm healing. Indeed, the role of the extent of coil thrombogenicity on aneurysm healing remains unclear. These coatings provide a basis for achieving thrombosis to different extents and in turn, studying the effect of the degree of coil thrombogenicity on aneurysm healing. In this regard, platelet adhesion and activation tests on the various surfaces developed here will certainly be the next step towards determining the control of thrombosis that could potentially be achieved by these coatings.

References

- [1] B. D. Ratner. *Biomaterials science an introduction to materials in medicine*. Academic Press, Massachusetts, USA, 3 edition, 2013.
- [2] A. A. Meyer-Plath, K. Schroder, B. Finke, and A. Ohl. Current trends in biomaterial surface functionalization - nitrogen-containing plasma assisted processes with enhanced selectivity. *Vacuum*, 71(3):391–406, 2003.
- [3] F. Truica-Marasescu, S. Guimond, and M. R. Wertheimer. Vuv-induced nitriding of polymer surfaces: Comparison with plasma treatments in nitrogen. *Nuclear Instruments and Methods in Physics Research Section B-Beam Interactions with Materials and Atoms*, 208:294–299, 2003.
- [4] F. Truica-Marasescu and M. R. Wertheimer. Vacuum ultraviolet-induced photochemical nitriding of polyolefin surfaces. *Journal of Applied Polymer Science*, 91(6):3886–3898, 2004.
- [5] K. S. Siow, L. Britcher, S. Kumar, and H. J. Griesser. Plasma methods for the generation of chemically reactive surfaces for biomolecule immobilization and cell colonization - a review. *Plasma Processes and Polymers*, 3(6-7):392–418, 2006.
- [6] A. G. Shard, J. D. Whittle, A. J. Beck, P. N. Brookes, N. A. Bullett, R. A. Talib, A. Mistry, D. Barton, and S. L. McArthur. A nexafs examination of unsaturation in plasma polymers of allylamine and propylamine. *Journal of Physical Chemistry B*, 108(33):12472–12480, 2004.
- [7] U. Oran, S. Swaraj, A. Lippitz, and W. E. S. Unger. Surface analysis of plasma deposited polymer films, 7 - "in situ" characterization of plasma deposited allylamine films by tof-ssims, xps and nexafs spectroscopy. *Plasma Processes and Polymers*, 3(3):288–298, 2006.

- [8] P. L. Girard-Lauriault, F. Mwale, M. Iordanova, C. Demers, P. Desjardins, and M. R. Wertheimer. Atmospheric pressure deposition of micropatterned nitrogen-rich plasma-polymer films for tissue engineering. *Plasma Processes and Polymers*, 2(3):263–270, 2005.
- [9] S. Babaei and P. L. Girard-Lauriault. Tuning the surface properties of oxygen-rich and nitrogen-rich plasma polymers: Functional groups and surface charge. *Plasma Chemistry and Plasma Processing*, 36(2):651–666, 2016.
- [10] F. Truica-Marasescu, S. Guimond, P. Jedrzejowski, and M. R. Wertheimer. Hydrophobic recovery of vuv/nh₃ modified polyolefin surfaces: Comparison with plasma treatments in nitrogen. *Nuclear Instruments and Methods in Physics Research Section B-Beam Interactions with Materials and Atoms*, 236:117–122, 2005.
- [11] F. Truica-Marasescu, P. Jedrzejowski, and M. R. Wertheimer. Hydrophobic recovery of vacuum ultraviolet irradiated polyolefin surfaces. *Plasma Processes and Polymers*, 1(2):153–163, 2004.
- [12] N. A. Bullett, D. P. Bullett, F. E. Truica-Marasescu, S. Lerouge, F. Mwale, and M. R. Wertheimer. Polymer surface micropatterning by plasma and vuv-photochemical modification for controlled cell culture. *Applied Surface Science*, 235(4):395–405, 2004.
- [13] P. S. Sit and R. E. Marchant. Surface-dependent conformations of human fibrinogen observed by atomic force microscopy under aqueous conditions. *Thrombosis and Haemostasis*, 82(3):1053–1060, 1999.
- [14] J. A. Broeders, A. U. Ahmed, A. J. Molyneux, W. Poncyłjusz, J. Raymond, P. M. White, and B. Steinfort. Bioactive versus bare platinum coils for the endovascular treatment of intracranial aneurysms: systematic review and meta-analysis of randomized clinical trials. *J Neurointerv Surg*, 2015.

- [15] G. Guglielmi, F. Vinuela, I. Sepetka, and V. Macellari. Electrothrombosis of saccular aneurysms via endovascular approach. part 1: Electrochemical basis, technique, and experimental results. *J Neurosurg*, 75(1):1–7, 1991.
- [16] L. K. Wang, Y. T. Hung, and N. K. Shamma. *Advanced physicochemical treatment technologies*, volume 5. Humana Press Inc., New Jersey USA, 2007.
- [17] A. Grill. *Cold plasma in materials fabrication: From fundamentals to applications*, volume 151. IEEE Press, New York, USA, 1994.
- [18] S. Samal. Thermal plasma technology: The prospective future in material processing. *Journal of Cleaner Production*, 142:3131–3150, 2017.
- [19] H. Yasuda. *Luminous chemical vapor deposition and interface engineering*. Marcel Dekker, New York, 2005.
- [20] D. Hegemann, M. M. Hossain, E. Korner, and D. J. Balazs. Macroscopic description of plasma polymerization. *Plasma Processes and Polymers*, 4(3):229–238, 2007.
- [21] R. d’Agostino and F. Palumbo. Comment on "ion-assisted processes of polymerization in low-pressure plasmas". *Plasma Processes and Polymers*, 9(9):844–849, 2012.
- [22] H. Biederman. *Plasma polymer films*. Imperial College Press, London, 2004.
- [23] F. F. Shi. Developments in plasma-polymerized organic thin films with novel mechanical, electrical, and optical properties. *Journal of Macromolecular Science-Reviews in Macromolecular Chemistry and Physics*, C36(4):795–826, 1996.
- [24] Z. Zhang, B. Menges, R. B. Timmons, W. Knoll, and R. Forch. Surface plasmon resonance studies of protein binding on plasma polymerized di(ethylene glycol) monovinyl ether films. *Langmuir*, 19(11):4765–4770, 2003.

- [25] S. Liu, M. M. L. M. Vareiro, S. Fraser, and A. T. A. Jenkins. Control of attachment of bovine serum albumin to pulse plasma-polymerized maleic anhydride by variation of pulse conditions. *Langmuir*, 21(19):8572–8575, 2005.
- [26] Q. Chen, R. Forch, and W. Knoll. Characterization of pulsed plasma polymerization allylamine as an adhesion layer for dna adsorption/hybridization. *Chemistry of Materials*, 16(4):614–620, 2004.
- [27] R. Forch, Z. H. Zhang, and W. Knoll. Soft plasma treated surfaces: Tailoring of structure and properties for biomaterial applications. *Plasma Processes and Polymers*, 2(5):351–372, 2005.
- [28] R. C. Chatelier, X. M. Xie, T. R. Gengenbach, and H. J. Griesser. Quantitative-analysis of polymer surface restructuring. *Langmuir*, 11(7):2576–2584, 1995.
- [29] P. Favia, M. V. Stendardo, and R. d’Agostino. Selective grafting of amine groups on polyethylene by means of nh₃-h₂ rf glow discharges. *Plasmas and Polymers*, 1(2):91–112, 1996.
- [30] A. A. Meyer-Plath, B. Finke, K. Schroder, and A. Ohl. Pulsed and cw microwave plasma excitation for surface functionalization in nitrogen-containing gases. *Surface and Coatings Technology*, 174:877–881, 2003.
- [31] F. Truica-Marasescu, P. L. Girard-Lauriault, A. Lippitz, W. E. S. Unger, and M. R. Wertheimer. Nitrogen-rich plasma polymers: Comparison of films deposited in atmospheric- and low-pressure plasmas. *Thin Solid Films*, 516(21):7406–7417, 2008.
- [32] F. Fally, C. Doneux, J. Riga, and J. J. Verbist. Quantification of the functional groups present at the surface of plasma polymers deposited from propylamine, allylamine, and propargylamine. *Journal of Applied Polymer Science*, 56(5):597–614, 1995.

- [33] I. Gancarz, J. Bryjak, G. Pozniak, and W. Tylus. Plasma modified polymers as a support for enzyme immobilization - ii. amines plasma. *European Polymer Journal*, 39(11):2217–2224, 2003.
- [34] B. Lassen and M. Malmsten. Competitive protein adsorption at plasma polymer surfaces. *Journal of Colloid and Interface Science*, 186(1):9–16, 1997.
- [35] T. R. Gengenbach and H. J. Griesser. Aging of 1,3-diaminopropane plasma-deposited polymer films: Mechanisms and reaction pathways. *Journal of Polymer Science Part a-Polymer Chemistry*, 37(13):2191–2206, 1999.
- [36] T. R. Gengenbach, R. C. Chatelier, and H. J. Griesser. Correlation of the nitrogen 1s and oxygen 1s xps binding energies with compositional changes during oxidation of ethylene diamine plasma polymers. *Surface and Interface Analysis*, 24(9):611–619, 1996.
- [37] P. Kingshott, H. Thissen, and H. J. Griesser. Effects of cloud-point grafting, chain length, and density of peg layers on competitive adsorption of ocular proteins. *Biomaterials*, 23(9):2043–2056, 2002.
- [38] M. Muller and C. Oehr. Plasma aminofunctionalisation of pvdf microfiltration membranes: comparison of the in plasma modifications with a grafting method using esca and an amino-selective fluorescent probe. *Surface and Coatings Technology*, 116:802–807, 1999.
- [39] P. L. Girard-Lauriault, P. Desjardins, W. E. S. Unger, A. Lippitz, and M. R. Wertheimer. Chemical characterisation of nitrogen-rich plasma-polymer films deposited in dielectric barrier discharges at atmospheric pressure. *Plasma Processes and Polymers*, 5(7):631–644, 2008.
- [40] P. L. Girard-Lauriault, F. Truica-Marasescu, A. Petit, H. T. Wang, P. Desjardins, J. Antoniou, F. Mwale, and M. R. Wertheimer. Adhesion of human u937 monocytes to

- nitrogen-rich organic thin films: novel insights into the mechanism of cellular adhesion. *Macromol Biosci*, 9(9):911–21, 2009.
- [41] J. G. Calderon, A. Harsch, G. W. Gross, and R. B. Timmons. Stability of plasma-polymerized allylamine films with sterilization by autoclaving. *Journal of Biomedical Materials Research*, 42(4):597–603, 1998.
- [42] Florina Truica-Marasescu and Michael R. Wertheimer. Nitrogen-rich plasma-polymer films for biomedical applications. *Plasma Processes and Polymers*, 5(1):44–57, 2008.
- [43] M. M. Hossain, A. S. Herrmann, and D. Hegemann. Incorporation of accessible functionalities in nanoscaled coatings on textiles characterized by coloration. *Plasma Processes and Polymers*, 4(2):135–144, 2007.
- [44] T. R. Gengenbach, R. C. Chatelier, and H. J. Griesser. Characterization of the ageing of plasma-deposited polymer films: Global analysis of x-ray photoelectron spectroscopy data. *Surface and Interface Analysis*, 24(4):271–281, 1996.
- [45] J. Dorst, M. Vandenbossche, M. Amberg, L. Bernard, P. Rupper, K. D. Weltmann, K. Fricke, and D. Hegemann. Improving the stability of amino-containing plasma polymer films in aqueous environments. *Langmuir*, 2017.
- [46] M. B. Zucker and V. T. Nachmias. Platelet activation. *Arteriosclerosis*, 5(1):2–18, 1985.
- [47] W. B. Tsai, J. M. Grunkemeier, and T. A. Horbett. Human plasma fibrinogen adsorption and platelet adhesion to polystyrene. *Journal of Biomedical Materials Research*, 44(2):130–139, 1999.
- [48] J. A. Chinn, B. D. Ratner, and T. A. Horbett. Adsorption of baboon fibrinogen and the adhesion of platelets to a thin film polymer deposited by radio-frequency glow discharge of allylamine. *Biomaterials*, 13(5):322–332, 1992.

- [49] G. Ladam, C. Gergely, B. Senger, G. Decher, J. C. Voegel, P. Schaaf, and F. J. G. Cuisinier. Protein interactions with polyelectrolyte multilayers: Interactions between human serum albumin and polystyrene sulfonate/polyallylamine multilayers. *Biomacromolecules*, 1(4):674–687, 2000.
- [50] Z. Adamczyk, B. Cichocki, M. L. Ekiel-Jezewska, A. Slowicka, E. Wajnryb, and M. Wasilewska. Fibrinogen conformations and charge in electrolyte solutions derived from dls and dynamic viscosity measurements. *Journal of Colloid and Interface Science*, 385:244–257, 2012.
- [51] R. J. Green, J. Davies, M. C. Davies, C. J. Roberts, and S. J. B. Tendler. Surface plasmon resonance for real time in situ analysis of protein adsorption to polymer surfaces. *Biomaterials*, 18(5):405–413, 1997.
- [52] B. Lassen and M. Malmsten. Structure of protein layers during competitive adsorption. *Journal of Colloid and Interface Science*, 180(2):339–349, 1996.
- [53] G. L. Francis. Albumin and mammalian cell culture: implications for biotechnology applications. *Cytotechnology*, 62(1):1–16, 2010.
- [54] T. A. Horbett. Adsorption of proteins from plasma to a series of hydrophilic-hydrophobic co-polymers. 2. compositional analysis with the prelabeled protein technique. *Journal of Biomedical Materials Research*, 15(5):673–695, 1981.
- [55] S. M. Slack and T. A. Horbett. The vroman effect - a critical review. *Proteins at Interfaces II*, 602:112–128, 1995.
- [56] J. L. Brash and T. A. Horbett. *Proteins at interfaces - An overview*, volume 602. ACS Symposium Series; American Chemical Society, Washington, DC, 1995.

- [57] W. K. Lee, J. McGuire, and M. K. Bothwell. Competitive adsorption of bacteriophage t4 lysozyme stability variants at hydrophilic glass surfaces. *Journal of Colloid and Interface Science*, 269(1):251–254, 2004.
- [58] J. E. Mahan. *Physical vapor deposition of thin films*. Wiley, 2000.
- [59] P. Chabert and N. Braithwaite. *Physics of radio-frequency plasmas*. Cambridge University Press, New York, USA, 2011.
- [60] S. Ligot, M. Guillaume, P. Raynaud, D. Thiry, V. Lemaire, T. Silva, N. Britun, J. Cornil, P. Dubois, and R. Snyders. Experimental and theoretical study of the plasma chemistry of ethyl lactate plasma polymerization discharges. *Plasma Processes and Polymers*, 12(5):405–415, 2015.
- [61] E. D. Hoffmann and V. Stroobant. *Mass spectrometry: Principles and applications*. John Wiley and Sons Ltd, West Sussex, UK, 3 edition, 2007.
- [62] D. Thiry, F. J. Aparicio, N. Britun, and R. Snyders. Concomitant effects of the substrate temperature and the plasma chemistry on the chemical properties of propanethiol plasma polymer prepared by icp discharges. *Surface and Coatings Technology*, 241:2–7, 2014.
- [63] L. Denis, P. Marsal, Y. Olivier, T. Godfroid, R. Lazzaroni, M. Hecq, J. Cornil, and R. Snyders. Deposition of functional organic thin films by pulsed plasma polymerization: A joint theoretical and experimental study. *Plasma Processes and Polymers*, 7(2):172–181, 2010.
- [64] L. O’Toole, R. D. Short, A. P. Ameen, and F. R. Jones. Mass-spectrometry of and deposition-rate measurements from radiofrequency-induced plasmas of methyl isobutyrate, methyl-methacrylate and n-butyl methacrylate. *Journal of the Chemical Society-Faraday Transactions*, 91(9):1363–1370, 1995.

- [65] B. C. Smith. *Fundamentals of fourier transform infrared spectroscopy*. Taylor and Francis, Florida, USA, 2 edition, 2011.
- [66] J. F. Watts and J. Wolstenholme. *An introduction to surface analysis by XPS and AES*. John Wiley and Sons Ltd, West Sussex, UK, 2003.
- [67] C. P. Klages, Z. Khosravi, and A. Hinze. Some remarks on chemical derivatization of polymer surfaces after exposure to nitrogen-containing plasmas. *Plasma Processes and Polymers*, 10(4):307–312, 2013.
- [68] C. P. Klages and S. Kotula. Critical remarks on chemical derivatization analysis of plasma-treated polymer surfaces and plasma polymers. *Plasma Processes and Polymers*, 13(12):1213–1223, 2016.
- [69] P. L. Girard-Lauriault, P. Dietrich, T. Gross, and W. E. S. Unger. Is quantitative chemical derivatization xps of plasma deposited organic coatings a valid analytical procedure? *Surface and Interface Analysis*, 44(8):1135–1140, 2012.
- [70] M. Agashe, V. Raut, S. J. Stuart, and R. A. Latour. Molecular simulation to characterize the adsorption behavior of a fibrinogen gamma-chain fragment. *Langmuir*, 21(3):1103–1117, 2005.
- [71] M. Strobel and C. S. Lyons. An essay on contact angle measurements. *Plasma Processes and Polymers*, 8(1):8–13, 2011.
- [72] I. L. Singer, S. D. Dvorak, K. J. Wahl, and T. W. Scharf. Role of third bodies in friction and wear of protective coatings. *Journal of Vacuum Science and Technology A*, 21(5):S232–S240, 2003.
- [73] D. Hegemann, H. Brunner, and C. Oehr. Plasma treatment of polymers for surface and adhesion improvement. *Nuclear Instruments and Methods in Physics Research Section B-Beam Interactions with Materials and Atoms*, 208:281–286, 2003.

- [74] M. R. Widmer, M. Heuberger, J. Voros, and N. D. Spencer. Influence of polymer surface chemistry on frictional properties under protein-lubrication conditions: implications for hip-implant design. *Tribology Letters*, 10(1-2):111–116, 2001.
- [75] L. Q. Chu, Q. Zhang, and R. Forch. Surface plasmon-based techniques for the analysis of plasma deposited functional films and surfaces. *Plasma Processes and Polymers*, 12(9):941–952, 2015.
- [76] Z. Zhang, W. Knoll, and R. Forch. Amino-functionalized plasma polymer films for dna immobilization and hybridization. *Surface and Coatings Technology*, 200(1-4):993–995, 2005.
- [77] R. Foerch, A. N. Chifen, A. Bousquet, H. L. Khor, M. Jungblut, L. Q. Chu, Z. Zhang, I. Osey-Mensah, E. K. Sinner, and W. Knoll. Recent and expected roles of plasma-polymerized films for biomedical applications. *Chemical Vapor Deposition*, 13(6-7):280–294, 2007.
- [78] L. Q. Chu, W. Knoll, and R. Forch. Pulsed plasma polymerized di(ethylene glycol) monovinyl ether coatings for nonfouling surfaces. *Chemistry of Materials*, 18(20):4840–4844, 2006.
- [79] T. Liebermann and W. Knoll. Surface-plasmon field-enhanced fluorescence spectroscopy. *Colloids and Surfaces a-Physicochemical and Engineering Aspects*, 171(1-3):115–130, 2000.
- [80] T. Neumann, M. L. Johansson, D. Kambhampati, and W. Knoll. Surface-plasmon fluorescence spectroscopy. *Advanced Functional Materials*, 12(9):575–586, 2002.
- [81] S. Roy, J. H. Kim, J. T. Kellis, A. J. Poulouse, C. R. Robertson, and A. P. Gast. Surface plasmon resonance/surface plasmon enhanced fluorescence: An optical technique for the detection of multicomponent macromolecular adsorption at the solid/liquid interface. *Langmuir*, 18(16):6319–6323, 2002.

- [82] V. Nelea, L. Luo, C. N. Demers, J. Antoniou, A. Petit, S. Lerouge, M. R. Wertheimer, and F. Mwale. Selective inhibition of type x collagen expression in human mesenchymal stem cell differentiation on polymer substrates surface-modified by glow discharge plasma. *Journal of Biomedical Materials Research Part A*, 75A:216–223, 2005.
- [83] F. Mwale, H. T. Wang, V. Nelea, L. Luo, J. Antoniou, and M. R. Wertheimer. The effect of glow discharge plasma surface modification of polymers on the osteogenic differentiation of committed human mesenchymal stem cells. *Biomaterials*, 27:2258–2264, 2006.
- [84] F. Mwale, P. L. Girard-Lauriault, H. T. Wang, S. Lerouge, J. Antoniou, and M. R. Wertheimer. Suppression of genes related to hypertrophy and osteogenesis in committed human mesenchymal stem cells cultured on novel nitrogen-rich plasma polymer coatings. *Tissue Engineering*, 12:2639–2647, 2006.
- [85] S. Lerouge, A. Major, P. L. Girard-Lauriault, M. A. Raymond, P. Laplante, G. Soulez, F. Mwale, M. R. Wertheimer, and M. J. Hébert. Nitrogen-rich coatings for promoting healing around stent-grafts after endovascular aneurysm repair. *Biomaterials*, 28(6):1209–1217, 2007.
- [86] A. Gigout, J. C. Ruiz, M. R. Wertheimer, M. Jolicoeur, and S. Lerouge. Nitrogen-rich plasma-polymerized coatings on pet and ptfe surfaces improve endothelial cell attachment and resistance to shear flow. *Macromolecular Bioscience*, 11(8):1110–1119, 2011.
- [87] C. Charbonneau, J. C. Ruiz, P. Lequoy, M. J. Hébert, G. De Crescenzo, M. R. Wertheimer, and S. Lerouge. Chondroitin sulfate and epidermal growth factor immobilization after plasma polymerization: A versatile anti-apoptotic coating to promote healing around stent grafts. *Macromolecular bioscience*, 12(6):812–821, 2012.

- [88] E. Gallino, S. Massey, M. Tatoulian, and D. Mantovani. Plasma polymerized allylamine films deposited on 316l stainless steel for cardiovascular stent coatings. *Surface and Coatings Technology*, 205(7):2461–2468, 2010.
- [89] P. K. Thalla, A. Contreras-Garcia, H. Fadlallah, J. Barrette, G. De Crescenzo, Y. Merhi, and S. Lerouge. A versatile star peg grafting method for the generation of nonfouling and nonthrombogenic surfaces. *Biomed Research International*, 2013.
- [90] K. Vasilev, V. R. Sah, R. V. Goreham, C. Ndi, R. D. Short, and H. J. Griesser. Antibacterial surfaces by adsorptive binding of polyvinyl-sulphonate-stabilized silver nanoparticles. *Nanotechnology*, 21(21):215102, 2010.
- [91] S. Taheri, A. Cavallaro, S. N. Christo, L. E. Smith, P. Majewski, M. Barton, J. D. Hayball, and K. Vasilev. Substrate independent silver nanoparticle based antibacterial coatings. *Biomaterials*, 35(16):4601–4609, 2014.
- [92] L. Štrbková, A. Manakhov, L. Zajíčková, A. Stoica, P. Veselý, and R. Chmelík. The adhesion of normal human dermal fibroblasts to the cyclopropylamine plasma polymers studied by holographic microscopy. *Surface and Coatings Technology*, 295:70–77, 2016.
- [93] C. Dehili, P. Lee, K. M. Shakesheff, and M. R. Alexander. Comparison of primary rat hepatocyte attachment to collagen and plasma-polymerised allylamine on glass. *Plasma Processes and Polymers*, 3(6-7):474–484, 2006.
- [94] B. Finke, F. Luethen, K. Schroeder, P. D. Mueller, C. Bergemann, M. Frant, A. Ohl, and B. J. Nebe. The effect of positively charged plasma polymerization on initial osteoblastic focal adhesion on titanium surfaces. *Biomaterials*, 28(30):4521–4534, 2007.
- [95] P. Hamerli, Th. Weigel, Th. Groth, and D. Paul. Surface properties of and cell adhesion onto allylamine-plasma-coated polyethylenterephthalat membranes. *Biomaterials*, 24(22):3989–3999, 2003.

- [96] M. Buddhadasa and P. L. Girard-Lauriault. Plasma co-polymerisation of ethylene, 1,3-butadiene and ammonia mixtures: Amine content and water stability. *Thin Solid Films*, 591:76–85, 2015.
- [97] K. Fricke, P. L. Girard-Lauriault, K. D. Weltmann, and M. R. Wertheimer. Plasma polymers deposited in atmospheric pressure dielectric barrier discharges: Influence of process parameters on film properties. *Thin Solid Films*, 603:119–125, 2016.
- [98] A. Harsch, J. Calderon, R. B. Timmons, and G. W. Gross. Pulsed plasma deposition of allylamine on polysiloxane: a stable surface for neuronal cell adhesion. *Journal of Neuroscience Methods*, 98(2):135–144, 2000.
- [99] L. Denis, D. Cossement, T. Godfroid, F. Renaux, C. Bittencourt, R. Snyders, and M. Hecq. Synthesis of allylamine plasma polymer films: Correlation between plasma diagnostic and film characteristics. *Plasma Processes and Polymers*, 6:199–208, 2009.
- [100] J. Ryssy, E. Prioste-Amaral, D. F. N. Assuncao, N. Rogers, G. T. S. Kirby, L. E. Smith, and A. Michelmore. Chemical and physical processes in the retention of functional groups in plasma polymers studied by plasma phase mass spectroscopy. *Physical Chemistry Chemical Physics*, 18(6):4496–4504, 2016.
- [101] K. Vasilev, L. Britcher, A. Casanal, and H. J. Griesser. Solvent-induced porosity in ultrathin amine plasma polymer coatings. *Journal of Physical Chemistry B*, 112:10915–10921, 2008.
- [102] A. Manakhov, L. Zajickova, M. Elias, J. Cechal, J. Polcak, J. Hnilica, S. Bitnerova, and D. Necas. Optimization of cyclopropylamine plasma polymerization toward enhanced layer stability in contact with water. *Plasma Processes and Polymers*, 11(6):532–544, 2014.

- [103] J. C. Ruiz, A. St-Georges-Robillard, C. Theresy, S. Lerouge, and M. R. Wertheimer. Fabrication and characterisation of amine-rich organic thin films: Focus on stability. *Plasma Processes and Polymers*, 7(9-10):737–753, 2010.
- [104] A. Contreras-García and M. R. Wertheimer. Low-pressure plasma polymerization of acetylene–ammonia mixtures for biomedical applications. *Plasma Chemistry and Plasma Processing*, 33(1):147–163, 2013.
- [105] A. E. Lefohn, N. M. Mackie, and E. R. Fisher. Comparison of films deposited from pulsed and continuous wave acetonitrile and acrylonitrile plasmas. *Plasmas and polymers*, 3(4):197–209, 1998.
- [106] D. Hegemann, E. Korner, and S. Guimond. Plasma polymerization of acrylic acid revisited. *Plasma Processes and Polymers*, 6(4):246–254, 2009.
- [107] C. Vandenabeele, M. Buddhadasa, P. L. Girard-Lauriault, and R. Snyders. Comparison between single monomer versus gas mixture for the deposition of primary amine-rich plasma polymers. *Thin Solid Films*, 2016.
- [108] S. Ligot, D. Thiry, P. A. Cormier, P. Raynaud, P. Dubois, and R. Snyders. In situ ir spectroscopy as a tool to better understand the growth mechanisms of plasma polymers thin films. *Plasma Processes and Polymers*, 12:1200–1207, 2015.
- [109] S. A. Voronin, M. Zelzer, C. Fotea, M. R. Alexander, and J. W. Bradley. Pulsed and continuous wave acrylic acid radio frequency plasma deposits: Plasma and surface chemistry. *Journal of Physical Chemistry B*, 111(13):3419–3429, 2007.
- [110] J. R. Durig, J. F. Sullivan, and C. M. Whang. Low frequency vibrational spectrum and conformational analysis of allylamine. *Spectrochimica Acta Part a-Molecular and Biomolecular Spectroscopy*, 41(1-2):129–154, 1985.

- [111] V. F. Kalasinsky, D. E. Powers, and W. C. Harris. Vibrational-spectra and conformations of cyclopropylamine. *Journal of Physical Chemistry*, 83(4):506–510, 1979.
- [112] H. E. Howard-Lock, C. J. L. Lock, G. Turner, and M. Zvagulis. The crystal structure and vibrational spectra of cis-dichlorobis (cyclopropylamine)-platinum (ii), $\text{PtCl}_2(\text{C}_3\text{H}_5\text{NH}_2)_2$. *Canadian Journal of Chemistry*, 59(18):2737–2745, 1981.
- [113] A. O. Diallo, Nguyenvanthanh, and I. Rossi. Infrared-spectra and conformation of cyclopropylamine, cpa. *Spectrochimica Acta Part a-Molecular and Biomolecular Spectroscopy*, 43(3):415–420, 1987.
- [114] T. Shimanouchi. *Tables of Molecular Vibrational Frequencies Consolidated*, volume 1. National Bureau of Standards, Washington D.C., 1972.
- [115] A. Maki, W. Quapp, S. Klee, G. C. Mellau, and S. Albert. The cn mode of hcn: A comparative study of the variation of the transition dipole and herman-wallis constants for seven isotopomers and the influence of vibration-rotation interaction. *Journal of Molecular Spectroscopy*, 174(2):365–378, 1995.
- [116] K. N. Choi and E. F. Barker. Infrared absorption spectrum of hydrogen cyanide. *Physical Review*, 42(6):0777–0785, 1932.
- [117] B. Smith. *Infrared Spectral Interpretation: A Systematic Approach*. CRC Press, London, 1999.
- [118] G. Socrates. *Infrared and Raman characteristic group frequencies: tables and charts*. John Wiley & Sons, Chichester, 2004.
- [119] K. B. K. Teo, M. Chhowalla, G. A. J. Amaratunga, W. I. Milne, D. G. Hasko, G. Pirio, P. Legagneux, F. Wyczisk, and D. Pribat. Uniform patterned growth of carbon nanotubes without surface carbon. *Applied Physics Letters*, 79(10):1534–1536, 2001.

- [120] Y. R. Luo. *Handbook of bond dissociation energies in organic compounds*. CRC press, Florida, USA, 2003.
- [121] D. Thiry, S. Konstantinidis, J. Cornil, and R. Snyders. Plasma diagnostics for the low-pressure plasma polymerization process: A critical review. *Thin Solid Films*, 606:19–44, 2016.
- [122] Z. Zhang, Q. Chen, W. Knoll, and R. Forch. Effect of aqueous solution on functional plasma polymerized films. *Surface and Coatings Technology*, 174:588–590, 2003.
- [123] J. Friedrich, G. Kuhn, R. Mix, A. Fritz, and A. Schonhals. Polymer surface modification with monofunctional groups of variable types and densities. *Journal of Adhesion Science and Technology*, 17:1591–1617, 2003.
- [124] A. Tarasova, P. Hamilton-Brown, T. Gengenbach, H. J. Griesser, and L. Meagher. Colloid probe afm and xps study of time-dependent aging of amine plasma polymer coatings in aqueous media. *Plasma Processes and Polymers*, 5:175–185, 2008.
- [125] B. Finke, K. Schroder, and A. Ohl. Structure retention and water stability of microwave plasma polymerized films from allylamine and acrylic acid. *Plasma Processes and Polymers*, 6:S70–S74, 2009.
- [126] D. Hegemann and M. M. Hossain. Influence of non-polymerizable gases added during plasma polymerization. *Plasma Processes and Polymers*, 2:554–562, 2005.
- [127] F. Truica-Marasescu and M. R. Wertheimer. Vacuum-ultraviolet photopolymerisation of amine-rich thin films. *Macromolecular Chemistry and Physics*, 209:1043–1049, 2008.
- [128] P. Hammer and F. Alvarez. Influence of chemical sputtering on the composition and bonding structure of carbon nitride films. *Thin Solid Films*, 398:116–123, 2001.

- [129] Y. H. Cheng, Y. P. Wu, J. G. Chen, X. L. Qiao, C. S. Xie, B. K. Tay, S. P. Lau, and X. Shi. On the deposition mechanism of a-c : H films by plasma enhanced chemical vapor deposition. *Surface and Coatings Technology*, 135:27–33, 2000.
- [130] Donald Pavia, Gary Lampman, George Kriz, and James Vyvyan. *Introduction to spectroscopy*. Harcourt, Orlando, FL, USA, 2001.
- [131] J. A. Dean. *Lange's Handbook of Chemistry*. McGraw-Hill, USA, 1999.
- [132] D. C. Montgomery, G. C. Runger, and N. M. Hubele. *Engineering Statistics*. Wiley, Hoboken, NJ, USA, 2011.
- [133] P. L. Girard-Lauriault, P. M. Dietrich, T. Gross, T. Wirth, and W. E. S. Unger. Chemical characterization of the long-term ageing of nitrogen-rich plasma polymer films under various ambient conditions. *Plasma Processes and Polymers*, 10:388–395, 2013.
- [134] J. Y. Yook, M. Lee, K. H. Song, J. Jun, and S. Kwak. Surface modification of poly(ethylene-2,6-naphthalate) using nh₃ plasma. *Macromolecular Research*, 22:534–540, 2014.
- [135] R. d'Agostino, F. Cramarossa, S. De Benedictis, and G. Ferraro. Kinetic and spectroscopic analysis of nh₃ decomposition under r.f. plasma at moderate pressures. *Plasma Chemistry and Plasma Processing*, 1:19–35, 1981.
- [136] J. E. Nicholas, A. I. Spiers, and N. A. Martin. Kinetics and mechanism in the decomposition of nh₃ in a radiofrequency pulse discharge. *Plasma Chemistry and Plasma Processing*, 6:39–51, 1986.
- [137] F. Arefi-Khonsari, J. Kurdi, M. Tatoulian, and J. Amouroux. On plasma processing of polymers and the stability of the surface properties for enhanced adhesion to metals. *Surface and Coatings Technology*, 142:437–448, 2001.

- [138] J. Y. Yook, J. Jun, and S. Kwak. Amino functionalization of carbon nanotube surfaces with nh₃ plasma treatment. *Applied Surface Science*, 256:6941–6944, 2010.
- [139] F. Arefi-Khonsari, M. Tatoulian, and J. Kurdi. Study of the surface properties and stability of polymer films treated by nh₃ plasma and its mixtures. *Journal of photopolymer science and technology.*, 11:277–292, 1998.
- [140] Y. Murayama, F. Vinuela, S. Tateshima, J. K. Song, N. R. Gonzalez, and M. P. Wallace. Bioabsorbable polymeric material coils for embolization of intracranial aneurysms: a preliminary experimental study. *J Neurosurg*, 94(3):454–63, 2001.
- [141] L. Feng, F. Vinuela, and Y. Murayama. Healing of intracranial aneurysms with bioactive coils. *Neurosurgery Clinics*, 16(3):487–499, 2005.
- [142] Y. Niimi, J. Song, M. Madrid, and A. Berenstein. Endosaccular treatment of intracranial aneurysms using matrix coils early experience and midterm follow-up. *Stroke*, 37(4):1028–1032, 2006.
- [143] L. Zhang, B. Casey, D. K. Galanakis, C. Marmorat, S. Skoog, K. Vorvolakos, M. Simon, and M. H. Rafailovich. The influence of surface chemistry on adsorbed fibrinogen conformation, orientation, fiber formation and platelet adhesion. *Acta Biomaterialia*, 54:164–174, 2017.
- [144] P. M. White, S. C. Lewis, A. Gholkar, R. J. Sellar, H. Nahser, C. Cognard, L. Forrester, J. M. Wardlaw, et al. Hydrogel-coated coils versus bare platinum coils for the endovascular treatment of intracranial aneurysms (helps): a randomised controlled trial. *The Lancet*, 377(9778):1655–1662, 2011.
- [145] J. Raymond, R. Klink, M. Chagnon, S. L. Barnwell, A. J. Evans, J. Mocco, B. H. Hoh, A. S. Turk, R. D. Turner, H. Desal, et al. Hydrogel versus bare platinum coils in patients with large or recurrent aneurysms prone to recurrence after endovascular treatment:

- A randomized controlled trial. *American Journal of Neuroradiology*, 38(3):432–441, 2017.
- [146] S. Saboohi, M. Jasieniak, B. R. Coad, H. J. Griesser, R. D. Short, and A. Michelmore. Comparison of plasma polymerization under collisional and collision-less pressure regimes. *Journal of Physical Chemistry B*, 119(49):15359–15369, 2015.
- [147] H. W. Strauss, R. R. Chromik, S. Hassani, and J. E. Klemberg-Sapieha. In situ tribology of nanocomposite ti-si-c-h coatings prepared by pe-cvd. *Wear*, 272(1):133–148, 2011.
- [148] H. Hertz. Über die berührung fester elastischer körper. *Journal fur die reine und angewandte Mathematik*, 92:156–171, 1881.
- [149] J. Voros. The density and refractive index of adsorbing protein layers. *Biophysical Journal*, 87(1):553–561, 2004.
- [150] J. A. Defeijter, J. Benjamins, and F. A. Veer. Ellipsometry as a tool to study adsorption behavior of synthetic and biopolymers at air-water-interface. *Biopolymers*, 17(7):1759–1772, 1978.
- [151] D. L. Pappas and J. Hopwood. Deposition of diamond-like carbon using a planar radio-frequency induction plasma. *Journal of Vacuum Science and Technology a-Vacuum Surfaces and Films*, 12(4):1576–1582, 1994.
- [152] A. Bubenzer, B. Dischler, G. Brandt, and P. Koidl. Rf-plasma deposited amorphous hydrogenated hard carbon thin-films - preparation, properties, and applications. *Journal of Applied Physics*, 54(8):4590–4595, 1983.
- [153] L. Vroman and A. L. Adams. Findings with recording ellipsometer suggesting rapid exchange of specific plasma proteins at liquid/solid interfaces. *Surface Science*, 16:438, 1969.

-
- [154] L. Vroman, A. L. Adams, G. C. Fischer, and P. C. Munoz. Interaction of high molecular-weight kininogen, factor-xii, and fibrinogen in plasma at interfaces. *Blood*, 55(1):156–159, 1980.
- [155] J. Benesch, A. Askendal, and P. Tengvall. Quantification of adsorbed human serum albumin at solid interfaces: a comparison between radioimmunoassay (ria) and simple null ellipsometry. *Colloids and Surfaces B-Biointerfaces*, 18(2):71–81, 2000.
- [156] R. J. Green, M. C. Davies, C. J. Roberts, and S. J. B. Tendler. Competitive protein adsorption as observed by surface plasmon resonance. *Biomaterials*, 20(4):385–391, 1999.
- [157] B. Lassen and M. Malmsten. Competitive protein adsorption studied with tifr and ellipsometry. *Journal of Colloid and Interface Science*, 179(2):470–477, 1996.